

Technische Universität Dresden  
Fachrichtung Mathematik

Institut für Wissenschaftliches Rechnen

**Interacting Particles in Flowing Solvents**  
**Modeling, Numerics and High-Performance Computing**

Diplomarbeit  
zur Erlangung des ersten akademischen Grades

**Diplommathematiker**

vorgelegt von

Name: Praetorius

Vorname: Simon

geboren am: 20.09.1985

in: Nordhausen

Tag der Einreichung: 7. Dez. 2010

Betreuer: Prof. Dr.rer.nat.habil. Axel Voigt



## Abstract

This paper presents a new mathematical model to describe colloidal particles in a flowing polymer solution. In contrast to former models this method is based on a partial differential equation for the interacting polymer coils and potential and diffuse domain based descriptions of the colloids. The model is applied to the calculation of depletion forces between two particles that are very close to each other. Simulations of flowing interacting particles around some spherical obstacles are performed and compared to Brownian dynamics simulations qualitatively. The model is comparable to dynamic density functional type models but it has the advantage of less computational effort due to local equations. Therefore it is now possible to solve bigger systems for longer periods of time and the coupling to other phenomena, other differential equations.

## Zusammenfassung

In dieser Arbeit wird ein neues Modell zur Beschreibung von Kolloiden, die sich in einer fließenden Lösung von Polymer-Knäulen befinden, hergeleitet und analysiert. Die Methode basiert auf der Lösung einer partiellen Differentialgleichung für die interagierenden Teilchen in der Lösung und einer Diffuse-domain Methode zusammen mit Potentialfeldern zur Beschreibung der Kolloidteilchen in der Flüssigkeit. Angewendet wird das Modell auf die Berechnung von Depletion-Kräften zwischen zwei Partikeln, die sich sehr nahe kommen, und zur Untersuchung von Partikeldichten in einer Umströmung von runden Hindernissen. Letzteres wird mit anderen Brownsche-dynamik Simulationen verglichen, bezüglich dem qualitativen Verhalten in der Nähe der Kugeln. Außerdem ist das Modell vergleichbar zu dynamischer Dichtefunktional Theorie, hat der gegenüber den Vorteil, dass es weniger rechenintensiv ist, aufgrund des lokalen Charakters der Differentialgleichung. Dies führt dazu, dass Simulationen von größeren Systemen und über einen längeren Zeitraum durchgeführt werden können und eine Kopplung an andere Phänomene vergleichsweise einfach realisierbar ist.

## Danksagungen

An dieser Stelle möchte ich einer Reihe von Leuten danken, die mich in der Zeit der Ausarbeitung der Diplomarbeit sehr unterstützt haben. Anfangen möchte ich bei meinen Eltern, die mir solch ein Studium überhaupt erst ermöglicht haben, mich finanziell unterstützt, aber mich auch motiviert und mir viel Geduld entgegen gebracht haben. Viele aus meiner Arbeitsgruppe haben mir ganz praktisch beigestanden, durch Unterstützung bei Problemen mit den Rechnern oder der Programmierung und Auswertung, durch Diskussionen über erhaltene Resultate und Ideen zur Verbesserung, den Austausch über Möglichkeiten der Implementierung verschiedener Ansätze und vieles weitere mehr. Stellvertretend möchte ich hier nennen Thomas Witkowski, Andreas Naumann, Sebastian Aland, Rainer Backofen, Ingo Nitschke, Roland Gärtner. Meinem Mentor und Betreuer Prof. Dr. Axel Voigt danke ich für die Heranführung an das Thema, die Motivation und Unterstützung, für die Diskussion über Ergebnisse und die Möglichkeit so in die Forschung Einblick zu gewinnen. Marion Koethe möchte ich ganz herzlich danken, für viele Korrekturen in Sprache und Stil.

# Contents

<b>1</b>	<b>Introduction</b>	<b>1</b>
1.1	Motivation . . . . .	1
1.1.1	Soft Matter systems . . . . .	2
1.1.2	Structure of this thesis . . . . .	4
1.2	Mathematical preliminaries . . . . .	5
1.2.1	Fourier transform and delta function . . . . .	5
1.2.2	Sobolev space and gradient flow . . . . .	8
<b>2</b>	<b>Modeling</b>	<b>12</b>
2.1	Physical derivation of Phase-Field Crystal equation . . . . .	12
2.1.1	Brownian motion . . . . .	12
2.1.2	Fokker-Planck equation . . . . .	14
2.1.3	Dynamic density functional theory . . . . .	16
2.1.4	Phase-Field Crystal model . . . . .	18
2.2	Colloids in polymer solution . . . . .	26
2.2.1	Moving colloids . . . . .	28
<b>3</b>	<b>Numerics</b>	<b>30</b>
3.1	Description of complex geometries . . . . .	30
3.1.1	Explicit triangulations . . . . .	30
3.1.2	Levelset method . . . . .	32
3.1.3	Phase-Field method . . . . .	33
3.2	Diffuse-Domain approach . . . . .	35
3.3	Navier-Stokes equations in diffuse domain . . . . .	41
3.4	Energy-Minimization . . . . .	43

3.5	Time-discretization . . . . .	46
3.5.1	Semi-implicit discretization . . . . .	47
3.5.2	Rosenbrock method . . . . .	49
3.5.3	Time-discretization of Navier-Stokes equations . . . . .	51
3.6	Space-discretization . . . . .	51
3.6.1	Semi-implicit time-discretization . . . . .	52
3.6.2	Rosenbrock method . . . . .	55
3.6.3	Space-discretization of Navier-Stokes equations . . . . .	57
<b>4</b>	<b>Simulations</b>	<b>59</b>
4.1	Validation . . . . .	60
4.1.1	Validation of mathematical properties . . . . .	63
4.2	Modification of the model . . . . .	64
4.2.1	Non-constant mobility . . . . .	65
4.2.2	Penalization of low densities . . . . .	66
4.3	Depletion forces . . . . .	68
<b>5</b>	<b>Conclusion and Outlook</b>	<b>75</b>
5.1	Conclusion . . . . .	75
5.2	Outlook . . . . .	77
5.3	Anisotropic PFC . . . . .	78
5.3.1	Transformed PFC-energy . . . . .	78
5.3.2	Modeling of nematic liquid crystals . . . . .	79
5.3.3	Simulation of stretched particles . . . . .	81
<b>A</b>	<b>Solution Theory</b>	<b>84</b>
<b>B</b>	<b>Stability analysis</b>	<b>86</b>
B.1	Energy-stability . . . . .	86
B.2	Linear stability analysis . . . . .	88
<b>C</b>	<b>Derivation of SIMPLE-R algorithm</b>	<b>92</b>

# Chapter 1

## Introduction

### 1.1 Motivation

In 1991 Pierre-Gilles de Gennes gave his Nobel lecture<sup>1</sup> on a topic referred to as *Soft Matter*. He explained an early experiment initiated by the Indians of the Amazon basin, who collected the sap from the hevea tree (rubber tree) and spread it onto their feet. The liquid reacted with the oxygen in the air, hardened and resulted in some kind of rubbery "boots". This experiment shows a typical property of a soft material, i.e. mild chemical action can introduce a significant change in mechanical properties.

De Gennes was not the first one to analyze these Soft Matter systems, but he was the most prominent one, sometimes called the "founding father of Soft Matter", who has achieved the Nobel price for his work. Today soft materials appear in a wide range of every day products, for example structural and packaging materials, foams and adhesives, detergents and cosmetics, paints, food additives, lubricants and fuel additives, rubber in tires, in biological materials, e.g. blood, muscle, milk, yogurt or Jell-o. Liquid Crystals, i.e. are one category of Soft Matter systems that are applied in display devices (LCDs).

Polymers and colloids are prominent ingredients to Soft Matter systems. The analysis of one-component systems, i.e. consisting of polymers or colloidal particles, is quite interesting but recently the combination of different basic elements was put more focus on. These mixtures exhibit new properties, which are not found in either system separately. The character of particle interactions can often be controlled and tuned by additives to the suspension and thus gel or glass formation can be found in these systems.

---

<sup>1</sup>[dG92] College de France, Paris

The analysis of multi-component systems, using physical models and mathematical descriptions became important, since simulation methods were developed. It can predict the behavior of different model systems in reasonable time and with qualitative agreement with experimental studies. All former methods, e.g. molecular dynamics, Brownian dynamics, (dynamic) density functional methods, have different drawbacks, computational expense due to solution of different time-scales, or due to difficult mathematical equations, i.e. integro-differential equations. In this thesis we want to introduce a new mathematical model to describe interacting Brownian particles –the Phase-Field Crystal model –that was used to describe nucleation and growth of crystalline patterns, for example, in the last years, and provides a tool to simulate configurations of colloids and polymers in a solvent.

### 1.1.1 Soft Matter systems

Classical fluids, like water, consist of molecules or particles of a size of about one angstrom. The structure is very homogeneous if you look at them from a mesoscopic point of view. The properties of these fluids depend heavily on the properties of the molecules or molecular particles. On the other hand, take a look at a liquid with solvated latex molecules or at a mixture of oil and water. The structure becomes inhomogeneous there. Particles of a size of about  $10^4$  times the size of an angstrom (i.e.  $1\text{nm}$  to  $10\mu\text{m}$ ) build structures that are coarser than in classical fluids. The particles are referred to as *macro molecules*. Since these structures are easily deformable, they are termed *Soft Matter* systems.

Basic elements to Soft Matter systems are *colloids* or *polymers*, upon others. Colloids are rigid particles with spherical or other convex shapes, dispersed in a liquid. They are small enough to exhibit thermal motion. Since these particles are thousand times larger than the solvent molecules, that have a typical size of  $1\text{ \AA}$ , they can be regarded as macroscopic objects on the liquid length scale. The behavior of these dispersions, are comparable to that of molecular systems in some aspects and are thus an interesting model to study fundamental processes, like crystallization or glass formation. Due to their large size and slow dynamics, i.e. relaxation times are on the order of seconds compared to time-scales of about  $10^{-15}\text{s}$  for the solvent, experimental studies of such systems can be done easily by direct techniques, such as confocal microscopy, or indirect techniques, like light-scattering and rheology. The interaction of colloidal particles is, in the simplest form, hard sphere interaction, which is zero at all separations and infinitely repulsive at contact. This can be modified by grafting polymers or varying solvent temperature or salinity, for example.

Polymers are, in principle, very large molecules, consisting of many basic units, i.e. monomers,



that are bound together by covalent bonds. Chains of monomers often build polymer coils of the same order of magnitude as that of classical colloidal particles but with a very large number of internal degrees of freedom, several orders of magnitude larger than what is needed for the colloids. In [LBHM00, LBF<sup>+</sup>02] a coarse-graining of polymers as soft particles is motivated and explained to be a good model system that can reflect basic properties of the polymer coils. Since the polymers can interpenetrate, soft interaction of the model particles is expected, with a range in the region of the radius of gyration of individual coils.

The interaction of repulsive colloids can be modified by introducing polymers in the solution. This mixture is additionally driven by *depletion interaction*, which can be understood as entropic forces. Two colloidal particles, that are close to each other, so that polymers do not fit between them, are forced by an attraction potential that comes from a possible increase of entropy in the system. These depletion forces are analyzed in several ways, by different approximations of particle correlations or particle densities and for different repulsive potentials of the colloidal particles. In [GED97] hard colloidal particles immersed in a hard sphere fluid, i.e. the polymer coils were approximated by hard spheres, were analyzed with respect to depletion forces and it was found that this entropic force is attractive for distances of the colloids smaller than the twice the gyration radius. There the depletion interaction comes from a volume exclusion mechanism. The authors of [DLL03] used a superposition argument and simulation of non-interacting particles to get a profile of depletion forces depending on the distance of the colloidal particles. Colloid-colloid and colloid-wall interactions in driven suspensions were analyzed in [KR07], where macroscopic spherical obstacles are mediated by non-interacting solvent particles. The authors compared superposition approximations with a method of reflection and solution of a Smoluchowski equation to calculate the forces between two colloids and one colloid and a wall. In the case of ellipsoidal solvent particles in [KGG<sup>+</sup>04] a molecular simulation and mesoscale study can be found to calculate interactions between dilute spherical particles. Coarse-grained simulations of depletion forces induced by interacting Brownian particles in the presents of two nearly approaching spherical obstacle were not found in literature. This study is the main goal of this thesis.

Hartmut Löwen visualized the grade of difficulty and complexity to model such Soft Matter systems in diagram 1.1. In this thesis a mixture of spheres with different properties in full and steady-state non-equilibrium is considered. An extension to rod-like/ellipsoidal particles will be given in the outlook of the paper and thus nearly the most complex systems of this diagram can be simulated. Here we are interested in basic properties of the solvent, the particle density of Brownian particles around spherical obstacles, and change in the interaction properties of colloids mediated

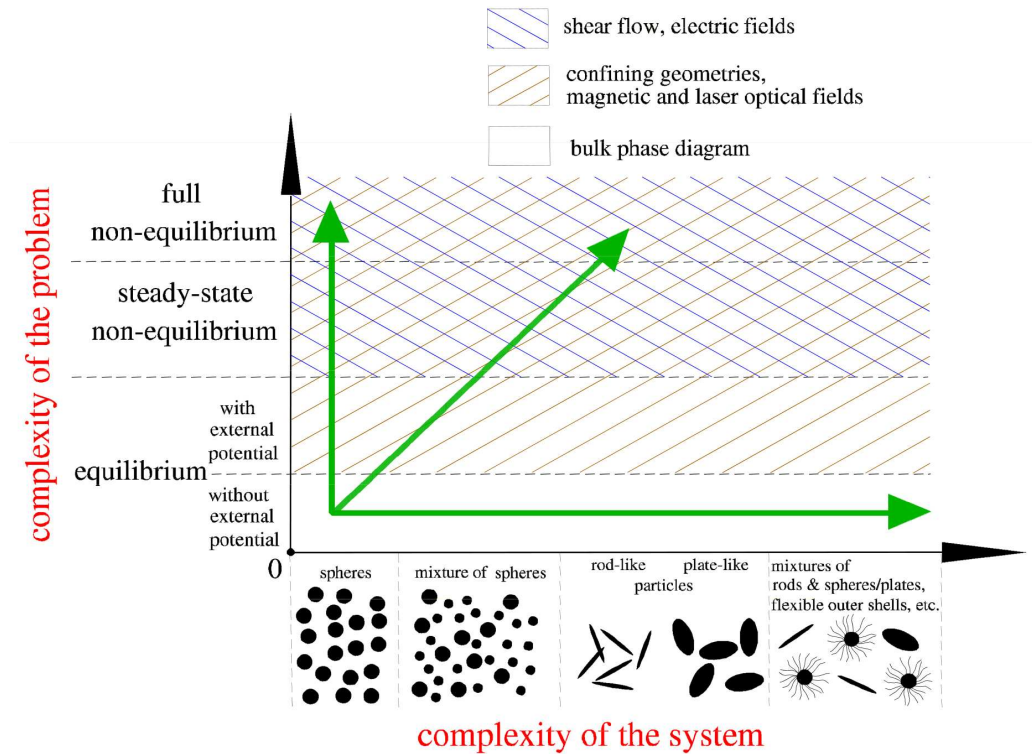


**Figure 1.1:** Diagram found in [L09], simulation and modeling complexity of Soft Matter systems. Green arrows point in the direction of higher complexity.

by this particles, i.e. depletion forces for dilute spheres.

### 1.1.2 Structure of this thesis

After some mathematical preliminaries at the end of this introduction, the Phase-Field Crystal model will be derived from other physical equation in chapter 2, starting from an equation of motion for the particles solved in a fluid. The dealing with the colloidal particles immersed in the fluid that act as macroscopic obstacles will be described in the second part of that chapter. A repulsive potential function is introduced to handle these obstacles.

Chapter 3 deals with the solution of the Phase-Field Crystal equations. Hence the partial differential equation must be discretization in time and space. We consider the minimization of an appropriate energy and mathematical description of the obstacles. A solution of the partial differential equation in a complex domain can be approximated by a diffuse domain method that is applied to the Phase-Field Crystal equations as well as to the Navier-Stokes equations. For the discretization in time a semi-implicit Euler discretization and a Rosenbrock-method is described.

The discretization in space is done using the Finite-Element Method.

In chapter 4 simulations of a system of Brownian particles that flow around spherical obstacles are presented. Starting from simulations of one colloid in a polymer solution, that can be compared to Brownian dynamics and density functional simulations qualitatively, we add a second colloid to the system, to calculate depletion forces between these particles.

In the Outlook in chapter 5 some extensions of the proposed model, are displayed. There a conclusion is drawn as to whether the proposed model is an appropriate simulation of Soft Matter systems.

## 1.2 Mathematical preliminaries

In this section some mathematical objects, notations and denotations are clarified. The examples given here are related to the Phase-Field Crystal model that is described in chapter 2.1 and analyzed throughout this paper.

### 1.2.1 Fourier transform and delta function

**Definition 1.2.1.** (from [Kab99], Definition 41.2)

Let  $f \in L_1(\mathbb{R}^d)$  be an integrable function, then the mapping  $\mathfrak{F} : f \mapsto \hat{f}$ , defined by

$$\mathfrak{F}[f](\mathbf{k}) := \hat{f}(\mathbf{k}) := (2\pi)^{-d/2} \int_{\mathbb{R}^d} f(\mathbf{x}) e^{-i\mathbf{x} \cdot \mathbf{k}} d\mathbf{x}, \quad \mathbf{k} \in \mathbb{R}^d$$

is called *Fourier transform* and the vector  $\mathbf{k}$  *wave number*.

The Fourier transform can also be defined for square integrable functions, sometimes called *Fourier-Planchel transform*, by

**Theorem 1.2.1.** *Let  $f \in L_2(\mathbb{R}^d)$  be a square integrable function, then the mapping*

$$\mathfrak{F}_2[f](\mathbf{k}) := \lim_{R \rightarrow \infty} (2\pi)^{-d/2} \int_{\|\mathbf{x}\| \leq R} f(\mathbf{x}) e^{-i\mathbf{x} \cdot \mathbf{k}} d\mathbf{x}$$

*is defined, where convergence in the sense of  $\|\cdot\|_{L_2}$  is given. It then holds  $\mathfrak{F}_2[f](\mathbf{k}) = \mathfrak{F}[f](\mathbf{k})$  almost everywhere.*

*Proof.* see [Wer06], Theorem V.2.9 □

**Example 1.2.1.** For Fourier transform of derivatives of functions  $f$  where  $D_x^\alpha f \in L_1(\mathbb{R}^d)$  holds, with  $\alpha$  is a multiindex, one can derive

$$\mathfrak{F}[D_x^\alpha f](\mathbf{k}) = i^{|\alpha|} \mathbf{k}^\alpha \hat{f}(\mathbf{k}) \quad . \quad (1.1)$$

Especially for the Laplacian  $\Delta f$  the Fourier transform is given by

$$\mathfrak{F}[\Delta f](\mathbf{k}) = -\mathbf{k}^2 \hat{f}(\mathbf{k}), \quad \text{with } \mathbf{k}^2 := \sum_i k_i^2 \quad .$$

Same results can be obtained for rapidly decreasing functions  $f \in \mathcal{S}(\mathbb{R}^d)$  (see [Wer06], Lemma V.2.4) or weakly differential functions  $f \in W^l(\mathbb{R}^d)$  for  $|\alpha| \leq l$  (see [Wer06], Lemma V.2.11).

**Example 1.2.2.** The duality of products and convolutions by Fourier transform is based on

$$\begin{aligned} \mathfrak{F}[f \cdot g](\mathbf{k}) &= \frac{1}{\sqrt{2\pi}^d} \{ \hat{f} * \hat{g} \}(\mathbf{k}) \\ \mathfrak{F}[f * g](\mathbf{k}) &= \frac{1}{\sqrt{2\pi}^d} \hat{f}(\mathbf{k}) \hat{g}(\mathbf{k}) \end{aligned}$$

where  $f, g \in L_1(\mathbb{R}^d)$ .

**Definition 1.2.2.** (from [Kab99], Definition 10.9.a)

A sequence  $(\delta_\epsilon)$  in  $\mathcal{L}_1(\mathbb{R}^d)$  ( $\epsilon > 0$ ) is called sequence of *nascent delta functions*, or *approximation to the identity*, if the following properties hold

- a)  $\delta_\epsilon \geq 0$
- b)  $\int_{\mathbb{R}^d} \delta_\epsilon(\mathbf{x}) \, d\mathbf{x} = 1$
- c)  $\lim_{\epsilon \rightarrow 0} \int_{\|\mathbf{x}\| \geq R} \delta_\epsilon(\mathbf{x}) \, d\mathbf{x} = 0, \quad \forall R > 0.$

The limit of such a sequence

$$\delta(\mathbf{x}) := \lim_{\epsilon \rightarrow 0} \delta_\epsilon(\mathbf{x})$$

is called *delta distribution* (sometimes (Dirac) *delta function*), since the limit is considered in a distributional sense, either that

$$\lim_{\epsilon \rightarrow 0} \int_{\mathbb{R}^d} \delta_\epsilon(\mathbf{x}) f(\mathbf{x}) \, d\mathbf{x} = f(0)$$

for all smooth functions  $f$  with compact support.

Some examples of nascent delta functions are given in chapter 3.1.2 and 3.1.3 where the Levelset-approach and Phase-field approach are described. Integration over the boundary of a domain in  $\mathbb{R}^d$  are approximated by multiplication with an approximation to a delta function. This situation occurs when the PDE is written in weak form and boundary terms are included in the equations. Since the integration over the whole domain is approximated in these methods, too, an approximation of a characteristic function that describes the domain is introduced. Here the relation of characteristic function and delta function is given. This works similarly for the approximated version of both "functions".

**Example 1.2.3.** For the *Heaviside step function*  $H := \chi_{[0,\infty)} \in L_1^{\text{loc}}(\mathbb{R})$  the weak derivative  $H'$  can be calculated by

$$\langle H', \vartheta \rangle = -\langle H, \vartheta' \rangle = -\int_{[0,\infty)} \vartheta'(\mathbf{x}) \, d\mathbf{x} = \vartheta(0)$$

since  $\vartheta \in C_0^\infty$ , because  $H$  has no compact support, where  $\langle a, b \rangle := \int_{\mathbb{R}} a \cdot b \, d\mathbf{x}$ . This gives the distributional representation  $H' = \delta$ .

**Example 1.2.4.** Weak gradients of multidimensional characteristic functions can also be expressed by multidimensional delta functions  $\delta_\Gamma$ , with respect to a manifold  $\Gamma$ , defined by

$$\int_{\mathbb{R}^d} \delta_\Gamma(\mathbf{x}) f(\mathbf{x}) \, d\mathbf{x} = \int_\Gamma f(\mathbf{x}) \, ds$$

for all test functions  $f$ .

For the derivative of a characteristic function  $\chi_\Omega := \{1 \text{ for } x \in \Omega; 0 \text{ otherwise}\}$ , where  $\Omega$  is a bounded domain subset of  $\mathbb{R}^d$ , a weak formulation leads to

$$\int_{\mathbb{R}^d} \nabla \chi_\Omega \vartheta \, d\mathbf{x} = -\int_{\mathbb{R}^d} \chi_\Omega \nabla \vartheta \, d\mathbf{x} = -\int_\Omega \nabla \vartheta \, d\mathbf{x} = -\int_{\partial\Omega} \mathbf{n} \vartheta \, ds = -\int_{\mathbb{R}^d} \mathbf{n} \delta_{\partial\Omega} \vartheta \, d\mathbf{x}$$

where  $\vartheta$  is a test function and  $\mathbf{n}$  is the perpendicular to  $\partial\Omega$  pointing outwards of  $\Omega$ . This leads to a distributional formulation

$$\nabla \chi_\Omega = -\mathbf{n} \delta_{\partial\Omega} \tag{1.2}$$

**Example 1.2.5.** The delta distribution can be represented by inverse Fourier transform, using

$$\delta(\mathbf{x}) = \mathfrak{F}^{-1}[(2\pi)^{-1/2}] \quad ,$$

since  $\mathfrak{F}[\delta(\mathbf{x})](\mathbf{k}) = (2\pi)^{-1/2} \int_{\mathbb{R}^d} e^{-i\mathbf{k}\cdot\mathbf{x}} \delta(\mathbf{x}) \, d\mathbf{x} = \frac{1}{\sqrt{2\pi}}$ . Also (weak) derivatives of the delta distribution can be described by Fourier transform:

$$\mathfrak{F}[\mathbf{x}^n](\mathbf{k}) = i^n \sqrt{2\pi} \delta^{(n)}(\mathbf{k})$$

where  $n \in \mathbb{N}$  and  $\delta^{(n)}$  the  $n^{\text{th}}$  (weak) derivative of the delta distribution.

## 1.2.2 Sobolev space and gradient flow

**Definition 1.2.3.** (Sobolev spaces, [Kab99, GR05])

Let  $\Omega \subseteq \mathbb{R}^d$  be an open set,  $k \in \mathbb{N}_{\geq 0}$ . One defines the space

$$\mathcal{W}^{k,2}(\Omega) := \{f \in L_2(\Omega) : D^\alpha f \in L_2(\Omega), \text{ for } |\alpha| \leq k\}$$

of  $L_2$ -functions with  $L_2$  derivatives up to order  $k$  in  $\Omega$ , with the norm

$$\|f\|_{\mathcal{W}^{k,2}} := \left( \sum_{|\alpha| \leq k} \int_{\Omega} \|D^\alpha f(\mathbf{x})\|^2 \, d\mathbf{x} \right)^{1/2} .$$

This gives a Hilbert space. We define the *Sobolev spaces*  $W^{k,2}(\Omega)$  and  $W_0^{k,2}(\Omega)$  as the closure of  $\overline{\mathcal{C}}^\infty(\Omega)$  and accordingly  $\mathcal{C}_0^\infty(\Omega)$  in  $\mathcal{W}^{k,2}$ . The spaces will also be denoted by  $H^k := W^{k,2}$  and  $H_0^k := W_0^{k,2}$ .

**Example 1.2.6.** Denoting the dual space to a Hilbert space  $H$  by  $H^*$ . Consider the Sobolev space  $\dot{H}_0^1(\Omega)$  of functions in  $H^1(\Omega)$  with compact support and zero average, the dual  $\dot{H}_0^1(\Omega)^*$  will be denoted by  $H^{-1}(\Omega)$ . For  $u, v \in \dot{H}_0^1(\Omega)$  the inner product is defined by  $(u, v)_{\dot{H}_0^1(\Omega)} := (\nabla u, \nabla v)_{L_2(\Omega)}$  and accordingly the norm as  $\|u\|_{\dot{H}_0^1(\Omega)} := \|\nabla u\|_{L_2(\Omega)}$ . We can derive the inner product of the dual space  $H^{-1}$  (see [Emm03]), as

$$(u^*, v^*)_{H^{-1}(\Omega)} = (u, v)_{\dot{H}_0^1(\Omega)} = (\nabla u, \nabla v)_{L_2(\Omega)} = - \int_{\Omega} \Delta^{-1}(u^*) v^* \, d\mathbf{x}$$

where  $u, v$  are the associates to  $u^*, v^*$ , and are related via the Poisson equation

$$-\Delta u = u^* \text{ in } \Omega, \quad \text{s.t. } \partial_{\mathbf{n}} u = 0 \text{ on } \partial\Omega, \quad \int_{\Omega} u \, d\mathbf{x} = 0 \quad .$$

**Example 1.2.7.** Let  $M(\mathbf{x}) > 0$  be a positive definite function that acts as a weight function. One can modify the  $L_2$  and  $H^{-1}$  space, including this weight, by modifying the inner products

$$\begin{aligned} (u, v)_{L_2(\Omega), M} &:= \int_{\Omega} M^{-1} u v \, d\mathbf{x} \\ (u, v)_{H^{-1}(\Omega), M} &:= - \int_{\Omega} (\nabla \cdot (M \nabla \cdot))^{-1} (u) v \, d\mathbf{x} \quad . \end{aligned} \tag{1.3}$$

**Definition 1.2.4.** Let  $H$  be a real Hilbert space with norm  $\|\cdot\|$ , inner product  $(\cdot, \cdot)$  and duality pairing  $\langle \cdot, \cdot \rangle_{H^* \times H}$ . Given a functional  $\mathcal{F} : H \rightarrow \mathbb{R}$  and a function  $\phi \in H$ , we say that  $\mathcal{F}$  is *differentiable* at  $\phi$ , if exists  $\delta_{\phi} \mathcal{F} \in H^*$  there, so that

$$\langle \delta_{\phi} \mathcal{F}, \vartheta \rangle = \left. \frac{d}{d\varepsilon} \mathcal{F}[\phi + \varepsilon \vartheta] \right|_{\varepsilon=0}, \quad \forall \vartheta \in H$$

i.e. the limit exists. The functional  $\delta_{\phi} \mathcal{F}$  is then called *functional derivative* (or variational derivative) of  $\mathcal{F}$  with respect to  $\phi$ . Sometimes the derivative will be denoted by  $\frac{\delta \mathcal{F}[\phi]}{\delta \phi}$ .

If  $\mathcal{F}$  is differentiable at  $\phi \in H$ , a unique  $w \in H$  exists (Riesz Representation Theorem), such that

$$\langle \delta_{\phi} \mathcal{F}, \vartheta \rangle = (w, \vartheta), \quad \forall \vartheta \in H \quad .$$

This  $w$  is denoted by  $\text{grad}_H \mathcal{F}[\phi]$  as the gradient of the functional  $\mathcal{F}$ . By limiting the direction of the derivative, i.e.  $\vartheta \in X \subset H$ , the gradient might not be unique anymore. Taking the set

$$G(\mathcal{F}, H, X, \phi) := \left\{ w \in H : \lim_{\varepsilon \rightarrow 0} \frac{1}{\varepsilon} (\mathcal{F}[\phi + \varepsilon \vartheta] - \mathcal{F}[\phi]) = (w, \vartheta), \quad \forall \vartheta \in X \right\}$$

where  $X$  denotes the limiting directions and  $G$  the set of candidates for the gradient, one can select the element of  $G$  with least norm and denote it by  $\text{grad}_H^X \mathcal{F}[\phi]$ .  $G$  is closed and convex and if  $X$  is dense subspace of  $H$ , it can be shown that  $G$  is empty or a singleton. So for appropriate spaces  $X$  we get a good choice of a gradient of  $\mathcal{F}$ . Details and proof of the above statements can be found in [Cow04].

**Example 1.2.8.** The simplified Phase-Field Crystal functional in Ginzburg-Landau form, related

to later studies (see chapter 2.1.4), is given by

$$\mathcal{F}[\phi] := \int_{\Omega} \frac{1}{2} \|\Delta\phi\|^2 - \|\nabla\phi\|^2 + f(\phi) \, d\mathbf{x}$$

where  $f$  is a differentiable function. The functional can be differentiated with respect to  $\phi$  in direction  $\vartheta$  as

$$\begin{aligned} \left. \frac{d}{d\varepsilon} \mathcal{F}[\phi + \varepsilon\vartheta] \right|_{\varepsilon=0} &= \left. \frac{d}{d\varepsilon} \int_{\Omega} \frac{1}{2} \|\Delta(\phi + \varepsilon\vartheta)\|^2 - \|\nabla(\phi + \varepsilon\vartheta)\|^2 + f(\phi + \varepsilon\vartheta) \, d\mathbf{x} \right|_{\varepsilon=0} \\ &= \int_{\Omega} \Delta\phi\Delta\vartheta - 2\nabla\phi\nabla\vartheta + f'(\phi)\vartheta \, d\mathbf{x} \\ &= \int_{\Omega} \Delta^2\phi\vartheta + 2\Delta\phi\vartheta + f'(\phi)\vartheta \, d\mathbf{x} \end{aligned}$$

where we assume appropriate boundary conditions.

a) The gradient with respect to  $L_2$  is then simply given by

$$\text{grad}_{L_2} \mathcal{F}[\phi] = \Delta^2\phi + 2\Delta\phi + f'(\phi) \quad . \quad (1.4)$$

b) Now consider the Hilbert space  $H^{-1}$  of example 1.2.6. We derive formally:

$$\begin{aligned} \int_{\Omega} \Delta^2\phi\vartheta + 2\Delta\phi\vartheta + f'(\phi)\vartheta \, d\mathbf{x} &= \int_{\Omega} \underbrace{(\Delta^2\phi + 2\Delta\phi + f'(\phi))}_{=:g} \vartheta \, d\mathbf{x} \\ &= \int_{\Omega} g\vartheta \, d\mathbf{x} \stackrel{!}{=} \int_{\Omega} -\Delta^{-1}(g^*)\vartheta \, d\mathbf{x} \quad \Leftrightarrow \quad g^* = -\Delta g \\ \Rightarrow \quad \langle \delta_{\phi}\mathcal{F}, \vartheta \rangle &= (-\Delta(\Delta^2\phi + 2\Delta\phi + f'(\phi)), \vartheta)_{H^{-1}(\Omega)} \end{aligned}$$

and this takes us to

$$\text{grad}_{H^{-1}} \mathcal{F}[\phi] = -\Delta(\Delta^2\phi + 2\Delta\phi + f'(\phi)) \quad . \quad (1.5)$$

An analogy to a gradient descent method for functions in  $\mathbb{R}^d$ , can now be defined for functionals in a Hilbert space setting. The motivation is to be consistent with the laws of thermodynamics, in the sense of decreasing an energy (functional) as much as possible at a given time step. In the finite dimensional case, this can be done by going in the negative gradient direction. Something similar is considered for the functional gradients.

**Definition 1.2.5.** (Gradient flow, e.g. [Dro05, Cow04])

Let  $H$  be a Hilbert space,  $\mathcal{F} \in H^*$  a functional,  $\text{grad}_H \mathcal{F}$  its gradient and  $M > 0$ . An evolution



equation, starting from an initial value  $\phi(t = 0) = \phi_0$ , that is defined by

$$\partial_t \phi = -M \operatorname{grad}_H \mathcal{F}[\phi]$$

and has to be understood in the sense

$$(\partial_t \phi, \vartheta)_H = -M \langle \delta_\phi \mathcal{F}[\phi], \vartheta \rangle_{H^* \times H}, \quad \forall \vartheta \in H$$

is called *gradient flow* of the functional  $\mathcal{F}$ , and  $M$  is called the *mobility* of the flow.

*Remark.* A gradient flow is a descent method, since  $-\operatorname{grad}_H \mathcal{F}[\phi]$  is a descent direction:

$$\partial_t \mathcal{F}[\phi] = \langle \delta_\phi \mathcal{F}[\phi], \partial_t \phi \rangle = (\operatorname{grad}_H \mathcal{F}[\phi], -M \operatorname{grad}_H \mathcal{F}[\phi]) = -M \|\operatorname{grad}_H \mathcal{F}[\phi]\| \leq 0 \quad .$$

**Example 1.2.9.** The gradient flow of the functional defined in example 1.2.8 is derived. The  $L_2$ -gradient flow simply gives

$$\partial_t \phi = -M \operatorname{grad}_{L_2} \mathcal{F}[\phi] = -M(\Delta^2 \phi + 2\Delta \phi + f'(\phi)) \quad .$$

This equation, a fourth order parabolic partial differential equation, is related to the so called *Swift-Hohenberg equation* (e.g. [SH77, WWL09]).

The  $H^{-1}$ -gradient flow of the same functional gives a six-order PDE:

$$\partial_t \phi = -M \operatorname{grad}_{H^{-1}} \mathcal{F}[\phi] = M\Delta(\Delta^2 \phi + 2\Delta \phi + f'(\phi))$$

and is related to the Phase-Field Crystal equations which we derive and explain in the next chapters.

# Chapter 2

## Modeling

### 2.1 Physical derivation of Phase-Field Crystal equation

In the work about relaxation dynamics of an assembly of interacting particles by Tarazona and Marconi [MT99], the authors introduce a theory that was developed further in many directions for few years. They assume that an ensemble of identical, spherical particles, that do not interact via hydrodynamic forces, can be modeled as Brownian particles with stochastic equations of motion. Later different approaches are presented to include hydrodynamic interactions (e.g. [Arc09], [RL08], [RL09], [PRDK07])

Starting from Newton's equation of motion, we want to sketch the derivation of dynamic density functional theory and from there the derivation of the Phase-Field Crystal equations that are used in the study of particle interactions.

#### 2.1.1 Brownian motion

Consider  $N$  identical spherical colloidal particles with position coordinates  $\vec{\mathbf{r}} = \{\mathbf{r}_1, \mathbf{r}_2, \dots, \mathbf{r}_N\}$ , and mass  $m$ , immersed in an incompressible fluid acting as a heat reservoir with well-defined temperature. Then the equation of motion of the  $i^{\text{th}}$  particle, with velocity  $\partial_t \mathbf{r}_i = \frac{1}{m} \mathbf{p}_i$ , reads

$$\partial_t \mathbf{p}_i = -\gamma(\mathbf{p}_i - \mathbf{u}(\mathbf{r}_i, t)) + F_i(\vec{\mathbf{r}}, t) + \boldsymbol{\eta}_i(t) \quad (2.1)$$

where  $\gamma = 2d\pi\eta_0 a$  is the friction coefficient, with  $d$  the space-dimension,  $\eta_0$  the shear viscosity of the solvent and  $a$  the radius of the colloidal particles. The sum of all forces acting on the particle  $i$  is solved in  $F_i$ . We assume that the forces contain contributions to an external potential and particle

interactions only. This force-term can then be expressed as

$$F_i(\vec{\mathbf{r}}, t) = -\nabla_{\mathbf{r}_i} V(\vec{\mathbf{r}}, t)$$

$$V(\vec{\mathbf{r}}, t) = \sum_i V_1(\mathbf{r}_i, t) + \frac{1}{2} \sum_{ij} V_2(\mathbf{r}_i, \mathbf{r}_j) + \frac{1}{6} \sum_{ijk} V_3(\mathbf{r}_i, \mathbf{r}_j, \mathbf{r}_k) + \dots$$

where  $V_1$  is the external one-particle potential,  $V_2$  the pair-interaction potential and where  $V_3$  represents the interaction of three particles and so on. In the case of homogeneous, isotropic fluids the pair-interaction function is a function of the distance of two particles ([Dho98])  $\|\mathbf{r}_i - \mathbf{r}_j\|$ . For systems that are dilute, events where three or more particles interact simultaneously are unlikely. Therefore we can neglect all interaction-potentials  $V_n$  with  $n \geq 3$  and approximate  $V_2$  by  $\bar{V}_2(\|\mathbf{r}_i - \mathbf{r}_j\|)$ . Because of the symmetry of  $\bar{V}_2$  in  $i, j$  we get

$$V(\vec{\mathbf{r}}, t) \approx \sum_i V_1(\mathbf{r}_i, t) + \sum_{i < j} \bar{V}_2(\|\mathbf{r}_i - \mathbf{r}_j\|) \quad .$$

If the mass of the colloidal particles is small compared to macroscopic objects, thermal fluctuations insert a velocity in the evolution. This is approximated by the random force  $\boldsymbol{\eta}_i(t) = (\eta_i^x(t), \eta_i^y(t), \eta_i^z(t))$ . By assuming that different collisions with fluid molecules are approximately independent, we get an average description of the fluctuations by its first two moments

$$\langle \eta_i^\alpha(t) \rangle = 0 \quad \text{and}$$

$$\langle \eta_i^\alpha(t) \eta_j^\beta(s) \rangle = q \delta_{ij} \delta_{\alpha\beta} \delta(t - s), \quad \forall \alpha, \beta \in \{x, y, z\}$$

where the term  $q \approx 2\gamma k_B T$  describes the fluctuation strength,  $k_B$  is Boltzmann's constant,  $T$  the temperature,  $\delta_{ij}$  the Kronecker delta and  $\delta(\cdot)$  the (Dirac) delta function (see (1.2.2) for description).

*Remark.* Fluctuation  $\boldsymbol{\eta}$  represents stochastic white noise that is characterized by the spectral density

$$S(\omega) = 2 \int_{\mathbb{R}} e^{-i\omega\tau} \langle \eta(\tau) \eta'(0) \rangle d\tau = 2 \int_{\mathbb{R}} e^{-i\omega\tau} q \delta(\tau) d\tau = 2q \quad .$$

The noise is called *white noise* because  $S(\omega)$  is independent of the frequency  $\omega$ , i.e. the spectral density is flat, like the optical spectrum of white light (within the visible range) ([Gar96], [Ris89]).

Hydrodynamic interactions, i.e. one particle induces a fluid flow that affects another particle, are approximately neglected. In general this is only reasonable for very dilute suspension (very large distances between particles). The friction force can then simply be written as  $-\frac{\gamma}{m} \mathbf{p}_i$  and is extended to  $-\frac{\gamma}{m} (\mathbf{p}_i - \mathbf{u})$ , because we have to use the velocity of the particles relative to the local velocity  $\mathbf{u}$

of the solvent instead of the absolute velocity of the Brownian particles. Throughout this paper we assume the velocity  $\mathbf{u}$  to be solenoidal, i.e.  $\nabla \cdot \mathbf{u} = 0$ .

*Remark.* In less dilute suspensions the friction coefficient depends on the momentum and position coordinates of all Brownian particles and can be described through friction matrices  $\mathbf{D}(\vec{\mathbf{r}})$ . This linear form occurs due to very low Reynolds numbers and the reduction of Navier-Stokes to simple Stokes flow, induced by the particles. (see [Dho98] for further explanations).

If the friction coefficient  $\gamma$  is large (overdamped dynamics, i.e. the system returns to equilibrium without oscillating), we can neglect the second derivative of the position, i.e.  $\partial_t \mathbf{p}_i = 0$ . By putting the mass  $m$  into the timescale and  $\frac{1}{\gamma}$  into the random force  $\bar{\boldsymbol{\eta}}_i := \frac{1}{\gamma} \boldsymbol{\eta}_i$  we obtain the Langevin equation of motion considered in this work

$$\begin{aligned} \partial_t \mathbf{r}_i &= \mathbf{u}(\mathbf{r}_i, t) + \frac{1}{\gamma} (F_i(\vec{\mathbf{r}}, t) + \boldsymbol{\eta}_i(t)) \\ &= \mathbf{u}(\mathbf{r}_i, t) - \frac{1}{\gamma} \left( \nabla_{\mathbf{r}_i} \left[ \sum_i V_1(\mathbf{r}_i, t) + \sum_{i < j} \bar{V}_2(\|\mathbf{r}_i - \mathbf{r}_j\|) \right] \right) + \bar{\boldsymbol{\eta}}_i(t) \quad . \end{aligned} \quad (2.2)$$

### 2.1.2 Fokker-Planck equation

The equation of motion (2.2) is a stochastic differential equation for each particle in the system. For many particles this coupled system becomes more and more complex. One attempt to describe the particle motion by only one equation, is the Fokker-Planck equation, that gives a probability density  $W(\vec{\mathbf{r}}, t)$  that determines the probability to find the set of  $N$  particles around the positions  $\mathbf{r}_1, \dots, \mathbf{r}_N$ .

Fokker-Planck's equations, or commonly called *Smoluchowski equations* in this case, for the  $N$ -particle probability density  $W(\vec{\mathbf{r}}, t)$  that are equivalent to the equation of motion (2.2) can be found in [Dho98] or [Ris89] for example, and are given by

$$\begin{aligned} \partial_t W(\vec{\mathbf{r}}, t) &= \mathcal{L}_S W(\vec{\mathbf{r}}, t) \\ \text{with } \mathcal{L}_S(\cdot) &= \sum_i \nabla_{\mathbf{r}_i} \cdot \left[ \left( -\mathbf{u}(\mathbf{r}_i, t) - \frac{1}{\gamma} F(\vec{\mathbf{r}}, t) + k_B T \nabla_{\mathbf{r}_i} \right) (\cdot) \right] \end{aligned} \quad (2.3)$$

with initial conditions  $W(\vec{\mathbf{r}}, t = t_0) = \delta(\vec{\mathbf{r}} - \vec{\mathbf{r}}_0)$  and appropriate boundary conditions. By defining the *probability current*  $\mathbf{J} = (J_i)_{i=1, \dots, N}$

$$J_i(\vec{\mathbf{r}}, t) := \frac{1}{\gamma} F(\vec{\mathbf{r}}, t) W(\vec{\mathbf{r}}, t) - k_B T \nabla_{\mathbf{r}_i} W(\vec{\mathbf{r}}, t)$$

we can set, for example, periodic boundary conditions for the boundary of a box-domain  $\Omega = [a, b]^3$ :

$$\begin{aligned}\lim_{\alpha \rightarrow b^-} W(r^{\vec{\alpha}}, t) &= \lim_{\alpha \rightarrow a^+} W(r^{\vec{\alpha}}, t) \\ \lim_{\alpha \rightarrow b^-} \mathbf{J}(r^{\vec{\alpha}}, t) &= \lim_{\alpha \rightarrow a^+} \mathbf{J}(r^{\vec{\alpha}}, t), \quad \text{for } \alpha \in \{x, y, z\}\end{aligned}$$

where  $r^{\vec{\alpha}} = (r_1^\alpha, r_2^\alpha, \dots, r_N^\alpha)$  represents the vector of one component of the coordinates.

*Remark.* The operator  $\mathcal{L}_S$  is called *Smoluchowski-operator*.

The Fokker-Planck equation can be seen as an abstract advection-diffusion equation with the current  $\mathbf{J}$ , using the identity  $\nabla_{\vec{\mathbf{r}}} \cdot (\dots) = \sum_i \nabla_{\mathbf{r}_i} \cdot (\dots)$

$$\partial_t W(\vec{\mathbf{r}}, t) + \nabla_{\vec{\mathbf{r}}} \cdot (\mathbf{u}(\vec{\mathbf{r}}, t) W(\vec{\mathbf{r}}, t)) = -\nabla_{\vec{\mathbf{r}}} \cdot \mathbf{J}(\vec{\mathbf{r}}, t) \quad (2.4)$$

with  $\mathbf{u}(\vec{\mathbf{r}}, t) = (\mathbf{u}(\mathbf{r}_i, t))_{i=1, \dots, N}$

Since it is not of any interest where all the individual particles can be found at a time, but rather what is the probability to find any particle at a given position, we can integrate the Smoluchowski equation (2.3) over  $N - 1$  of the  $N$  variables to obtain a one-particle density distribution. Therefore we introduce the  $n$ -particle density  $\rho^{(n)}$  by integrating the Smoluchowski equation (2.3)  $(N - n)$ -times, using the  $(n)$ -particle density

$$\rho^{(n)}(\mathbf{r}_1, \dots, \mathbf{r}_n, t) = \frac{N!}{(N - n)!} \int W(\vec{\mathbf{r}}, t) d\mathbf{r}_{n+1} \dots d\mathbf{r}_N$$

we obtain the continuity equation

$$\begin{aligned}\partial_t \rho(\mathbf{r}, t) + \nabla \cdot (\rho(\mathbf{r}, t) \mathbf{u}(\mathbf{r}, t)) &= -\nabla \cdot \mathbf{j}(\mathbf{r}, t) \\ \gamma \mathbf{j}(\mathbf{r}, t) &= -\rho(\mathbf{r}, t) \nabla V_1(\mathbf{r}, t) - k_B T \nabla \rho(\mathbf{r}, t) \\ &\quad - \int \rho^{(2)}(\mathbf{r}, \mathbf{r}', t) \nabla \bar{V}_2(\|\mathbf{r} - \mathbf{r}'\|) d\mathbf{r}'\end{aligned} \quad (2.5)$$

where we have dropped the superscript for the one-particles density  $\rho^{(1)} =: \rho$  and the subscript in the positions. Detailed calculations can be found in [L ow09].

Neglecting the pair-interaction term containing the two-particle density  $\rho^{(2)}$ , the equation (2.5) reduces to Fick's diffusion equation in a flowing heat bath with an external potential  $U_1 := (k_B T)^{-1} V_1$  and diffusion coefficient  $D := k_B T \gamma^{-1}$ .

**Problem 1.** Let  $\Omega \subset \mathbb{R}^d$  and  $D > 0$ . Find  $\rho(\mathbf{r}, t)$  for  $(\mathbf{r}, t) \in \Omega \times [0, \infty)$  with

$$\begin{aligned} \partial_t \rho(\mathbf{r}, t) + \nabla \cdot (\rho(\mathbf{r}, t) \mathbf{u}(\mathbf{r}, t)) &= -\nabla \cdot \mathbf{j}(\mathbf{r}, t) \\ D^{-1} \mathbf{j}(\mathbf{r}, t) &= -\rho(\mathbf{r}, t) \nabla U_1(\mathbf{r}, t) - \nabla \rho(\mathbf{r}, t) \quad \text{in } \Omega \end{aligned}$$

subject to initial and boundary conditions

$$\begin{aligned} \rho(\mathbf{r}, 0) &= \rho_0(\mathbf{r}) \quad \text{in } \bar{\Omega} \\ \rho(\mathbf{r}, t) &= 0 \quad \text{in } \partial\Omega \times [0, \infty) \end{aligned}$$

with compatibility condition  $\rho_0(\mathbf{r}) = 0$  in  $\partial\Omega$ .

### 2.1.3 Dynamic density functional theory

In the equation of the noise averaged one-particle density (2.5) the interaction-term depends on the time and the aim is to approximate this by an interaction term in equilibrium (time-independent). If we apply an additional external potential  $\Psi(\mathbf{r})$  to our Fokker-Planck equation, we can achieve a system with equilibrium density distribution  $\rho^*(\mathbf{r}) = \rho(\mathbf{r}, t)$ . The existence of such a potential is proven by density functional theory but requires some properties of the equilibrium state.

For flows that are not curl-free (e.g. shear-flow, stokes-flow) no reversibility condition (*detailed balance*) for the Fokker-Planck equation is satisfied, as is described in [VR07] or [PRDK07]. So the restriction of the following derivation to simple potential flows is necessary. The velocity field can then be written as the gradient of a scalar field,  $\mathbf{u}(\mathbf{r}) = -\frac{1}{\gamma} \nabla \Phi(\mathbf{r})$ . Driven steady states are currently under massive research, e.g. by R. Evans, who pronounced that "Detailed balance has a counterpart in non-equilibrium steady states" ([Eva05]). Density functional theory requires an equilibrium state where detailed balance is satisfied. So in the future it is unavoidable to extend the density function theory to driven steady states (if possible) and to include this extension in the following derivation.

Replacing the external potential  $V_1$  by  $U^*(\mathbf{r}) = V_1(\mathbf{r}) + \Phi(\mathbf{r}) + \Psi(\mathbf{r})$  in the particle-density equation (2.5), where we assume that  $V_1(\mathbf{r}, t) = V_1(\mathbf{r})$  in equilibrium, and taking the stationary

state, with necessarily  $\partial_t \rho(\mathbf{r}, t) = 0$ , implies the following so called *Yvon-Born-Green-hierarchy*

$$\begin{aligned}
0 &= \nabla \cdot [\rho(\mathbf{r}, t) \nabla (V_1(\mathbf{r}, t) + \Phi(\mathbf{r})) + k_B T \nabla \rho(\mathbf{r}, t) + \int \rho^{(2)}(\mathbf{r}, \mathbf{r}', t) \nabla \bar{V}_2(\|\mathbf{r} - \mathbf{r}'\|) d\mathbf{r}'] \\
&= \nabla \cdot [\rho(\mathbf{r}) \nabla (V_1(\mathbf{r}) + \Phi(\mathbf{r})) + k_B T \nabla \rho(\mathbf{r}) + \int \rho^{(2)}(\mathbf{r}, \mathbf{r}') \nabla \bar{V}_2(\|\mathbf{r} - \mathbf{r}'\|) d\mathbf{r}'] \\
&= \nabla \cdot \underbrace{[\rho^*(\mathbf{r}) \nabla U^*(\mathbf{r}) + k_B T \nabla \rho^*(\mathbf{r}) + \int \rho^{*(2)}(\mathbf{r}, \mathbf{r}') \nabla \bar{V}_2(\|\mathbf{r} - \mathbf{r}'\|) d\mathbf{r}']}_{=const, \text{ must vanish for } \mathbf{r} \rightarrow \infty} \\
\Rightarrow 0 &= \rho^*(\mathbf{r}) \nabla U^*(\mathbf{r}) + k_B T \nabla \rho^*(\mathbf{r}) + \int \rho^{*(2)}(\mathbf{r}, \mathbf{r}') \nabla \bar{V}_2(\|\mathbf{r} - \mathbf{r}'\|) d\mathbf{r}' \\
\gamma \mathbf{u}(\mathbf{r}) \rho^* &= \rho^*(\mathbf{r}) \nabla (V_1(\mathbf{r}) + \Psi(\mathbf{r})) + k_B T \nabla \rho^*(\mathbf{r}) + \int \rho^{*(2)}(\mathbf{r}, \mathbf{r}') \nabla \bar{V}_2(\|\mathbf{r} - \mathbf{r}'\|) d\mathbf{r}' \quad (2.6)
\end{aligned}$$

with an equilibrium two-particle density  $\rho^{*(2)}(\mathbf{r}, \mathbf{r}')$  for the modified system. Density functional theory states, that the equilibrium density distribution is a minimizer of the grand canonical functional

$$\mathcal{F}^*[\rho(\mathbf{r})] := \mathcal{F}_{\text{id}}[\rho(\mathbf{r})] + \mathcal{F}_{\text{ext}}^*[\rho(\mathbf{r})] + \mathcal{F}_{\text{ex}}[\rho(\mathbf{r})]$$

with the ideal solution part  $\mathcal{F}_{\text{id}}[\rho(\mathbf{r})] = \int k_B T \rho(\mathbf{r}) (\ln(\rho(\mathbf{r}) \Lambda^d) - 1) d\mathbf{r}$ , where  $\Lambda$  is the thermal wavelength, a description for an external potentials  $\mathcal{F}_{\text{ext}}^*[\rho(\mathbf{r})] = \int \rho(\mathbf{r}) U^*(\mathbf{r}) d\mathbf{r}$  and the excess free energy for particle interactions  $\mathcal{F}_{\text{ex}}[\rho(\mathbf{r})]$ , that is unknown for general systems.

The Euler-Lagrange equation for  $\mathcal{F}$  is given by

$$\gamma \mathbf{u}(\mathbf{r}) = \nabla (V_1(\mathbf{r}) + \Psi(\mathbf{r})) + \frac{k_B T}{\rho^*(\mathbf{r})} \nabla \rho^*(\mathbf{r}) + \nabla \left. \frac{\delta \mathcal{F}_{\text{ex}}[\rho]}{\delta \rho} \right|_{\rho^*(\mathbf{r})} \quad (2.7)$$

Compared with the last equation of (2.6), this results in an equation for the interaction-term

$$\int \rho^{*(2)}(\mathbf{r}, \mathbf{r}') \nabla \bar{V}_2(\|\mathbf{r} - \mathbf{r}'\|) d\mathbf{r}' = \rho^*(\mathbf{r}) \nabla \left. \frac{\delta \mathcal{F}_{\text{ex}}[\rho]}{\delta \rho} \right|_{\rho^*(\mathbf{r})} = -k_B T \rho^*(\mathbf{r}) \nabla c^{(1)}(\mathbf{r}, \rho^*(\mathbf{r})) \quad .$$

If we now assume that the density correlations  $c^{(1)}$  at time  $t$  in non-equilibrium, with density  $\rho(\mathbf{r}, t)$ , are the same as in an equilibrium system with additional potential  $\Psi(\mathbf{r})$  and mean density  $\rho^*(\mathbf{r})$ , we get a compact form of the density evolution

$$\partial_t \rho(\mathbf{r}, t) + \nabla \cdot (\rho(\mathbf{r}, t) \mathbf{u}(\mathbf{r})) = \nabla \cdot \left( \frac{1}{\gamma} \rho(\mathbf{r}, t) \nabla \frac{\delta \mathcal{F}[\rho(\mathbf{r}, t)]}{\delta \rho(\mathbf{r}, t)} \right) \quad (2.8)$$

with the free energy functional

$$\mathcal{F}[\rho(\mathbf{r}, t)] := \mathcal{F}_{\text{id}}[\rho(\mathbf{r}, t)] + \mathcal{F}_{\text{ext}}[\rho(\mathbf{r}, t)] + \mathcal{F}_{\text{ex}}[\rho(\mathbf{r}, t)]$$

with  $\mathcal{F}_{\text{ext}}[\rho(\mathbf{r}, t)] = \int \rho(\mathbf{r}, t) V_1(\mathbf{r}, t) \, \text{d}\mathbf{r}$ .

### 2.1.4 Phase-Field Crystal model

The dynamic density functional evolution equation (2.8) still contains the unknown free energy part  $\mathcal{F}_{\text{ex}}$ . Further approximations are necessary to solve this equation and different approaches were proposed in the past, e.g. mean-field approximation for very soft interactions

$$\mathcal{F}_{\text{ex}}[\rho] \approx \frac{1}{2} \iint \rho(\mathbf{r}) \rho(\mathbf{r}') \nabla \bar{V}_2(\|\mathbf{r} - \mathbf{r}'\|) \, \text{d}\mathbf{r} \text{d}\mathbf{r}' \quad .$$

Other approximations (for hard particles) are based on the Rosenfeld fundamental measure theory [Löw09, Eva09], or weighted density approximations [GL99]. The third well-known ansatz is a *Ramakrishnan-Yussouff* (RY) approximation [RY79], that will be explained in more detail, since it is the base for further approximations in the Phase-Field Crystal theory.

Consider the relative density deviation from a constant reference liquid density:  $\Delta\rho(\mathbf{r}) := \rho(\mathbf{r}) - \rho_L$ . The excess free part of the energy must be approximated in the RY-approximation by expansion around the liquid density  $\rho_L$  up to second order, in the sense of generalized gradient expansions

$$\begin{aligned} \mathcal{F}_{\text{ex}}[\rho(\mathbf{r})] - \mathcal{F}_{\text{ex}}[\rho_L] &=: \Delta\mathcal{F}_{\text{ex}}[\rho(\mathbf{r})] \approx \int \Delta\rho(\mathbf{r}) \frac{\delta\mathcal{F}_{\text{ex}}[\rho_L]}{\delta\rho(\mathbf{r})} \, \text{d}\mathbf{r} + \frac{1}{2} \iint \Delta\rho(\mathbf{r}) \Delta\rho(\mathbf{r}') \frac{\delta^2(\mathcal{F}_{\text{ex}}[\rho_L])}{\delta\rho(\mathbf{r})\delta\rho(\mathbf{r}')} \, \text{d}\mathbf{r} \text{d}\mathbf{r}' \\ &= -k_B T \int \Delta\rho(\mathbf{r}) c^{(1)}(\mathbf{r}, \rho_L) \, \text{d}\mathbf{r} - \frac{k_B T}{2} \iint \Delta\rho(\mathbf{r}) c^{(2)}(\mathbf{r}, \mathbf{r}', \rho_L) \Delta\rho(\mathbf{r}') \, \text{d}\mathbf{r} \text{d}\mathbf{r}' \end{aligned} \quad (2.9)$$

with the direct (two point) correlation function, given by

$$c^{(2)}(\mathbf{r}_1, \mathbf{r}_2, \rho) = \frac{\delta c^{(1)}(\mathbf{r}_1, \rho)}{\delta\rho(\mathbf{r}_2)} = -\frac{1}{k_B T} \frac{\delta^2(\mathcal{F}_{\text{ex}}[\rho])}{\delta\rho(\mathbf{r}_1)\delta\rho(\mathbf{r}_2)} \quad .$$

In [Jaa06] another form of  $c^{(1)}$  in the liquid reference fluid is explained to be equal to the above definition:

$$c^{(1)}(\mathbf{r}, \rho_L) = \ln(\rho_L \Lambda^d) - \frac{\mu_L}{k_B T}$$



with  $\mu_L$  the constant chemical potential of the reference liquid.

The ideal gas part  $\mathcal{F}_{\text{id}}$  of the energy can be rewritten as

$$\mathcal{F}_{\text{id}}[\rho(\mathbf{r})] - \mathcal{F}_{\text{id}}[\rho_L] =: \Delta\mathcal{F}_{\text{id}}[\rho(\mathbf{r})] = k_B T \int \Delta\rho(\ln(\rho_L \Lambda^d) - 1) + \rho(\mathbf{r}) \ln\left(\frac{\rho(\mathbf{r})}{\rho_L}\right) d\mathbf{r} \quad .$$

Combining both, ideal gas end excess free part of the energy (relative to the reference liquid state) results in

$$\begin{aligned} \Delta\mathcal{F}_{\text{id}}[\rho(\mathbf{r})] + \Delta\mathcal{F}_{\text{ex}}[\rho(\mathbf{r})] &= k_B T \int \underbrace{\Delta\rho(\mathbf{r})\left(\frac{\mu_L}{k_B T} - 1\right)}_{f_1(\rho(\mathbf{r}))} + \underbrace{\rho(\mathbf{r}) \ln\left(\frac{\rho(\mathbf{r})}{\rho_L}\right)}_{f_2(\rho(\mathbf{r}))} \\ &\quad - \frac{1}{2} \int \underbrace{\Delta\rho(\mathbf{r})\bar{c}^{(2)}(\mathbf{r}, \mathbf{r}', \rho_L) \Delta\rho(\mathbf{r}')}_{f_3(\rho(\mathbf{r}'))} d\mathbf{r} \quad . \end{aligned}$$

Since  $\bar{V}_2$  depends on the distance  $\|\mathbf{r} - \mathbf{r}'\|$  only, this property is assumed to be true for the direct pair correlation function also, especially in the liquid phase, so  $c^{(2)}(\mathbf{r}, \mathbf{r}', \rho) = \bar{c}^{(2)}(\|\mathbf{r} - \mathbf{r}'\|, \rho)$  and the rotational symmetry of  $\bar{c}^{(2)}$  follows immediately.

Now consider the Fourier transformed correlation function, by rewriting  $f_3(\rho)$  as

$$f_3(\rho(\mathbf{r})) = \frac{1}{2} \Delta\rho(\mathbf{r}) \left[ \bar{c}^{(2)}(\|\circ\|, \rho) * \Delta\rho \right](\mathbf{r})$$

where  $(a * b)(\mathbf{r}) := \int a(\mathbf{r} - \mathbf{r}')b(\mathbf{r}')d\mathbf{r}'$  is the convolution of  $a$  and  $b$  and  $\circ$  the multiplication-operator  $\circ(\mathbf{k}) = \mathbf{k}$ . Since the correlation-function is rotational symmetric the Fourier-cosine-transform of  $\bar{c}^{(2)}$  is sufficient:

$$\mathfrak{F}[\bar{c}^{(2)}] =: \hat{c}(\mathbf{k}, \rho) = \frac{1}{\sqrt{2\pi^d}} \int_{\mathbb{R}^d} \bar{c}^{(2)}(\|\mathbf{r}\|, \rho) \cos(\mathbf{k} \cdot \mathbf{r}) d\mathbf{r} \quad .$$

Expanding  $\hat{c}$  around  $\mathbf{k}_0 = 0$  [EPB<sup>+</sup>07] leads to

$$\hat{c}(\mathbf{k}, \rho) = \underbrace{\hat{c}(0, \rho)}_{\hat{C}_0} + \mathbf{k}^2 \underbrace{\frac{1}{2}\hat{c}''(0, \rho)}_{\hat{C}_2} + \mathbf{k}^4 \underbrace{\frac{1}{24}\hat{c}^{(4)}(0, \rho)}_{\hat{C}_4} + \dots$$

with  $\mathbf{k}^m := \sum_i k_i^m$ . The coefficients with odd derivatives vanish, because

$$\hat{c}^{(m)}(\mathbf{k}_0, \rho) = \pm \frac{1}{\sqrt{2\pi^d}} \int_{\mathbb{R}^d} \mathbf{r}^m \bar{c}^{(2)}(\|\mathbf{r}\|, \rho) \underbrace{\sin(\mathbf{k}_0 \cdot \mathbf{r})}_{=0 \text{ for } \mathbf{k}_0=0} d\mathbf{r}, \quad \text{for odd } m \quad .$$

We can now write the Fourier transform of  $f_3$  as

$$\begin{aligned}\mathfrak{F}[f_3(\rho)](\mathbf{k}) &= \frac{1}{2\sqrt{2\pi}^d} \left[ \hat{\Delta}\rho * (\sqrt{2\pi}^d \hat{c}(o, \rho) \hat{\Delta}\rho) \right] (\mathbf{k}) \\ &= \frac{1}{2} \left[ \hat{\Delta}\rho * (\hat{C}_0 + \hat{C}_2 \circ^2 + \hat{C}_4 \circ^4 + \dots) \hat{\Delta}\rho \right] (\mathbf{k}) =: \hat{f}_3(\rho) \quad .\end{aligned}$$

The inverse Fourier transform leads to the real space analogy

$$\begin{aligned}\mathfrak{F}^{-1}[\hat{f}_3(\rho)](\mathbf{r}) &= \frac{\sqrt{2\pi}^d}{2} \Delta\rho(\mathbf{r}) (\hat{C}_0 - \hat{C}_2 \Delta + \hat{C}_4 \Delta^2 - + \dots) \Delta\rho(\mathbf{r}) \\ &=: \frac{1}{2} \Delta\rho(\mathbf{r}) (C_0 - C_2 \Delta + C_4 \Delta^2 - + \dots) \Delta\rho(\mathbf{r}) \\ &\approx \frac{1}{2} \Delta\rho(\mathbf{r}) (C_0 - C_2 \Delta + C_4 \Delta^2) \Delta\rho(\mathbf{r})\end{aligned}$$

where this gradient-expansion was truncated at fourth order.

*Remark.* In the literature, e.g. [vTBVL09, EPB<sup>+</sup>07, Jaa06], often a non-unitary Fourier transform is used, so that the coefficients of the expansion in Fourier space change to  $\hat{C}_i := C_i$ . This has to be taken into account when concrete values are compared.

To obtain the standard form of the PFC model we assume constant mobility in equation (2.8) on the right-hand side. This leads to a more complex ideal solution term in the evolution, since it can not be simplified to  $\Delta\rho$  any more. The key to this difficulty is an expansion of the logarithmic term in the energy around the mean density  $\bar{\rho}$ . Therefore we introduce a new variable  $\phi(\mathbf{r}, t) := (\rho(\mathbf{r}, t) - \bar{\rho})/\bar{\rho} = (\Delta\rho(\mathbf{r}, t) - \bar{\rho})/\bar{\rho} + \rho_L/\bar{\rho}$ , the dimensionless *density modulation*, and truncate the expansions at fourth order. For  $\phi$  the property  $\int \phi(\mathbf{r}, t) d\mathbf{r} = 0$  holds. The expansions of  $f_i(\rho)$  in terms of  $\phi$ , neglecting all linear terms, since they vanish due to integration, yield

$$\begin{aligned}\frac{1}{\bar{\rho}} (f_1(\rho(\mathbf{r})) - f_1(\bar{\rho})) &= \phi(\mathbf{r}, t) \left( \frac{\mu_L}{k_B T} - 1 \right) = \text{(linear term)} \\ \frac{1}{\bar{\rho}} (f_2(\rho(\mathbf{r})) - f_2(\bar{\rho})) &\approx \frac{1}{2} \phi(\mathbf{r}, t)^2 - \frac{1}{6} \phi(\mathbf{r}, t)^3 + \frac{1}{12} \phi(\mathbf{r}, t)^4 + \text{(linear terms)} \\ \frac{1}{\bar{\rho}} (f_3(\rho(\mathbf{r})) - f_3(\bar{\rho})) &\approx \frac{\bar{\rho}}{2} \phi(\mathbf{r}, t) (C_0 - C_2 \Delta + C_4 \Delta^2) \phi(\mathbf{r}, t) + \text{(linear terms)} \quad .\end{aligned}$$

The third term in the energy, containing the external potentials,  $\Delta\mathcal{F}_{\text{ext}}[\rho] = \int \Delta\rho V_1 =: \int f_4(\rho)$ , can also be expressed in terms of  $\phi$ , as

$$\frac{1}{\bar{\rho}} (f_4(\rho(\mathbf{r})) - f_4(\bar{\rho})) = \phi(\mathbf{r}, t) V_1(\mathbf{r}, t) \quad .$$

In conclusion we can define the total free energy relative to the mean density by summation of the

energy parts

$$\begin{aligned}
\frac{1}{\bar{\rho}}(\Delta\mathcal{F}[\rho(\mathbf{r},t)] - \Delta\mathcal{F}[\bar{\rho}]) &= \frac{1}{\bar{\rho}}(\mathcal{F}[\rho(\mathbf{r},t)] - \mathcal{F}[\bar{\rho}]) \approx \mathcal{F}_2[\phi(\mathbf{r},t)] \\
&:= k_B T \int \frac{1}{2}\phi(\mathbf{r},t)^2 - \frac{1}{6}\phi(\mathbf{r},t)^3 + \frac{1}{12}\phi(\mathbf{r},t)^4 \, \mathbf{d}\mathbf{r} \\
&\quad - \frac{k_B T \bar{\rho}}{2} \int \phi(\mathbf{r},t)(C_0 - C_2\Delta + C_4\Delta^2)\phi(\mathbf{r},t) \, \mathbf{d}\mathbf{r} \\
&\quad + \int \phi(\mathbf{r},t)V_1(\mathbf{r},t) \, \mathbf{d}\mathbf{r}
\end{aligned} \tag{2.10}$$

where the denotation  $\mathcal{F}_2$  comes from the original name *PFC2-model* in [vTBVL09]. The evolution equation with respect to  $\phi(\mathbf{r},t)$  with constant mobility  $\bar{\rho}$  can now be written as

$$\begin{aligned}
\partial_t \phi(\mathbf{r},t) + \nabla \cdot (\phi(\mathbf{r},t) \mathbf{u}(\mathbf{r})) &= \frac{\bar{\rho}}{\gamma} \Delta \frac{\delta \mathcal{F}_2[\phi(\mathbf{r},t)]}{\delta \phi(\mathbf{r},t)} \\
&= \frac{k_B T \bar{\rho}}{\gamma} \Delta \left( \phi(\mathbf{r},t) - \frac{1}{2}\phi(\mathbf{r},t)^2 + \frac{1}{3}\phi(\mathbf{r},t)^3 \right. \\
&\quad \left. + (k_B T)^{-1} V_1(\mathbf{r},t) - \bar{\rho}(C_0 - C_2\Delta + C_4\Delta^2)\phi(\mathbf{r},t) \right)
\end{aligned} \tag{2.11}$$

and is an approximation, due to the expansion of the correlation function, of the dynamic density functional evolution equation (2.8).

### PFC in standard-form

The simplest form of the phase-field crystal energy was proposed by Swift and Hohenberg in 1977 [SH77], but the relation to molecular dynamics or dynamic density functional theory was currently shown by [EPB<sup>+</sup>07, Jaa06] and others. Swift and Hohenberg introduced a functional, nowadays often called *Swift-Hohenberg energy*, extended by contribution to an external potential, given by

$$\frac{\mathcal{F}_{\text{SH}}[\psi(\mathbf{r},t)]}{k_B T} = \int \frac{1}{2}\psi(\mathbf{r},t)(\alpha\Delta T + \lambda(q_0^2 + \Delta)^2)\psi(\mathbf{r},t) + \frac{g}{4}\psi(\mathbf{r},t)^4 + \psi(\mathbf{r},t)\frac{V_1(\mathbf{r},t)}{k_B T} \, \mathbf{d}\mathbf{r} \tag{2.12}$$

where  $\alpha$ ,  $\Delta T$ ,  $\lambda$ ,  $q_0$  and  $g$  are phenomenological constants. To get a connection of (2.12) to the energy (2.10) we rewrite the latter in terms of bulk-modulus and lattice constants which are relations to basic properties of a material to simulate [EPB<sup>+</sup>07]:

$$\begin{aligned}
B_L &:= 1 - \bar{\rho}C_0 && \dots \text{liquid phase isothermal compressibility} \\
B_S &:= \bar{\rho} \frac{C_2^2}{4|C_4|} && \dots \text{bulk modulus of the crystal} \\
\frac{1}{R} &:= \sqrt{\frac{2|C_4|}{C_2}} && \dots \text{lattice constant} \quad .
\end{aligned} \tag{2.13}$$

The energy can be reformulated with the new parameters

$$\begin{aligned} \frac{\mathcal{F}_2[\phi(\mathbf{r}, t)]}{k_B T} &= \int \frac{1}{2} B_L \phi(\mathbf{r}, t)^2 - \frac{1}{6} \phi(\mathbf{r}, t)^3 + \frac{1}{12} \phi(\mathbf{r}, t)^4 \, d\mathbf{r} \\ &+ \int \frac{1}{2} B_S \phi(\mathbf{r}, t) (2R^2 \Delta + R^4 \Delta^2) \phi(\mathbf{r}, t) \, d\mathbf{r} \\ &+ \int \phi(\mathbf{r}, t) \frac{V_1(\mathbf{r}, t)}{k_B T} \, d\mathbf{r} \quad . \end{aligned} \quad (2.14)$$

For a special choice of parameters one can obtain the standard Swift-Hohenberg energy.

$$\alpha \Delta T = B_L - B_S - \frac{1}{4}, \quad q_0 = \frac{1}{R}, \quad \lambda = B_S R^4, \quad g = \frac{1}{3} \quad (2.15)$$

with the new variable  $\psi := \phi - \frac{1}{2}$ , where linear and constant terms are ignored. The relation between the energies can be written as  $\mathcal{F}_2[\phi] = \mathcal{F}_{\text{SH}}[\psi(\phi)] + \text{const.}$  .

Elder and Grant [EG05] derived another form of the PFC-equation by phenomenological considerations. They took a Ginzburg-Landau energy which describes phase-transitions, e.g. spinodal decomposition among other phenomena and tried to modify the functional so that fast phase changes can be solutions to an energy-minimization. Ginzburg-Landau functional with bulk free energy  $f$ , e.g. a double-well, for the order parameter field  $\varrho$  is a nonlinear Dirichlet-energy

$$\mathcal{F}_{\text{GL}}[\varrho] = \int K_1 \|\nabla \varrho\|^2 + f(\varrho) \, d\mathbf{x} \quad (2.16)$$

where  $K_1$  is a phenomenological constant. A typical example of such a functional is the Cahn-Hilliard energy, where  $f$  is similar to  $f(\varrho) = \frac{1}{4\epsilon^2} (\varrho^2 - 1)^2$ , that forces the quantity  $\varrho$  to have  $\|\varrho\| \approx 1$ . Minimization of (2.16) leads to a phase-field  $\varrho$  with regions nearly constant, since gradients in the quantity  $\varrho$  are energetically unfavorable. Only a transition area between two phases with different values of  $\varrho$  of width  $\mathcal{O}(\epsilon)$  has a positive value of the gradient  $\|\nabla \varrho\|$ .

Periodic system can be achieved by changing the sign of the gradient term to minus. So phase changes are preferred. But this leads to an unbounded energy, since this change generates infinite gradients in  $\varrho$ . To overcome this problem Elder and Grant regularized the functional by introducing the next higher order term  $\|\Delta \varrho\|^2$ . This leads to an energy of the form

$$\mathcal{F}_{\text{PFC}(\text{GL})}[\varrho] = \int -K_1 \|\nabla \varrho\|^2 + K_2 \|\Delta \varrho\|^2 + f(\varrho) \, d\mathbf{x} \quad (2.17)$$

Specification of  $f$  to  $f(\varrho) := (1+r)\varrho + \varrho^3$  makes this energy related to the Swift-Hohenberg energy

in the following way.

By changing the length-scale of (2.12) to  $\mathbf{x} := q_0 \mathbf{r}$  and defining new parameters, a dimensionless form of this energy will be obtained

$$\begin{aligned} r &:= \frac{\alpha \Delta T}{\lambda q_0^4} \quad \dots \text{undercooling} \\ \varrho &:= \psi \sqrt{\frac{g}{\lambda q_0^4}} \quad \dots \text{normed density} \end{aligned} \quad (2.18)$$

This provides the necessity to define a new external potential and velocity field, by

$$\begin{aligned} U(\mathbf{x}, t) &:= \sqrt{\frac{g}{\lambda^3 q_0^{12}}} (k_B T)^{-1} V_1(q_0^{-1} \mathbf{x}, t) \\ \mathbf{u}(\mathbf{x}, t) &:= q_0 \mathbf{u}(q_0^{-1} \mathbf{x}, t) \end{aligned}$$

All derivatives have to be modified, like  $\Delta_{\mathbf{r}} \rightarrow q_0^2 \Delta_{\mathbf{x}}$ . The Swift-Hohenberg-energy can then be written as

$$\frac{\mathcal{F}[\varrho(\mathbf{x}, t)]}{k_B T} = \frac{\lambda^2 q_0^{8-d}}{g} \int \frac{1}{2} \varrho(\mathbf{x}, t) (r + (1 + \Delta_{\mathbf{x}})^2) \varrho(\mathbf{x}, t) + \frac{1}{4} \varrho(\mathbf{x}, t)^4 + \varrho(\mathbf{x}, t) U(\mathbf{x}, t) \, d\mathbf{x} \quad (2.19)$$

This gives, after scaling and partial integration, the Phase-Field Crystal functional  $\mathcal{F}_{\text{PFC(GL)}}$  of Elder and Grant, extended by an external potential.

In the following evolution equation, all derivatives are interpreted with respect to the scaled variable  $\mathbf{x}$ , so the subscript will be dropped. For the variational derivative, the chain-rule has to be considered, as

$$\frac{\delta \mathcal{F}_2[\phi]}{\delta \phi} = \frac{\delta \mathcal{F}_2[\phi]}{\delta \varrho} \frac{\delta \varrho}{\delta \psi} \frac{\delta \psi}{\delta \phi} = \frac{\delta \mathcal{F}[\varrho]}{\delta \varrho} \sqrt{\frac{g}{\lambda q_0^4}}$$

Then the *Phase-Field Crystal equation* with mobility  $M$  follows, by variable transform (2.18)

$$\begin{aligned} \partial_t \varrho(\mathbf{x}, t) + \nabla \cdot (\mathbf{u}(\mathbf{x}, t) \varrho(\mathbf{x}, t)) &= \frac{\bar{\rho} k_B T \lambda q_0^{6-d}}{\gamma} \Delta \mu =: M \Delta \mu \\ \mu &= (r + (1 + \Delta)^2) \varrho(\mathbf{x}, t) + \varrho(\mathbf{x}, t)^3 + U(\mathbf{x}, t) \quad . \end{aligned} \quad (2.20)$$

### Conservation Law

Equation (2.20) shows the structure of a general continuity equation  $\partial_t \varrho + \nabla \cdot \mathbf{j} = 0$ , that is a local form of a *conservation law*. A quantity  $\varrho$  is conserved as it evolves under the flow  $\mathbf{j}$  of a conservation law if the total amount of the substance contained in any fixed volume  $\Omega$  can only change by the

amount that passes through the boundary  $\partial\Omega$  of the domain. For the concrete flux that defines the PFC-equation,  $\mathbf{j} := \varrho \mathbf{u} - M \nabla \mu$ , we find that

$$\frac{d}{dt} \int_{\Omega} \varrho \, d\mathbf{x} = - \int_{\Omega} \nabla \cdot \mathbf{j} \, d\mathbf{x} = \int_{\Omega} \nabla \cdot (M \nabla \mu) - \nabla \cdot (\varrho \mathbf{u}) \, d\mathbf{x} = \int_{\partial\Omega} M \partial_{\mathbf{n}} \mu - \varrho \mathbf{u} \cdot \mathbf{n} \, ds = \int_{\partial\Omega} -\varrho \mathbf{u} \cdot \mathbf{n} \, ds \quad .$$

To obtain conservation of density, the amount of quantity that is transported into the domain must equal the amount that flows out. So the last boundary integral must vanish, i.e. the additional coupling constrained

$$\int_{\partial\Omega} \varrho \mathbf{u} \cdot \mathbf{n} \, ds = 0 \tag{2.21}$$

must be fulfilled.

The complete Phase-Field Crystal problem, including initial and boundary conditions, can be formulated

**Problem 2.** *Let  $\Omega \subset \mathbb{R}^3$ ,  $M > 0$ . Find  $\varrho := \varrho(\mathbf{x}, t)$ ,  $\mu := \mu(\mathbf{x}, t)$  and  $\nu := \nu(\mathbf{x}, t)$  for  $(\mathbf{x}, t) \in \Omega \times (0, T]$  with  $T > 0$  that fulfill the evolution equation*

$$\begin{aligned} \partial_t \varrho + \nabla \cdot (\varrho \mathbf{u}) &= \Delta \mu \\ M^{-1} \mu &= (1+r)\varrho + \varrho^3 + 2\nu + \Delta \nu + U && \text{in } \Omega \\ \nu &= \Delta \varrho \end{aligned} \tag{2.22}$$

*subject to initial and boundary conditions*

$$\begin{aligned} \varrho(\mathbf{x}, 0) &= \varrho_0(\mathbf{x}) && \text{in } \bar{\Omega} \\ \partial_n \varrho(\mathbf{x}, t) = \partial_n \mu(\mathbf{x}, t) = \partial_n \nu(\mathbf{x}, t) &= 0 && \text{in } \partial\Omega \times (0, T] \end{aligned}$$

*with compatibility conditions  $\partial_n|_{\partial\Omega} \varrho_0 = 0$ ,  $\partial_n|_{\partial\Omega} (\Delta \varrho_0) = 0$  and  $\partial_n|_{\partial\Omega} (\Delta^2 \varrho_0) = 0$ .*

### Selection of parameters

In the final form of the PFC model (2.20) there is only one parameter left that describes the general behavior of the system:  $r$ . The mobility  $M$  can be put into the time-scale and is, thus, only responsible for the speed of relaxation/minimization of the energy. To get an idea of a good choice of the parameter  $r$  to simulate specific states of a material, a stability analysis of the equation can be performed. In liquids a constant density profile is expected, since the particles can move more

freely than in a solid state. A steady solution of the differential equation (2.20) has to be stable in the sense that small perturbations of the solution tend to zero. In Appendix B.2 a linear stability analysis of the PFC equation is performed to obtain the relation

$$3\bar{\varrho}^2 + r > 0$$

that is fulfilled when small perturbations of a constant solution  $\bar{\varrho}$  vanish during the evolution. This relation is visualized in figure 2.1.

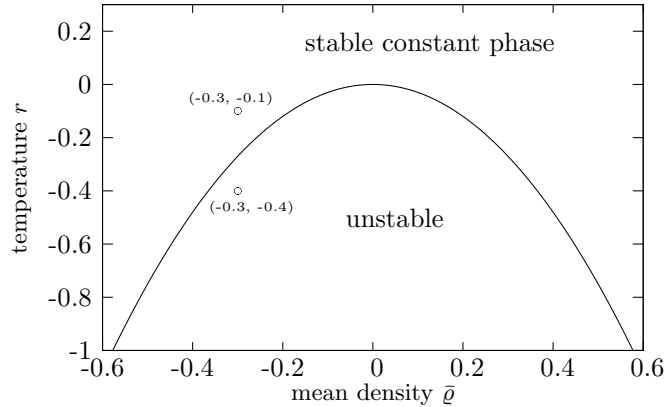


**Figure 2.1:** Stability-diagram depending on the parameters  $\bar{\varrho}$  and  $r$  of the PFC model. The stable regions are called *liquid* and the unstable *solid*.

Using this inequality for the parameters  $\bar{\varrho}$  and  $r$  we take

$$\bar{\varrho} = -0.3, \quad r_{\text{solid}} = -0.4, \quad r_{\text{liquid}} = -0.1$$

as parameters for the simulations. The solid state describes crystallization/solidification of colloidal crystals and is analyzed in [BRV07, vTBVL09, CW08] among many others. In figure 2.2 a sequence of snapshot of such a simulation is shown. The final state is a hexagonal configuration of maxima in the density profile, that can be interpreted as the positions of the individual particles.

An appropriate initial value for Problem P2 can be a perturbation around the mean density  $\bar{\varrho}$ , that is a conserved quantity and stays fixed during the evolution. For solved particles the temperature parameter for liquid  $r_{\text{liquid}}$  is convenient and without obstacles or walls, that change the behavior of the system, we would get a constant density field. Including an external potential that models obstacles, like big colloidal particles in the solution of small particles, will lead to qualitatively other density profiles. First simulations using density-functional theory, or for non-interacting particles a

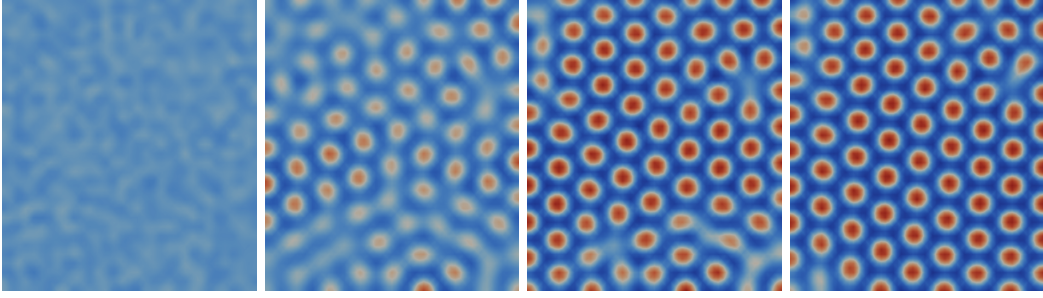


**Figure 2.2:** Solidification of particle density profile, using parameters  $\bar{\varrho} = -0.3$  and  $r = -0.4$ , at different simulation times, starting from perturbed constant density. Result is a hexagonal pattern, where the maxima (red) indicate positions of particles.

diffusion model, were performed by [PDT03, PRDK07], for example.

## 2.2 Colloids in polymer solution

Polymer coils and colloids are assumed to swim in a bath of Brownian particles that collide randomly and are transported by a flow-field  $\mathbf{u}$ . This leads to the transportation of big particles. In comparison to the colloids the polymer coils are rather small. This is the reason why we assume that the latter do not interact via hydrodynamic forces. However, the colloids do effect the flow-field. If the colloids

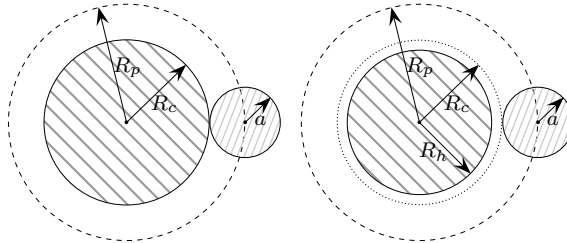


**Figure 2.3:** Left: hard colloidal particle, right: slightly soft colloidal particle, with the hydrodynamic interaction radius  $R_h$  smaller than  $R_c = R_p - a$ .

were soft particles, the interaction with the flowing solvent would be active in a region defined by a hydrodynamic interaction radius  $R_h$  only. The polymer coils, with interaction radius  $a$ , can approach the colloidal particles up to a distance  $R_p$  and the colloids themselves have a radius of  $R_c$ . Hard colloidal particles are characterized by  $R_h = R_c$ . In figure 2.3 the interaction radii for two different systems are plotted.

The interaction of colloids and polymer coils is modeled by an external potential of the general



form

$$U(\mathbf{x}) = C_1 \cdot \exp\left(-\frac{\|\mathbf{x}\|^p}{C_2^p}\right) \quad (2.23)$$

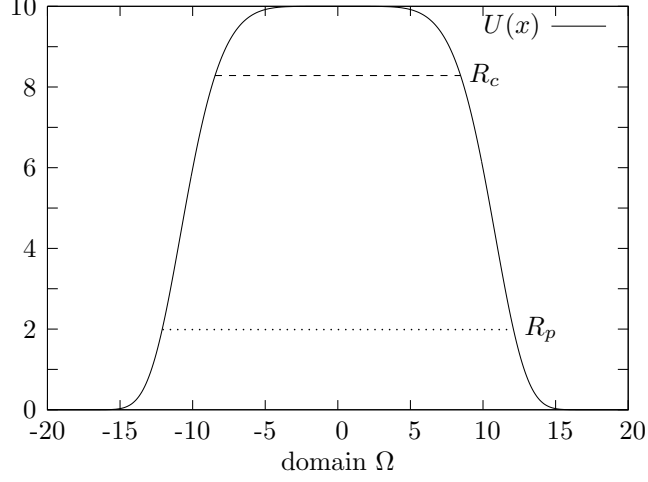


**Figure 2.4:** Plot of 1d potential function  $U(\mathbf{x})$  for  $R^* = 0.7$

with parameters  $C_1, C_2$  and  $p$  subject to a specific interaction model (e.g. (ultra-)soft interaction, hard interaction). These parameters should be chosen in such a way that the limit  $R_c = R_h$  defines a hard sphere interaction potential

$$U_{\text{HS}}(\mathbf{x}) = \begin{cases} \infty & \text{for } \|\mathbf{x}\| \leq R_c \\ 0 & \text{otherwise} \end{cases} .$$

Furthermore the slope of  $U$  in the interval  $[R_c, R_p]$  should be approximately independent of the colloid radius  $R_c$ . To obtain such parameters the following conditions were introduced, depending on a "hardness" function  $f$  that is up to some constraints arbitrary.  $C_2$  and  $p$  should be determined so that

$$U(x; \|\mathbf{x}\| = R_p) = f(R_c, R_h)$$

$$U(x; \|\mathbf{x}\| = R_c) = C_1 - f(R_c, R_h)$$

is fulfilled. Hardness  $f$  must be chosen so that it is monotone in both of its arguments and

$$f(R_c, R_h = R_c) = 0 \quad \text{and} \quad f(R_c, R_h < R_c) \in (0, C_3]$$

for some scaling factor  $C_3 > 0$ . A simple choice of  $f$  that we have used to model hard and soft colloidal interactions can be written as a linear relation

$$f(R_c, R_h) = C_3 \left(1 - \frac{R_c}{R_h}\right) \quad .$$

The limit  $R_c = R_h$  that results in an hard interaction potential will be obtained by defining  $C_1$  by  $C_1 := \frac{C_4}{f(R_c, R_h)}$ . In our model the new parameters  $C_3$  and  $C_4$  were chosen as  $C_3 = 10$  and  $C_4 = 20$ . Now we can calculate values for  $C_2$  and  $p$ , assuming  $R_h < R_c$ , with

$$p = \ln \left[ \ln \left( \frac{f(R_c, R_h)^2}{C_4} \right) / \ln \left( \frac{(C_4 - f(R_c, R_h)^2)}{C_4} \right) \right] / \ln \left[ \frac{R_p}{R_c} \right]$$

$$C_2 = R_p \left[ -\ln \left( \frac{f(R_c, R_h)^2}{C_4} \right) \right]^{-\frac{1}{p}} \quad .$$

By the fraction  $\frac{R_p}{R_c} =: R^*$  a characteristic length is set. This is used by the authors of [PRDK07].

More than one colloid with potential  $U_i$  that interacts with the particles in the environment can simply be superposed to get the entire external potential, by

$$U(\mathbf{x}) = \sum_i U_i(\mathbf{x}) \quad .$$

Colloids act as hard spherical obstacles with radius  $R_h$  in the flow-field. For these objects no-slip boundary conditions were used to avoid flow into the colloids. Each colloid  $i$  is a part of the simulation domain  $\Omega$ , called  $\Omega_{c_i} \subset \Omega$ , with  $\bigcap_i \Omega_{c_i} = \emptyset$  and  $\bigcup_i \Omega_{c_i} =: \Omega_c$ . Because of some numerical reasons we assume, that  $\partial\Omega_c \cap \partial\Omega = \emptyset$ .

### 2.2.1 Moving colloids

The colloids immersed in an aqueous solution move due to different local and global forces. In chapter 2.1 an equation of motion was derived for small colloidal particles. Since thermal fluctuation induce small oscillations of the particles, equation (2.2) describes the Brownian motion. If we assume that the colloidal particles are bigger than the particles in the solvent, i.e. the diameter in the range of  $100nm - 10\mu m$ , then the random fluctuations can be neglected and the particles move due to inter-particle interactions, global potential fields or transport in a flow, only with an equation of motion, that can be derived from (2.2) by crossing out some terms:

$$\gamma \partial_t \mathbf{r}_i = F_i(\vec{\mathbf{r}}, t) \quad . \tag{2.24}$$

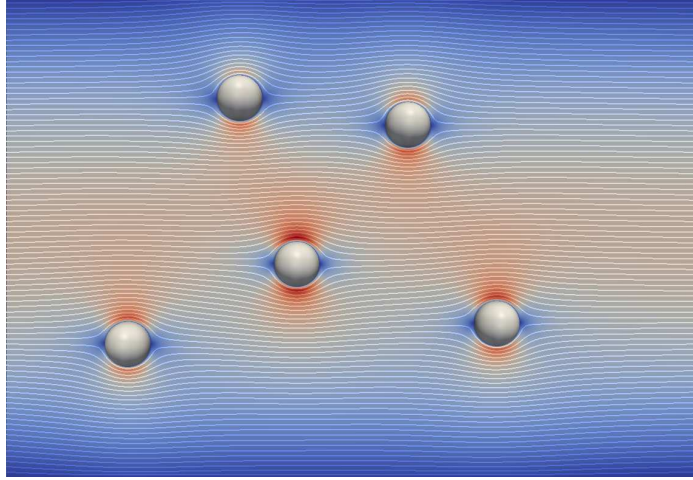


**Figure 2.5:** Five colloidal particles in a flow field. The fluid flows from left to right with a parabolic inflow profile with maximum in the center of the left side of the simulation box. Very low Reynolds numbers do not lead to turbulence behind the colloids. Top and bottom boundary of simulation box are physical boundaries with no-slip boundary condition.

For more than one colloid the external potentials are positioned with respect to  $\mathbf{r}_i$ , i.e.  $U_i(\mathbf{x}, t) = U(\mathbf{x} - \mathbf{r}_i(t))$ . The equation of motion for this potential function can be written as

$$\partial_t U_i(\mathbf{x}, t) = -\nabla U_i(\mathbf{x}, t) \cdot \partial_t \mathbf{r}(t) \quad .$$

# Chapter 3

## Numerics

### 3.1 Description of complex geometries

For a long time different methods to describe geometries in two or three dimensions have been known. One main difficulty is the representation of the domain of interest in a discrete way, e.g. by triangulation. Further difficulties arise when the domain is allowed to evolve in time, move, shrink or expand and sometimes change its topology, i.e. collapse or merge. In the most simple case the translation of the domain is the only aspect considered. Let  $\Omega_0(t)$  be a domain in  $\mathbb{R}^d$  at time  $t$  and  $\mathbf{x} \in \Omega_0$ , then

$$\partial_t \mathbf{x} = \mathbf{y}, \quad \text{with } \mathbf{x}(t=0) = \mathbf{x}_0 \quad \Rightarrow \quad \partial_t \Omega_0 = \mathbf{y}, \quad \text{with } \Omega_0(t=0) = \Omega_0^0$$

where  $\mathbf{y}$  the velocity of  $\Omega_0$ , that is constant in the whole domain. This situation can be handled by the following methods by translation of the coordinate system.

The aim of this section is to introduce and compare several methods that can describe  $N$  colloids as macroscopic objects in a bounded finite size simulation box (see figure 3.1 for a box with one colloid modeled as a circular object). If there is one colloid it would be sufficient to translate a domain only. However, if we deal with more than one colloid, more complex methods are needed.

#### 3.1.1 Explicit triangulations

The standard approach decomposes a polygonal domain into simple elements, like triangles or quadruples. Curved boundaries can be replaced by polygonal chains or must be handled by curved triangles and parametrization of the boundary curves. In two dimensions this gives quite reason-

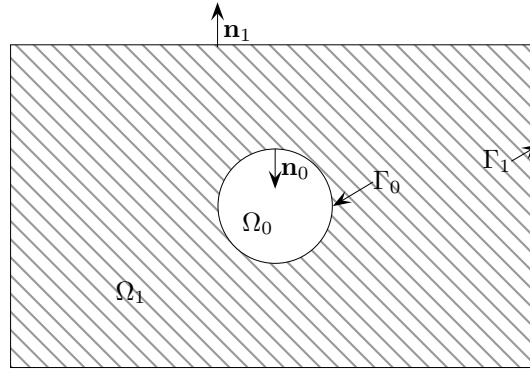


**Figure 3.1:**  $\Omega_0$  and  $\Omega_1$  are embedded in simpler domain  $\Omega := \Omega_0 \cup \Omega_1$  with boundary  $\partial\Omega = \Gamma_1$ . Normal vectors  $\mathbf{n}_0$  and  $\mathbf{n}_1$  on the boundaries  $\Gamma_0$  and  $\Gamma_1$  point out of the domain  $\Omega_1$ .

able results. An example of such a triangulation of a rectangular domain with circular hole that is approximated by a polygonal chain can be seen in figure 3.2. A polygonal chain that approximates

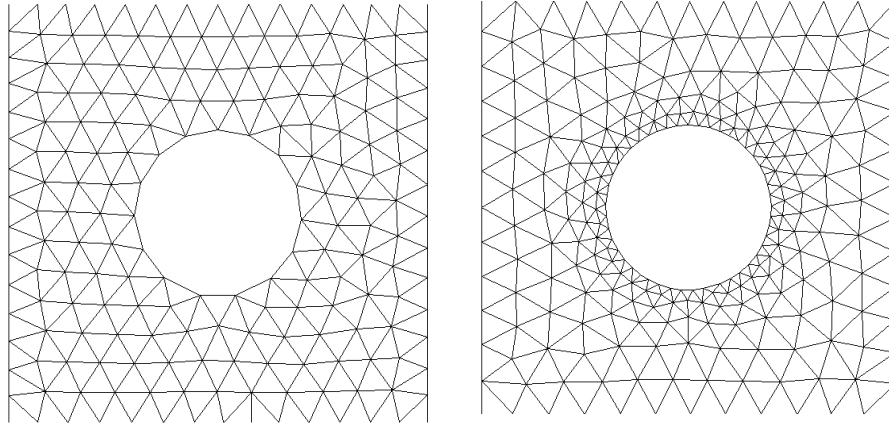


**Figure 3.2:** Left: coarse mesh with nearly equal sized elements, right: mesh refined on the boundary of the circular hole.

the boundary very closely can be achieved by the refinement of the mesh around this boundary. The appropriate triangulation can be obtained in two dimensions by mesh relaxation, for instance. Per-Olof Persson and Gilbert Strang [PS04] have written a simple mesh generator in MATLAB that produced the two shown examples in figure 3.2.

Motion of the domain  $\Omega_0$  translates into the motion of the boundary  $\Gamma_0$ . The polygonal chain that describes this boundary changes and thus, re-meshing or relaxing of the mesh are necessary. Shrinking or expanding boundaries need re-parametrization and topological changes often need a complete new build-up of data structures and management of several separate boundaries that can be merged or broken up again. So moving boundaries are rather difficult to implement. If this was

done, it would give a method that only needs triangulation points inside the domain of interest and thus the algebraic systems would be small accordingly.

### 3.1.2 Levelset method

In 1988 Osher and Sethian proposed [OS88] a method for front-propagation called *Levelset-method* that found many applications in image processing and two-phase flows in recent years. It is an implicit sharp interface approach where the boundary of the geometry  $\Omega_0$  is treated as a levelset of a function  $\phi : \mathbb{R}^d \rightarrow \mathbb{R}$ , commonly the zero levelset. The levelset-function  $\phi$  is embedded in a domain  $\Omega$  and will be propagated during the evolution of the interface of  $\Omega_0$  by a simple transport-equation

$$\partial_t \phi + \mathbf{u} \cdot \nabla \phi = 0 \quad .$$

An implicit description of domains, which is often used, is a signed distance-function, that has some convenient properties concerning the extraction of the zero-levelset, for example.

**Definition 3.1.1.** A function  $\mathfrak{d} : \mathbb{R}^d \rightarrow \mathbb{R}$  is called *signed distance-function* for a domain  $\Omega_0 \subset \mathbb{R}^d$  if it is a distance-function, i.e.  $|\mathfrak{d}(x)| := \text{dist}(x, \Omega_0)$  with signum

$$\text{sign}[\mathfrak{d}(x)] = \begin{cases} 1 & \text{if } x \notin \Omega_0 \\ 0 & \text{if } x \in \partial\Omega_0 \\ -1 & \text{if } x \in \Omega_0 \end{cases} \quad .$$

In [SS03] an example is given for using the levelset-method in two-phase-flow problems. The main idea is to replace normal vectors and delta-functions in the boundary conditions in terms of the levelset-function  $\phi$ . Smearred out delta-functions can be expressed as

$$\delta_\epsilon(\mathbf{x}) := \begin{cases} \frac{1}{2\epsilon} (1 + \cos(\pi\phi(\mathbf{x})/\epsilon)) & \text{for } -\epsilon \leq \phi(\mathbf{x}) \leq \epsilon \\ 0 & \text{otherwise} \end{cases}$$

where  $\epsilon$  is a small parameter that defines the width of the smeared out region of the delta-function. In a similar manner the characteristic function that represents the domain  $\Omega_0$  can be smeared out,

e.g. by

$$\chi_\epsilon(\mathbf{x}) := \begin{cases} 0 & \text{if } \phi(\mathbf{x}) < -\epsilon \\ \frac{1}{2}\left(1 + \frac{\phi(\mathbf{x})}{\epsilon} + \frac{1}{\pi} \sin(\pi\phi(\mathbf{x})/\epsilon)\right) & \text{if } -\epsilon \leq \phi(\mathbf{x}) \leq \epsilon \\ 1 & \text{if } \phi(\mathbf{x}) > \epsilon \end{cases} . \quad (3.1)$$

For the normal vector and the mean curvature of the levelset curve a direct representation with the implicit function  $\phi$  can be written as

$$\mathbf{n} := \frac{\nabla\phi}{\|\nabla\phi\|}, \quad \kappa := \nabla \cdot \frac{\nabla\phi}{\|\nabla\phi\|} .$$

The advantages of levelset-methods include the ability to compute geometric properties of the domain  $\Omega_0$  easily. The extension to higher dimensions can be done without many difficulties. A main advantage in comparison to explicit geometric descriptions and parametrization of the boundary is the possibility to allow topological changes without any extra carefulness in implementation.

Since one is interested in the signed distance values, some careful strategies are necessary to preserve the distance property and often a re-distancing step and some smoothing of norms are inevitable. These are some disadvantages of the methods that can be worked out but produce a higher computational effort.

### 3.1.3 Phase-Field method

The Phase-Field approach takes a quite similar way. Domains will be defined implicitly by a signed distance-functions  $\mathfrak{d}(x)$  like in the levelset-method. Nevertheless we are not interested in the distance property but in the sign of the distance-function. The main ingredient to phase-field methods is a smeared out characteristic function that can be transformed and transported during the evolution of the domain.

**Definition 3.1.2.** Let  $\epsilon > 0$  and  $\Omega_0 \subset \Omega$  a domain in  $\mathbb{R}^d$ , that can be described by a signed distance-function  $\mathfrak{d}$  with sign so that  $\mathfrak{d}(x) < 0 \Leftrightarrow x \in \Omega_0$ . Then the function

$$\varphi_\epsilon(x) := \frac{1}{2}(1 - \tanh(3\mathfrak{d}(x)/\epsilon)) \quad (3.2)$$

will be called *phase-field function*.

The phase-field function can be compared to the smeared out characteristic function of the

levelset-framework (3.1). Similar to the levelset-method one can derive approximations of the delta-

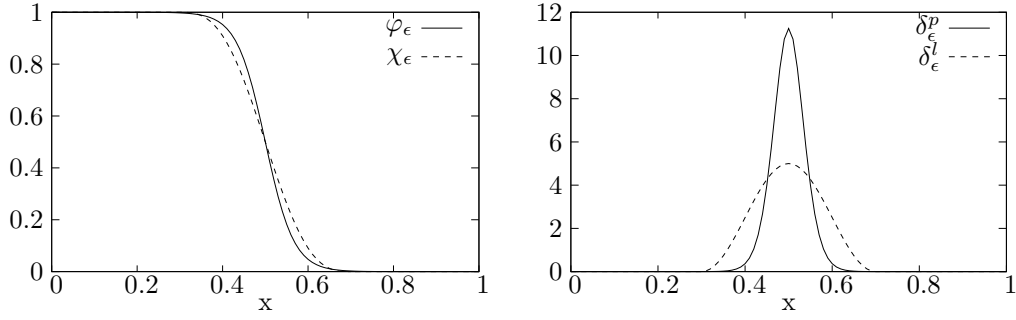


**Figure 3.3:** Left: Comparison of phase-field function to smeared out characteristic function of levelset-method, right: delta-function  $\delta_\epsilon^l$  of levelset-method and delta-function  $\delta_\epsilon^p$  of phase-field method.

function from the phase-field variable  $\varphi$

$$\delta(\mathbf{x}) = \lim_{\epsilon \rightarrow 0} \|\nabla \varphi_\epsilon(\mathbf{x})\| = \lim_{\epsilon \rightarrow 0} \epsilon^{-1} B(\varphi_\epsilon), \quad \text{with } B(\varphi) := C\varphi^2(1-\varphi)^2$$

where  $B(\varphi)$  is called *double-well* of  $\varphi$  and  $C = 36$  is a scaling-factor depending on the scaling of  $\mathbf{x}$  in the tanh-function. These approximations are indeed nascent delta-functions as defined in definition 1.2.2. In figure 3.4 the phase-field function and delta-function approximation are plotted using the double-well for different band-widths  $\epsilon$ .

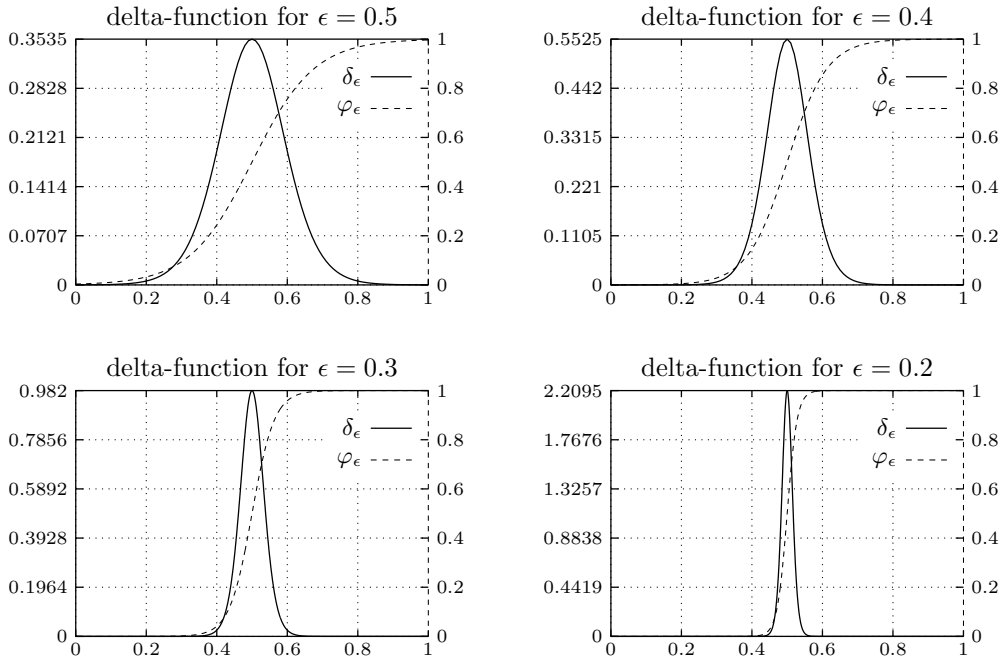


**Figure 3.4:** Phase-field  $\varphi_\epsilon$  and delta-function approximation  $\delta_\epsilon := \sim B(\varphi_\epsilon)$  for different values of  $\epsilon$  in the interval  $\mathbf{x} \in [0, 1]$



Since the domain  $\Omega_1$  is not discretized explicitly but embedded in a bigger domain  $\Omega$ , the complete domain must be discretized and thus, a local refinement is necessary to preserve computational resources. It is also necessary to solve the  $\epsilon$ -band around the interface very finely. In the domain  $\Omega_1$  the discretization needs to solve the PFC-solution. Outside  $\Omega_1$ , in the domain  $\Omega_0$ , a coarse discretization is sufficient. Figure 3.5 shows an example of a discretization of a domain where a spherical obstacle is included in the center of the box.

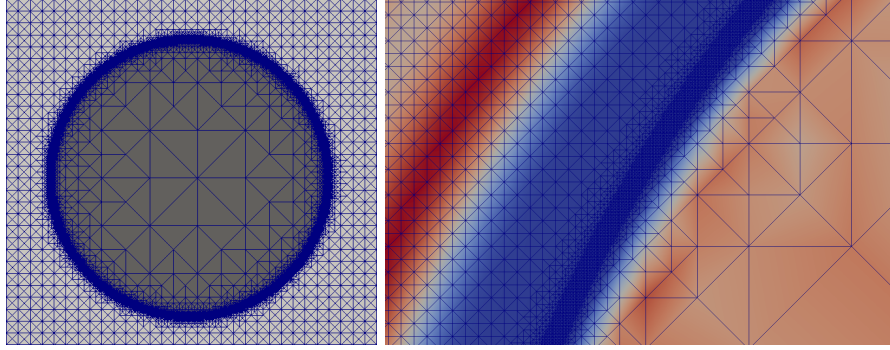


**Figure 3.5:** Mesh used to discretize spherical obstacle. Number of points: 320729, number of elements: 639408. The width of the  $\epsilon$ -band around the phase-change is discretized by approximately 10 degrees of freedom and in the region  $\Omega_1$  a grid-size of approximately  $h = \frac{a}{5}$ , where  $a$  is the half distance of particles in the solvent. The domain  $\Omega_0$ , the interior of the obstacle, is discretized as coarse as possible, since this region has no contribution to the solution of the differential equations.

*Remark.* The phase-field function that separates two domains is highly related to a stationary solution of the Cahn-Hilliard equation

$$\partial_t c = \Delta \left( \frac{1}{\epsilon} W(c) - \epsilon \Delta c \right)$$

that minimizes the Cahn-Hilliard energy similar to (2.16).  $c$  describes a concentration field and  $W$  a double-well. The evolution produces separated regions with constant concentration and transition areas of width proportional to  $\epsilon$ . In figure 3.6 a stationary solution of a Cahn-Hilliard evolution is compared to the tanh function, that is the base for the phase-field approach.

## 3.2 Diffuse-Domain approach

Solutions of evolution equations in complex geometries with standard types of boundary conditions, i.e. Dirichlet, Neumann and Robin boundary conditions, and diffuse description of the domains by phase-field functions was described by the authors of [LLVAR09]. The base of their approach is a modification of a partial differential equation using characteristic and delta functions to include the

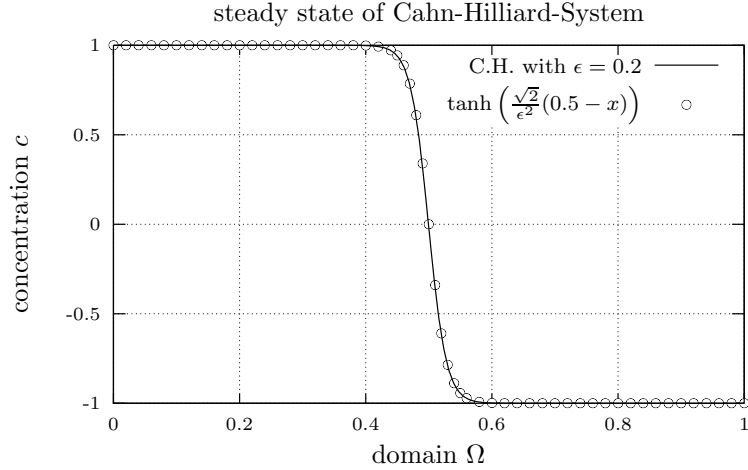


**Figure 3.6:** A numerically solved Cahn-Hilliard equation in 1d is compared to a tanh-function.

boundary conditions in the equations and to extend the equations to a bigger, simpler domain. The second step is an approximation of the characteristic function by a phase-field function and of the delta function by a double-well or an other nascent delta-function. To conclude that the approximated equations tend to the sharp ones for the diffuseness parameter  $\epsilon$  tend to zero, asymptotic analysis is performed. This method is based on the matching of outer and inner expansions. A detailed description can be found in [Emm03].

The considered domain  $\Omega_1$  of the PDEs in [LLVAR09] has the property to be embedded strictly in the bigger domain  $\Omega$ , i.e.  $\Omega_1 \subsetneq \Omega$  and  $\partial\Omega_1 \cap \partial\Omega = \emptyset$ , and thus, the boundary of  $\Omega$  and boundary conditions to  $\partial\Omega$  do not influence the solution of embedded PDEs. In the case of colloids in the simulation domain, that are cut out of  $\Omega$ , this property does not hold any more. So the derivation of the equations for the inclusion of boundary conditions must be changed slightly. It turns out that the resulting equations are in fact the same as in the original ones but, in addition, the boundary conditions to  $\partial\Omega$  must be set to the one of  $\partial\Omega_1 \cap \partial\Omega = \Gamma_1$ . The derivation of these equations are performed here.

A general parabolic partial differential equation of second order is considered for the derivation of the diffuse domain method:

$$H\partial_t y - \nabla \cdot (A\nabla y) + (b \cdot \nabla)y + cy = f, \quad \text{in } \Omega_1(t) \quad (3.3)$$

with  $H \in \mathbb{R}_{\geq 0}$  a positive constant,  $A = A(\mathbf{x}, t, y, \nabla y) \in \mathbb{R}^{d \times d}$  a positive definite matrix function,  $b = b(\mathbf{x}, t, y, \nabla y) \in \mathbb{R}^d$  a vector function,  $c = c(\mathbf{x}, t, y, \nabla y) \in \mathbb{R}$  and  $f = f(\mathbf{x}, t)$ . The equation

is considered with respect to boundary conditions on  $\Gamma_{0/1}(t)$ , not necessary the same on both boundaries. For  $i \in \{0, 1\}$

a) Dirichlet boundary condition

$$y = g, \quad \text{on } \Gamma_i(t) \quad (3.4)$$

b) Neumann boundary condition

$$A\nabla y \cdot \mathbf{n}_i - HyV_{n_i} = g, \quad \text{on } \Gamma_i(t) \quad (3.5)$$

where  $V_{n_i}$  is the normal velocity of  $\Gamma_i(t)$  pointing in the direction of  $\mathbf{n}_i$

c) Robin boundary condition

$$A\nabla y \cdot \mathbf{n}_i - HyV_{n_i} = k(y - g), \quad \text{on } \Gamma_i(t) \quad (3.6)$$

for  $k \in \mathbb{R}$

Multiplying equation (3.3) by a time and space dependent test function  $\vartheta(\mathbf{x}, t)$  and integrating over  $\Omega_1(t)$  and over the time interval  $[0, T]$  the weak form of the equation can be obtained

$$\int_0^T \int_{\Omega_1(t)} Hy\vartheta \partial_t y \, d\mathbf{x}dt + \int_0^T \int_{\Omega_1(t)} \{-\nabla \cdot (A\nabla y) + b \cdot \nabla y + cy\} \vartheta \, d\mathbf{x}dt = \int_0^T \int_{\Omega_1(t)} f\vartheta \, d\mathbf{x}dt \quad (3.7)$$

In the following some identities are used. We assume that the domain  $\Omega$  is fixed but  $\Omega_0$  can change in time, so  $V_{n_1} = 0$

$$\begin{aligned} \nabla \chi_{\Omega_1} &= -\delta_{\partial\Omega_1} \mathbf{n} = -(\delta_{\Gamma_0} \mathbf{n}_0 + \delta_{\Gamma_1} \mathbf{n}_1) \\ \frac{d\chi_{\Omega_1}}{dt} &= \nabla \chi_{\Omega_1} \dot{\mathbf{x}} = -\delta_{\Gamma_0} \mathbf{n}_0 V = -\delta_{\Gamma_0} V_{n_0} \quad . \end{aligned} \quad (3.8)$$

Partial integration of (3.7) in time can be done, using

$$\begin{aligned} \int_0^T \int_{\Omega_1(t)} \vartheta \partial_t y + y \partial_t \vartheta \, d\mathbf{x}dt &= \int_0^T \int_{\Omega_1(t)} \partial_t (y\vartheta) \, d\mathbf{x}dt = \int_0^T \int_{\Omega} \partial_t (y\vartheta) \chi_{\Omega_1(t)} \, d\mathbf{x}dt \\ &= \int_0^T \int_{\Omega} y\vartheta \delta_{\Gamma_0(t)} V_{n_0} \, d\mathbf{x}dt + \left[ \int_{\Omega} y(t)\vartheta(t) \chi_{\Omega_1(t)} \, d\mathbf{x} \right]_{t=0}^T \\ &= \int_0^T \int_{\Gamma_0(t)} y\vartheta V_{n_0} \, dsdt + \left[ \int_{\Omega_1(t)} y(t)\vartheta(t) \, d\mathbf{x} \right]_{t=0}^T \quad . \end{aligned}$$

Since in the final PFC and Navier-Stokes equations only Dirichlet and Neumann boundary conditions are considered, the derivation of embedded formulas can be restricted to these two cases. Robin boundary conditions can be included in a similar manner.

a) For Neumann boundary conditions we consider

$$[(A\nabla y) \cdot \mathbf{n}_0 - HyV_{n_0}]|_{\Gamma_0} = g \quad \text{and} \quad [(A\nabla y) \cdot \mathbf{n}_1]|_{\Gamma_1} = h \quad .$$

Partial integration in space and time of (3.7) leads to

$$\begin{aligned} & - \int_0^T \int_{\Omega_1(t)} Hy \partial_t \vartheta \, d\mathbf{x} dt + \int_0^T \int_{\Omega_1(t)} \nabla \vartheta \cdot (A\nabla y) \, d\mathbf{x} dt + \int_0^T \int_{\Omega_1(t)} \{b \cdot \nabla y + cy - f\} \vartheta \, d\mathbf{x} dt \\ &= \int_0^T \int_{\Gamma_0(t)} \underbrace{[(A\nabla y) \cdot \mathbf{n}_0 - HyV_{n_0}]}_g \vartheta \, ds dt + \int_0^T \int_{\Gamma_1} \underbrace{(A\nabla y) \cdot \mathbf{n}_1}_h \vartheta \, ds dt - \left[ \int_{\Omega_1(t)} y(t) \vartheta(t) \, d\mathbf{x} \right]_{t=0}^T . \end{aligned}$$

Replacing integration in the domain  $\int_{\Omega_1}$  by  $\int_{\Omega} \chi_{\Omega_1}$  and on the boundary  $\int_{\Gamma}$  by  $\int_{\Omega} \delta_{\Gamma}$  gives

$$\begin{aligned} & - \int_0^T \int_{\Omega} H \chi_{\Omega_1(t)} y \partial_t \vartheta \, d\mathbf{x} dt + \int_0^T \int_{\Omega} \chi_{\Omega_1(t)} \nabla \vartheta \cdot (A\nabla y) \, d\mathbf{x} dt + \int_0^T \int_{\Omega} \chi_{\Omega_1(t)} \{b \cdot \nabla y + cy - f\} \vartheta \, d\mathbf{x} dt \\ & \quad - \int_0^T \int_{\Omega} \delta_{\Gamma_0(t)} g \vartheta \, d\mathbf{x} dt = \int_0^T \int_{\Gamma_1} h \vartheta \, ds dt - \left[ \int_{\Omega_1(t)} y(t) \vartheta(t) \, d\mathbf{x} \right]_{t=0}^T . \end{aligned}$$

Again partial integration in space and time leads to

$$\begin{aligned} & \int_0^T \int_{\Omega} H \vartheta \partial_t (\chi_{\Omega_1(t)} y) \, d\mathbf{x} dt - \int_0^T \int_{\Omega} \vartheta \nabla \cdot (\chi_{\Omega_1(t)} A\nabla y) \, d\mathbf{x} dt + \int_0^T \int_{\Omega} \chi_{\Omega_1(t)} \{b \cdot \nabla y + cy - f\} \vartheta \, d\mathbf{x} dt \\ & \quad - \int_0^T \int_{\Omega} \delta_{\Gamma_0(t)} g \vartheta \, d\mathbf{x} dt = - \int_0^T \int_{\Gamma_1} \underbrace{\chi_{\Omega_1(t)}}_{=1 \text{ on } \Gamma_1} h \vartheta \, ds dt + \int_0^T \int_{\Gamma_1} h \vartheta \, ds dt . \end{aligned}$$

This integral equation is equivalent to the strong formulation

$$H \partial_t (\chi_{\Omega_1(t)} y) - \nabla \cdot (\chi_{\Omega_1(t)} A\nabla y) + \chi_{\Omega_1(t)} \{b \cdot \nabla y + cy\} - \delta_{\Gamma_0(t)} g = \chi_{\Omega_1(t)} f \quad \text{s.t.} \quad [(A\nabla y) \cdot \mathbf{n}_1]|_{\Gamma_1} = h \quad (3.9)$$

that has to be understood in the sense of distributions.

b) Dirichlet boundary conditions  $y|_{\Gamma_0} = g$ ,  $y|_{\Gamma_1} = h$  can be included in the same manner. The following derivation only considers the Laplace term, since the time derivative and first/zero order terms are not related to these boundary conditions. The time-dependency of the domain will be ignored in this derivation, too. Consider the weak form of the Poisson equation  $\Delta v = f$  in  $\Omega_1$  and

perform partial integration twice:

$$\begin{aligned}
& \int_{\Omega_1} \vartheta \Delta y \, d\mathbf{x} = \int_{\Omega_1} \vartheta f \, d\mathbf{x} \\
& \int_{\Omega_1} \Delta \vartheta y \, d\mathbf{x} + \int_{\Gamma_0} \vartheta \partial_{\mathbf{n}_0} y - g \partial_{\mathbf{n}_0} \vartheta \, ds + \int_{\Gamma_1} \vartheta \partial_{\mathbf{n}_1} y - h \partial_{\mathbf{n}_1} \vartheta \, ds = \int_{\Omega_1} \vartheta f \, d\mathbf{x} \\
& \underbrace{\int_{\Omega} \chi_{\Omega_1} \Delta \vartheta y + \delta_{\Gamma_0} (\vartheta \partial_{\mathbf{n}_0} y - g \partial_{\mathbf{n}_0} \vartheta) \, d\mathbf{x}}_A + \int_{\Gamma_1} \vartheta \partial_{\mathbf{n}_1} y - h \partial_{\mathbf{n}_1} \vartheta \, ds = \int_{\Omega} \chi_{\Omega_1} \vartheta f \, d\mathbf{x} \quad .
\end{aligned}$$

Further calculations lead to

$$\begin{aligned}
A &= - \underbrace{\int_{\Omega} \nabla(\chi_{\Omega_1} y) \cdot \nabla \vartheta \, d\mathbf{x}}_B + \int_{\Gamma_1} \chi_{\Omega_1} h \partial_{\mathbf{n}_1} \vartheta \, ds \\
B &= \int_{\Omega} \Delta(\chi_{\Omega_1} y) \vartheta \, d\mathbf{x} - \int_{\Gamma_1} \vartheta \partial_{\mathbf{n}_1} (\chi_{\Omega_1} y) \, ds \quad .
\end{aligned}$$

With  $\partial_{\mathbf{n}_1} \chi_{\Omega_1}|_{\Gamma_1} = 0$  and  $\chi_{\Omega_1}|_{\Gamma_1} = 1$ , we get the equation

$$\int_{\Omega} \Delta(\chi_{\Omega_1} y) \vartheta + \delta_{\Gamma_0} (\vartheta \partial_{\mathbf{n}_0} y - g \partial_{\mathbf{n}_0} \vartheta) \, d\mathbf{x} = \int_{\Omega} \chi_{\Omega_1} \vartheta f \, d\mathbf{x} \quad .$$

Splitting the Laplace term in  $\Delta(\chi_{\Omega_1} y) = \nabla \chi_{\Omega_1} \cdot \nabla y + y \Delta \chi_{\Omega_1} + \nabla \cdot (\chi_{\Omega_1} \nabla y)$ , using (3.8) and assuming  $\partial_{\mathbf{n}_0} g|_{\Gamma_0} = 0$  gives two replacements for the boundary-terms

$$\begin{aligned}
\int_{\Omega} \vartheta \nabla \chi_{\Omega_1} \cdot \nabla y \, d\mathbf{x} &= - \int_{\Omega} \vartheta \delta_{\Gamma_0} \partial_{\mathbf{n}_0} y \, d\mathbf{x} \\
\int_{\Omega} \vartheta g \Delta \chi_{\Omega_1} \, d\mathbf{x} &= \int_{\Omega} \partial_{\mathbf{n}_0} (\vartheta g) \delta_{\Gamma_0} \, d\mathbf{x} - \underbrace{\int_{\Gamma_1} \vartheta g \delta_{\Gamma_0}}_{=0 \text{ since } \Gamma_0 \cap \Gamma_1 = \emptyset} \\
&= \int_{\Omega} \delta_{\Gamma_0} g \partial_{\mathbf{n}_0} \vartheta \, d\mathbf{x} \quad .
\end{aligned}$$

In the conclusion this leads us to the associated strong formulation

$$\nabla \cdot (\chi_{\Omega_1} \nabla y) + (y - g) \Delta \chi_{\Omega_1} = \chi_{\Omega_1} f, \quad \text{s.t. } y|_{\Gamma_1} = h \quad . \quad (3.10)$$

The inclusion of time-derivatives and first/zero order terms leads to a formula similar to (3.9) where the boundary term  $\delta_{\Gamma_0} g$  is replaced by  $(y - g) \Delta \chi_{\Omega_1}$ .

Replacing  $\chi_{\Omega_1}$  by the phase-field function  $\varphi_\epsilon$  and  $\delta_{\Gamma_0}$  by  $\delta_\epsilon$  gives the approximation of (3.9) and (3.10). Boundary terms like  $(y - g) \Delta \chi_{\Omega_1}$  or  $\delta_{\Gamma_0} g$  are inserted in the abstract expression  $BC$ , that

is used to encapsulate all kinds of boundary conditions.

$$\begin{aligned}
H\partial_t(\varphi_\epsilon y) - \nabla \cdot (\varphi_\epsilon A \nabla y) + \varphi_\epsilon b \cdot \nabla y + \varphi_\epsilon c y + BC &= \varphi_\epsilon f \quad \text{in } \Omega \\
\text{s.t. } [(A \nabla y) \cdot \mathbf{n}_1]_{|\Gamma_1} &= h \quad \text{or} \quad y|_{\Gamma_1} = h \quad .
\end{aligned} \tag{3.11}$$

In [LLVAR09] other forms of  $BC$  than the one we obtained above are described and justified by asymptotic analysis. Especially the inclusion of Dirichlet boundary conditions by  $(y - g)\Delta\chi_{\Omega_1}$  appears to be numerically very unstable and unfavorable. The authors proposed some penalty terms to force the solution to fulfill the Dirichlet boundary conditions. In table 3.1 some of the boundary terms used are listed. Using (3.11) and boundary conditions in table 3.1 we can rewrite

Dirichlet boundary conditions		$BC = \epsilon^{-3}(1 - \varphi_\epsilon)(y - g)$
Neumann boundary conditions		$BC = -\epsilon g \ \nabla \varphi_\epsilon\ ^2$
Robin boundary conditions		$BC = -\epsilon k(y - g)\ \nabla \varphi_\epsilon\ ^2$

**Table 3.1:** Boundary terms for the diffuse domain method

the PFC equations (2.20) in terms of the diffuse domain approach. The boundary conditions  $\partial_{\mathbf{n}}\varrho = 0$ ,  $\partial_{\mathbf{n}}\mu = 0$  and  $\partial_{\mathbf{n}}\nu = 0$  produce no boundary term, since  $g$  and  $h$  can be set to zero. We arrive at the diffuse domain Phase-Field Crystal model:

**Problem 3.** *PFC problem: Let  $\Omega \subset \mathbb{R}^d$ ,  $M > 0$  and  $\varphi_\epsilon$  described by (3.2) for  $\epsilon > 0$  sufficiently small,  $r > -1$ . Find  $\varrho := \varrho(\mathbf{x}, t)$ ,  $\mu := \mu(\mathbf{x}, t)$  and  $\nu := \nu(\mathbf{x}, t)$  for  $(\mathbf{x}, t) \in \Omega \times (0, T]$  with  $T > 0$  that fulfill the evolution equation*

$$\begin{aligned}
\partial_t(\varphi_\epsilon \varrho) + \varphi_\epsilon \mathbf{u} \cdot \nabla \varrho &= \nabla \cdot (\varphi_\epsilon \nabla \mu) \\
M^{-1} \varphi_\epsilon \mu &= (1 + r)\varphi_\epsilon \varrho + \varphi_\epsilon \varrho^3 + 2\varphi_\epsilon \nu + \nabla \cdot (\varphi_\epsilon \nabla \nu) + \varphi_\epsilon U \quad \text{in } \Omega \\
\varphi_\epsilon \nu &= \nabla \cdot (\varphi_\epsilon \nabla \varrho)
\end{aligned} \tag{3.12}$$

subject to initial and boundary conditions

$$\begin{aligned}
\varrho(\mathbf{x}, 0) &= \varrho_0(\mathbf{x}) && \text{in } \bar{\Omega} \\
\partial_n \varrho(\mathbf{x}, t) = \partial_n \mu(\mathbf{x}, t) = \partial_n \nu(\mathbf{x}, t) &= 0 && \text{in } \partial\Omega \times (0, T]
\end{aligned}$$

with compatibility conditions  $\partial_n|_{\partial\Omega} \varrho_0 = 0$ ,  $\partial_n|_{\partial\Omega} (\Delta \varrho_0) = 0$  and  $\partial_n|_{\partial\Omega} (\Delta^2 \varrho_0) = 0$ .

The transport term in the first equation in (3.12) has been modified in comparison to the sharp interface equation (2.22), to be consistent with the diffuse domain ansatz of equation (3.3). Since

the velocity field is incompressible, we find

$$\nabla \cdot (\boldsymbol{\rho} \mathbf{u}) = \mathbf{u} \cdot \nabla \boldsymbol{\rho} + \boldsymbol{\rho} \nabla \cdot \mathbf{u} = \mathbf{u} \cdot \nabla \boldsymbol{\rho} \quad .$$

The integral coupling-constrained (2.21) leads to a diffuse domain constrained

$$\int_{\partial\Omega} \boldsymbol{\rho} \mathbf{u} \cdot \mathbf{n} \, ds = \int_{\Omega} \boldsymbol{\rho} \overline{\mathbf{u}}|_{\Gamma_0} \cdot \nabla \varphi_\epsilon \, d\mathbf{x} \quad (3.13)$$

where  $\overline{\mathbf{u}}|_{\Gamma_0}$  indicates an extension of  $\mathbf{u}|_{\Gamma_0}$  to  $\Omega$ .

### 3.3 Navier-Stokes equations in diffuse domain

For viscous incompressible fluids the motion is governed by the Navier-Stokes equations

$$\begin{aligned} \partial_t \mathbf{u} + (\mathbf{u} \cdot \nabla) \mathbf{u} &= -\nabla p + \eta \Delta \mathbf{u} \\ \nabla \cdot \mathbf{u} &= 0 \end{aligned} \quad (3.14)$$

where  $\mathbf{u}(\mathbf{x}, t) = (u_i(\mathbf{x}, t))_{i=1, \dots, d}$  is the velocity vector,  $p$  the scaled pressure variable and  $\eta$  the kinematic viscosity of the fluid. The derivative operators  $\partial_t$ ,  $\nabla^\top$  and  $\Delta$  have to be understood component-wise. By specifying initial and boundary conditions, the statement of the problem can be made complete. Taking the equations (3.14) in a domain  $\Omega_1$  with boundary  $\partial\Omega_1 = \Gamma_0 \cup \Gamma_1$ , one can set boundary conditions of Dirichlet type:

$$\mathbf{u}|_{\Gamma_0} = \mathbf{g} \quad \text{and} \quad \mathbf{u}|_{\Gamma_1} = \mathbf{h}, \quad \text{for all } t \in (0, T]$$

where  $\mathbf{g} : \Gamma_0 \times (0, T] \rightarrow \mathbb{R}^d$  and  $\mathbf{h} : \Gamma_1 \times (0, T] \rightarrow \mathbb{R}^d$ , for  $T > 0$ , define the boundary velocities. The initial condition specifies a velocity field  $\mathbf{u}_0$  at time  $t = 0$ :

$$\mathbf{u}|_{t=0} = \mathbf{u}_0 \quad \text{in } \bar{\Omega} \quad .$$

Compatibility of initial and boundary conditions has to be guaranteed. First of all, we assume that  $\mathbf{u}_0$  is solenoidal, i.e.  $\nabla \cdot \mathbf{u}_0 = 0$  in  $\Omega_1$ , then the initial velocity field must be consistent with the boundary conditions

$$\mathbf{u}_0|_{\Gamma_0} = \mathbf{g}|_{t=0} \quad \text{and} \quad \mathbf{u}_0|_{\Gamma_1} = \mathbf{h}|_{t=0} \quad .$$

By integrating the continuity equation over  $\Omega_1$ , we obtain a condition on the boundary functions

$$0 = \int_{\Omega_1} \nabla \cdot \mathbf{u} \, d\mathbf{x} = \int_{\partial\Omega_1} \mathbf{u} \cdot \mathbf{n} \, ds = \int_{\Gamma_0} \mathbf{g} \cdot \mathbf{n}_0 \, ds + \int_{\Gamma_1} \mathbf{h} \cdot \mathbf{n}_1 \, ds \quad . \quad (3.15)$$

The case of fixed colloids in a flowing solvent can be handled by

$$\mathbf{u}|_{\Gamma_0} = 0 \quad \text{and} \quad \mathbf{u}|_{\Gamma_1} = \mathbf{h} \quad .$$

Moving colloids in a closed box are described by

$$\mathbf{u}|_{\Gamma_0} = \mathbf{g} \quad \text{and} \quad \mathbf{u}|_{\Gamma_1} = 0 \quad .$$

Both cases set one boundary function to zero, so we get only one integral constrained like

$$0 = \int_{\Gamma_0} \mathbf{g} \cdot \mathbf{n}_0 \, ds \quad \text{or} \quad 0 = \int_{\Gamma_1} \mathbf{h} \cdot \mathbf{n}_1 \, ds \quad .$$

On the one hand these constraints can be understood as that the amount of fluid that flows into the domain equals the amount that flows out. On the other hand that the velocity of a colloid is equal all over the surface of the colloid.

To extend the Navier-Stokes equations to a simpler domain  $\Omega$  with  $\partial\Omega = \Gamma_1$  we apply the general diffuse domain equation for parabolic PDEs (3.11) to the first set of equations, using the Dirichlet boundary expression of table 3.1 for the boundary  $\Gamma_0$ :

$$\partial_t(\varphi_\epsilon u_j) + \varphi_\epsilon \mathbf{u} \cdot \nabla u_j = \varphi_\epsilon \nabla p - \eta \nabla \cdot (\varphi_\epsilon \nabla u_j) - \frac{\beta}{\epsilon^3} (1 - \varphi_\epsilon)(u_j - \bar{g}_j) \quad j = 1, \dots, d$$

where  $\beta$  is an additional scaling factor for the penalty term. Writing the incompressibility condition  $0 = \nabla \cdot \mathbf{u}$  in a weak form, we obtain

$$\begin{aligned} 0 &= \int_{\Omega_1} \vartheta \nabla \cdot \mathbf{u} \, d\mathbf{x} = - \int_{\Omega_1} \mathbf{u} \cdot \nabla \vartheta \, d\mathbf{x} + \int_{\Gamma_0} \mathbf{g} \cdot \mathbf{n}_0 \vartheta \, ds + \int_{\Gamma_1} \mathbf{h} \cdot \mathbf{n}_1 \vartheta \, ds \\ &= - \int_{\Omega} \chi_{\Omega_1} \mathbf{u} \cdot \nabla \vartheta \, d\mathbf{x} - \int_{\Omega} \nabla(1 - \chi_{\Omega_0}) \cdot \mathbf{g} \vartheta \, d\mathbf{x} + \int_{\Gamma_1} \mathbf{h} \cdot \mathbf{n}_1 \vartheta \, ds \\ &= \int_{\Omega} \nabla \cdot (\chi_{\Omega_1} \mathbf{u}) \vartheta \, d\mathbf{x} - \int_{\Omega} \nabla(1 - \chi_{\Omega_0}) \cdot \mathbf{g} \vartheta \, d\mathbf{x} - \int_{\Gamma_1} \chi_{\Omega_1} \mathbf{h} \cdot \mathbf{n}_1 \vartheta \, ds + \int_{\Gamma_1} \mathbf{h} \cdot \mathbf{n}_1 \vartheta \, ds \\ &= \int_{\Omega} \nabla \cdot (\chi_{\Omega_1} \mathbf{u}) \vartheta - \nabla(1 - \chi_{\Omega_0}) \cdot \mathbf{g} \vartheta \, d\mathbf{x} \\ &\approx \int_{\Omega} \nabla \cdot (\varphi_\epsilon \mathbf{u}) \vartheta - \nabla \varphi_\epsilon \cdot \mathbf{g} \vartheta \, d\mathbf{x} \end{aligned}$$



for test functions  $\vartheta$ . We arrive formally at the strong formulation

$$\nabla \cdot (\varphi_\epsilon \mathbf{u}) = \nabla \varphi_\epsilon \cdot \mathbf{g} \quad . \quad (3.16)$$

This results in the diffuse-domain Navier-Stokes formulation:

**Problem 4.** *Navier-Stokes problem:* Let  $\Omega \subset \mathbb{R}^d$  and  $\varphi_\epsilon$  be described by (3.2) for  $\epsilon > 0$  sufficiently small,  $\eta > 0$  and  $\beta > 0$ . Furthermore let the boundary function  $\mathbf{g}, \mathbf{h}$  fulfill the integral condition (3.15) and let  $\bar{\mathbf{g}} : \Omega \times [0, T] \rightarrow \mathbb{R}^d$  be the extension of  $\mathbf{g}$  to  $\Omega$  and  $\mathbf{h} : \partial\Omega \times [0, T] \rightarrow \mathbb{R}^d$ . Find velocity  $\mathbf{u} := (u_j(\mathbf{x}, t))_{j=1, \dots, d}$  and pressure  $p := p(\mathbf{x}, t)$  for  $(\mathbf{x}, t) \in \Omega \times (0, T]$  with  $T > 0$  that fulfill the diffuse domain Navier-Stokes equations

$$\begin{aligned} \partial_t(\varphi_\epsilon u_j) + \varphi_\epsilon \mathbf{u} \cdot \nabla u_j &= \varphi_\epsilon \nabla p - \eta \nabla \cdot (\varphi_\epsilon \nabla u_j) - \frac{\beta}{\epsilon^3} (1 - \varphi_\epsilon)(u_j - \bar{g}_j) \quad j = 1, \dots, d \\ \nabla \cdot (\varphi_\epsilon \mathbf{u}) &= \nabla \varphi_\epsilon \cdot \bar{\mathbf{g}} \quad \text{in } \Omega \end{aligned} \quad (3.17)$$

subject to initial and boundary conditions

$$\begin{aligned} \mathbf{u}(\mathbf{x}, 0) &= \mathbf{u}_0(\mathbf{x}) \quad \text{in } \bar{\Omega} \\ \mathbf{u}(\mathbf{x}, t) &= \mathbf{h}(\mathbf{x}, t) \quad \text{in } \partial\Omega \times (0, T] \\ \int_{\Omega} \varphi_\epsilon(\mathbf{x}, t) p(\mathbf{x}, t) \, d\mathbf{x} &= 0 \quad \text{in } [0, T] \end{aligned}$$

with compatibility conditions  $\mathbf{u}_0|_{\Gamma_1} = \mathbf{h}$  and  $\nabla \cdot (\varphi_\epsilon \mathbf{u}_0) = \nabla \varphi_\epsilon \cdot \bar{\mathbf{g}}$ .

Here we have set the integral condition on the pressure, to define the constant that makes the pressure variable unique.

### 3.4 Energy-Minimization

Starting from the principle of energy dissipation we want to show that the PFC-energy (2.19) is decreasing in time, using a  $H^{-1}$ -gradient-flow approach and the mentioned approximation of a characteristic function, to describe the energy evolution in a complex domain.

$$\begin{aligned} \mathcal{F}(\varrho) &= \int_{\Omega_1} \frac{1}{4} \varrho^4 + \frac{1}{2} (1+r) \varrho^2 + \varrho \Delta \varrho + \frac{1}{2} (\Delta \varrho)^2 + \varrho U \, d\mathbf{x} \\ &\approx \int_{\Omega} \varphi_\epsilon \left\{ \frac{1}{4} \varrho^4 + \frac{1}{2} (1+r) \varrho^2 + \frac{\varrho}{\varphi_\epsilon} \nabla \cdot (\varphi_\epsilon \nabla \varrho) + \frac{1}{2} \left( \frac{1}{\varphi_\epsilon} \nabla \cdot (\varphi_\epsilon \nabla \varrho) \right)^2 + \varrho U \right\} \, d\mathbf{x} \quad (3.18) \\ &=: \mathcal{F}_\epsilon(\varrho) \end{aligned}$$

where we have approximated the integration over the domain  $\Omega_1$  by multiplication with a phase-field function. The Laplace operators have been replaced by a restriction of the second order operator to a (smaller) domain:

$$(\Delta\varrho)_{\Omega_1} \approx \frac{1}{\varphi_\epsilon} \nabla \cdot (\varphi_\epsilon \nabla \varrho)$$

that comes from a weak diffuse domain Poisson equation. We can write the evolution of the energy  $\partial_t \mathcal{F} = \int \partial_t \varrho \cdot \delta_\varrho \mathcal{F} \, d\mathbf{x}$  with first variation of  $\mathcal{F}$ . To show that the energy is decreasing for our choice of  $\partial_t \varrho$  we have to prove the energy-decreasing property  $\partial_t \mathcal{F} \leq 0$ .

*Remark.* The property  $\partial_t \mathcal{F} \leq 0$  is required to characterize  $\mathcal{F}$  as Lyapunov function to the continuous dynamical system  $\partial_t \varrho = \Delta \mu$ , with  $\mu = \delta_\varrho \mathcal{F}$  defined as above. In Appendix B.1 this property is proved to hold also for a time-discrete dynamical system if the discretization is done with care, since  $\mathcal{F}$  is not a convex functional but consists of convex and concave parts.

Starting with the exact PFC-energy  $\mathcal{F}$  in  $\Omega_1$ , we can make the ansatz to use a continuity equation  $\partial_t \varrho = \nabla \cdot J$  in  $\Omega_1$  with a flux  $J$  proportional to the gradient of the variational derivative of  $\mathcal{F}$ :  $J = M \nabla \delta_\varrho \mathcal{F}$ , with  $M > 0$ . The variational derivative of  $\mathcal{F}$  can be found as

$$\delta_\varrho \mathcal{F} = \varrho^3 + (1+r)\varrho + 2\Delta\varrho + \Delta(\Delta\varrho) + U \quad . \quad (3.19)$$

This results in the energy-decreasing inequality for the exact PFC-energy:

$$\begin{aligned} \partial_t \mathcal{F} &= \int_{\Omega_1} \partial_t \varrho \cdot \delta_\varrho \mathcal{F} \, d\mathbf{x} = \int_{\Omega_1} \nabla \cdot \{M \nabla \delta_\varrho \mathcal{F}\} \cdot \delta_\varrho \mathcal{F} \, d\mathbf{x} \\ &= -M \int_{\Omega_1} \nabla \delta_\varrho \mathcal{F} \cdot \nabla \delta_\varrho \mathcal{F} \, d\mathbf{x} \\ &= -M (\text{grad}_{H^{-1}} \mathcal{F}, \text{grad}_{H^{-1}} \mathcal{F})_{H^{-1}(\Omega_1)} = -M \|\text{grad}_{H^{-1}} \mathcal{F}\|_{H^{-1}(\Omega_1)}^2 \leq 0 \end{aligned} \quad (3.20)$$

where  $(\cdot, \cdot)_{H^{-1}(\Omega_1)}$  is a product defined in  $\Omega_1$  by

$$(a^*, b^*)_{H^{-1}(\Omega_1)} := \int_{\Omega_1} \nabla a \cdot \nabla b \, d\mathbf{x}$$

with  $a^*, b^*$  associated to  $a, b$  by the Riesz-mapping theorem. This is a real scalar-product indeed and  $\|a\|_{H^{-1}(\Omega_1)} := (a, a)_{H^{-1}(\Omega_1)}^{1/2}$  defines the associated norm (see introduction for some details).

For the approximated energy  $\mathcal{F}_\epsilon$  the variational derivative can be calculated as

$$\delta_\varrho \mathcal{F}_\epsilon = \varphi_\epsilon \varrho^3 + \varphi_\epsilon(1+r)\varrho + 2\nabla \cdot (\varphi_\epsilon \nabla \varrho) + \nabla \cdot \left( \varphi_\epsilon \nabla \left( \frac{1}{\varphi_\epsilon} \nabla \cdot (\varphi_\epsilon \nabla \varrho) \right) \right) + \varphi_\epsilon U \quad . \quad (3.21)$$

If we use the continuity equation  $\partial_t \varrho = \nabla \cdot J_\epsilon$  in  $\Omega$  with the current  $J_\epsilon$  proportional to the gradient of the variational derivative of the energy:  $J_\epsilon = M \nabla \delta_\varrho \mathcal{F}_\epsilon$ , and assuming  $\partial_t \varphi_\epsilon = 0$ , we find that the energy is also decreasing in time:

$$\begin{aligned} \partial_t \mathcal{F}_\epsilon &= \int_\Omega \partial_t \varrho \cdot \delta_\varrho \mathcal{F}_\epsilon \, d\mathbf{x} = \int_\Omega \nabla \cdot (M \nabla \delta_\varrho \mathcal{F}_\epsilon) \cdot \delta_\varrho \mathcal{F}_\epsilon \, d\mathbf{x} \\ &= -M \int_\Omega \nabla \delta_\varrho \mathcal{F}_\epsilon \cdot \nabla \delta_\varrho \mathcal{F}_\epsilon \, d\mathbf{x} \\ &= -M (\text{grad}_{H^{-1}} \mathcal{F}_\epsilon, \text{grad}_{H^{-1}} \mathcal{F}_\epsilon)_{H^{-1}(\Omega)} = -M \|\text{grad}_{H^{-1}} \mathcal{F}_\epsilon\|_{H^{-1}(\Omega)}^2 \leq 0 \quad . \end{aligned} \quad (3.22)$$

On the one hand we can start with the exact PFC-energy, derive the evolution equation and then do the approximation of the domain, on the other hand we can do the approximation first and continue the derivation with  $\mathcal{F}_\epsilon$ . Both approaches give different evolution equations. For (3.20) we get

$$\begin{aligned} \varphi_\epsilon \partial_t \varrho &= \nabla \cdot (\varphi_\epsilon M \nabla \mu) \\ \varphi_\epsilon \mu &= \varphi_\epsilon \varrho^3 + \varphi_\epsilon(1+r)\varrho + 2\varphi_\epsilon \nu + \nabla \cdot (\varphi_\epsilon \nabla \nu) + \varphi_\epsilon U \\ \varphi_\epsilon \nu &= \nabla \cdot (\varphi_\epsilon \nabla \varrho) \end{aligned} \quad (3.23)$$

but for the other approach (3.22) we get the slightly altered system

$$\begin{aligned} \partial_t \varrho &= \nabla \cdot (M \nabla \mu) \\ \mu &= \varphi_\epsilon \varrho^3 + \varphi_\epsilon(1+r)\varrho + 2\varphi_\epsilon \nu + \nabla \cdot (\varphi_\epsilon \nabla \nu) + \varphi_\epsilon U \\ \varphi_\epsilon \nu &= \nabla \cdot (\varphi_\epsilon \nabla \varrho) \end{aligned} \quad (3.24)$$

Since both approaches tend to the same equilibrium configuration we use the equation (3.23) that approximates the differential equation as described in (3.12). It is supposed that this leads to more stable numerical simulations.

The key point of this section is, that we only approximate the gradient flow by a diffuse domain ansatz. This could cause some trouble in the energy minimization, since it is not clear whether the diffuse PFC equation is a decent direction any more. But for small  $\epsilon$  it seems to be a small perturbation of the original direction and thus, a good choice for minimizing the PFC functional.

Taking an approximated energy from the beginning leads to a system with well defined gradient direction, but the resulting PDE is not conform to the diffuse domain approach and could cause some trouble in numerical considerations. The left hand side of equation (3.24) does not require a fine mesh around the interface, but the right hand side does. The first equation does not contain any contribution to the phase-field variable and thus, the mobility is positive everywhere in the domain. Regions that are not of interest, e.g.  $\Omega_0$ , are driven by this system, as well as the original domain  $\Omega_1$ . So the system, if it is solvable, needs much more computational effort than the equation (3.23) that we will use throughout this paper.

### 3.5 Time-discretization

In order to solve the initial boundary value problem P3 numerically one has to discretize the partial differential equation in space and time. The space-discretization is considered in chapter 3.6. Here we will have a look at the semi-discretization in time.

Two strategies are well known to split the discretizations in space and time. If the discretization with respect to the spacial variable is done first, the method will be called (vertical) *method of lines*. Consider a domain  $\Omega \subseteq \mathbb{R}^d$  with smooth boundary  $\partial\Omega$  and the abstract parabolic initial boundary-value problem

$$\begin{aligned}
\partial_t Y &= F[\mathbf{x}, t, Y, Z] && \text{in } \Omega \times [0, T] \\
G[\mathbf{x}, t, Y, Z] &= 0 && \text{in } \Omega \times [0, T] \\
\mathcal{B}[t, Y] &= 0 && \text{on } \partial\Omega \times [0, T] \\
Y(\mathbf{x}, 0) &= Y_0(\mathbf{x}) && \text{in } \bar{\Omega}
\end{aligned} \tag{3.25}$$

where  $F$  and  $G$  are differential operators and  $\mathcal{B}$  a boundary (differential) operator that defines the boundary condition of the problem. By discretizing (3.25) with respect to the space variable  $\mathbf{x}$ , e.g. by Finite-Differences, Finite-Volume method or Finite-Element method, we arrive at an ordinary initial value problem. Writing this with discretized operators  $F_h, G_h$ , where the boundary conditions are solved, and space-discrete variants of the data and unknowns  $Y_h(t), Z_h(t)$  in a strong formulation:

$$\begin{aligned}
\partial_t Y_h &= F_h[\mathbf{x}, t, Y_h, Z_h] && \text{in } (0, T] \\
G_h[\mathbf{x}, t, Y_h, Z_h] &= 0 && \text{in } (0, T] \\
Y_h(0) &= Y_0
\end{aligned} \tag{3.26}$$

this leads to an initial-value problem of differential-algebraic equations that has to be solved. Now an integrator for DAEs can be applied to (3.26), like a Rung-Kutta method, a Rosenbrock method or a modified multi-step solver. Since the number of degrees of freedom, i.e. the dimension of the solution-vector  $Y_h$ , is in general fixed, problems arise when the mesh is to be refined adaptively over time. This situation occurs in moving front propagation, structure-coarsening or diffuse-domain problems with moving boundaries, for example. The requirement for this problems is a globally refined grid, that solves all front positions or phase boundary geometries from the beginning. Alternatively interpolation techniques and careful implementations could be used to save computational resources. This can be interpreted as perturbations to the ODE in each time step.

Another strategy discretizes in the time variables first and solves an elliptic boundary value problem in each time step. This method is called *Rothe-method* or horizontal method of lines. In this paper two discretizations in time direction are presented: an (semi) implicit Euler-method and a Rosenbrock method.

### 3.5.1 Semi-implicit discretization

If we split the time-interval  $[0, T]$  in intervals  $0 = t_0 < t_1 < \dots < t_N = T$  and define the discrete time step  $\tau^k := t_{k+1} - t_k$  and the values  $\varrho^k := \varrho(t_k)$ ,  $\mu^k := \mu(t_k)$ ,  $\nu^k := \nu(t_k)$ ,  $\varphi^k := \varphi(t_k)$ ,  $\mathbf{u}^k = (u_i^k)_i := \mathbf{u}(t_k)$ , we can rewrite the PFC-equation (2.20) with an Euler-method for the time-derivative as

$$\frac{\varrho^{k+1} - \varrho^k}{\tau^k} + \mathbf{u}^{k+1} \cdot \nabla \varrho^{k+1} = \nabla \cdot \{ M \nabla [(1+r)\varrho^{k+1} + 2(\lambda \Delta \varrho^{k+1} + (1-\lambda)\Delta \varrho^k) + \Delta^2 \varrho^{k+1} + \tilde{f}(\varrho^k, \varrho^{k+1}) + U] \}$$

where  $\lambda \in [0, 1]$  and the function  $\tilde{f}$  stands for a discretization of the non-linear term  $f(\varrho) := \varrho^3$ . The treatment of this cubic term is handled differently in literature. Cheng and Warren [CW08] use  $\tilde{f} := \varrho^k$  in their analysis. Wise, Wang and Lowengrub [WWL09] in contrast analyze an implicit scheme  $\tilde{f} := \varrho^{k+1}$ . Backofen, Rätz and Voigt [BRV07] introduce a linearization of  $f$  as

$$\tilde{f} := 3(\varrho^k)^2 \varrho^{k+1} - 2(\varrho^k)^3 \quad .$$

In the following we will use the linearized version of the non-linear term in the time-discretization since numerical tests show good performance of the scheme.

The parameter  $\lambda$  defines the treatment of the Laplace term, that causes some discussion in the literature. Wise et.al. [WWL09] expect that the implicit treatment, i.e.  $\lambda = 1$ , leads to a system,

that is not unconditionally uniquely solvable. Their convex splitting scheme takes  $\lambda = 0$ , as it is done by [CW08]. The authors of [BRV07], however, claim good behavior for  $\lambda = 1$ , i.e. the ability to take large time steps and numerically analyzed energy decreasing property.

For the explicit treatment a linear stability analysis is performed by Cheng and Warren and is extended to an implicit cubic term in the Appendix B.2. Since the linearized version is in between explicit and implicit discretization, the same stability-analysis should also hold for the most restrictive result of explicit and implicit stability analysis.

Wise et.al. analyzes the energy-stability of their scheme, i.e. that the discrete energy-evolution decreases the energy in each time step:  $\mathcal{F}[\varrho^k] \geq \mathcal{F}[\varrho^{k+1}]$ . This analysis could not be applied to the explicit or linearized treatment of the non-linear term, so it is not clear whether this property holds for these schemes, too. In Appendix B.1 this stability analysis is extended to include the external potential and a transport by potential flow of the density.

Now consider the diffuse-domain PFC-equation (3.12) in a non-stationary domain  $\Omega = \Omega(t)$  described by the phase-field function  $\varphi_\epsilon(\mathbf{x}, t)$ . Time-derivative and differential-operators contain this phase-field function as well as the non-linear term. The latter can be handled by Taylor expansion of  $\tilde{f}_\varphi(\varphi, \varrho) := \varphi \varrho^3$  around  $(\varphi^k, \varrho^k)$  by

$$\tilde{f}_\varphi(\varphi^{k+1}, \varrho^{k+1}) \approx 3\varphi^{k+1}(\varrho^k)^3 + \varphi^k \varrho^{k+1}(\varrho^k)^2 - 3\varphi^k(\varrho^k)^3$$

or, if  $\varphi^{k+1}$  is known before  $\varrho^{k+1}$  is calculated, an expansion around  $(\varphi^{k+1}, \varrho^k)$

$$\tilde{f}_\varphi(\varphi^{k+1}, \varrho^{k+1}) \approx 3\varphi^{k+1} \varrho^{k+1}(\varrho^k)^2 - 2\varphi^{k+1}(\varrho^k)^3 \quad .$$

The discretized evolution equation in time can then be written as

$$\begin{aligned} \frac{\varphi^{k+1} \varrho^{k+1} - \varphi^k \varrho^k}{\tau^k} + \varphi^{k+1} \mathbf{u}(t_{k+1}) \cdot \nabla \varrho^{k+1} &= \nabla \cdot \{M \varphi^{k+1} \nabla \mu^{k+1}\} \\ \varphi^{k+1} \mu^{k+1} &= (1+r) \varphi^{k+1} \varrho^{k+1} + 2\varphi^{k+1} \nu^{k+1} + \nabla \cdot (\varphi^{k+1} \nabla \nu^{k+1}) \\ &\quad + 3\varphi^{k+1} \varrho^{k+1}(\varrho^k)^2 - 2\varphi^{k+1}(\varrho^k)^3 + U(t_{k+1}) \\ \varphi^{k+1} \nu^{k+1} &= \nabla \cdot (\varphi^{k+1} \nabla \varrho^{k+1}) \quad . \end{aligned} \tag{3.27}$$

### 3.5.2 Rosenbrock method

An alternative to semi-implicit time-discretization (3.27) is a time-stepping method of Rosenbrock type for nonlinear parabolic partial differential equation systems (see [Lan01]) of the abstract form

$$\begin{aligned} H\partial_t Y(\mathbf{x}, t) &= F[\mathbf{x}, t, Y] && \text{in } \Omega \times (0, T] \\ \mathcal{B}[\mathbf{x}, t, Y] &= 0 && \text{on } \partial\Omega \times (0, T] \\ Y(\mathbf{x}, 0) &= Y_0(\mathbf{x}) && \text{on } \bar{\Omega} \end{aligned} \quad (3.28)$$

with  $H$  a constant real-valued matrix that may be singular,  $Y$  the (vector-valued) unknown and  $F$  is supposed to be sufficiently differentiable. The domain  $\Omega \subset \mathbb{R}^d$  is a bounded open domain with smooth boundary  $\partial\Omega$  and  $T > 0$ .  $\mathcal{B}$  is a boundary operator that implies boundary conditions to  $Y$ .

The PFC-equation (2.20) can be put into this form, using  $Y = (\nu, \varrho, \mu)$ ,  $H = \text{diag}(0, 1, 0)$  and  $F[\mathbf{x}, t, Y] = F[\mathbf{x}, t, \nu, \varrho, \mu]$  given by

$$F[\mathbf{x}, t, \nu, \varrho, \mu] := \begin{pmatrix} \nu - \Delta\varrho \\ \Delta\mu - \mathbf{u}(\mathbf{x}, t) \cdot \nabla\varrho \\ \mu - (1+r)\varrho - 2\nu - \Delta\nu - \varrho^3 - U(\mathbf{x}, t) \end{pmatrix}. \quad (3.29)$$

Furthermore the boundary-operator is given by

$$\mathcal{B}[\mathbf{x}, t, \nu, \varrho, \mu] := \begin{pmatrix} \partial_{\mathbf{n}}|_{\partial\Omega}\nu \\ \partial_{\mathbf{n}}|_{\partial\Omega}\varrho \\ \partial_{\mathbf{n}}|_{\partial\Omega}\mu \end{pmatrix}.$$

In order to integrate (3.28) in time semi implicit methods, like (3.27), or fully implicit discretization methods coupled with a Newton-like iteration for the nonlinear equation can be applied. By working the exact Jacobian directly into a discretization-formula one obtains an efficient integrator for stiff problems that arise in discretizations of partial differential equations using fine meshes. The method described here is a linearly implicit method of Rosenbrock type, introduced by [Ros63] to solve nonlinear ordinary differential equations.

Rosenbrock methods are usually implemented in a form which is different to the original one. By that some matrix-vector multiplications can be avoided. A slightly modified procedure of the one described in [Lan01] is presented now.

**Definition 3.5.1.** Let  $\tau > 0$  be the step size and  $t_k := k\tau$  for  $0 < k < N$  the discrete time with

$t_N = T$ . The so-called  $s$ -stage *Rosenbrock method* in transformed form reads

$$\begin{aligned}
\left(\frac{1}{\tau\gamma}H - F_Y[\mathbf{x}, t_k, Y^k]\right) X_i^k &= F[\mathbf{x}, t_k + \alpha_i\tau, Y^k + \sum_{j=1}^{i-1} a_{ij}X_j^k] + H \sum_{j=1}^{i-1} \frac{c_{ij}}{\tau} X_j^k \\
&\quad + \tau\gamma_i F_t[\mathbf{x}, t_k, Y^k] \qquad \qquad \qquad i = 1, \dots, s \\
Y^{k+1} &= Y^k + \sum_{i=1}^s m_i X_i^k
\end{aligned} \tag{3.30}$$

where  $\gamma > 0$ ,  $\alpha_i, a_{ij}, c_{ij}, \gamma_i$  and  $m_i$  are coefficients that should be chosen to guarantee consistency and stability of the scheme and that define the order of convergence. The operators  $F_Y$  and  $F_t$  name the derivatives of  $F$  with respect to  $Y$  and time.  $X_i^k$  is called the  $i^{\text{th}}$  stage solutions at time step  $k$ .

The solution procedure consists of the iterative solution of elliptic partial differential equations in each time step. It is shown that for coefficients that are chosen well  $Y^k$  is an approximation to the solution  $Y(t_k)$ . This approximation is called to be of order  $p$  if the local error satisfies

$$Y(t_k + \tau) - Y^{k+1} = \mathcal{O}(\tau^{p+1}), \quad \text{for } Y^k = Y(t_k) \quad .$$

In [Lan01] a proof for convergence of the discretization in time and space, using Finite Element discretization in space, is given and some sets of parameters for different approximation orders are displayed.

Time step control can be used in Rosenbrock methods and is described in [Lan01] and [EG96]. The basic idea is to use two Rosenbrock schemes that differ only in coefficients  $m_i$ . Thus a solution of different order can be calculated simply by summing up the stage solutions with different weights. Using two solutions of different approximation order a new time step can be calculated.

Derivatives of the system function  $F$  with respect to  $Y$  and time  $t$  for the PFC-equation can be found as:

$$F_Y[\mathbf{x}, t, Y, X] = \begin{pmatrix} \mathbf{n} - \Delta\mathbf{r} \\ \Delta\mathbf{m} - \mathbf{u}(\mathbf{x}, t) \cdot \nabla\mathbf{r} \\ \mathbf{m} - (1+r)\mathbf{r} - 2\mathbf{n} - \Delta\mathbf{n} - 3\varrho^2\mathbf{r} \end{pmatrix}, \quad F_t[\mathbf{x}, t, Y] = \begin{pmatrix} 0 \\ -\partial_t\mathbf{u}(\mathbf{x}, t) \cdot \nabla\varrho \\ -\partial_t U(\mathbf{x}, t) \end{pmatrix}$$

with  $X = (\mathbf{n}, \mathbf{r}, \mathbf{m})$ .



### 3.5.3 Time-discretization of Navier-Stokes equations

Navier-Stokes equations are nonlinear and this nonlinearity is not as "harmless" as it is in the Phase-Field Crystal equations. Especially for high Reynolds numbers nonlinear effects make the Navier-Stokes equations very hard to solve. Since we are in a regime of very low Reynolds numbers an approximation as Stokes-flow is possible and the nonlinearity does not cause too much difficulty. This gives the reason to apply simple linearization to the non-linear term by treating it explicitly.

For time-discrete variables  $\mathbf{u}^k = (u_i^k)_i := (u_i(t_k))_i$  and  $p^k := p(t_k)$  a discretization of the diffuse domain Navier-Stokes equations by semi-implicit Euler method is given by

$$\begin{aligned} \frac{\varphi_\epsilon^{k+1} u_j^{k+1} - \varphi_\epsilon^k u_j^k}{\tau^k} + \varphi_\epsilon^{k+1} \mathbf{u}^k \cdot \nabla u_j^{k+1} &= \varphi_\epsilon^{k+1} \nabla p^{k+1} - \eta \nabla \cdot (\varphi_\epsilon^{k+1} \nabla u_j^{k+1}) \\ &\quad - \frac{\beta}{\epsilon^3} (1 - \varphi_\epsilon^{k+1}) (u_j^{k+1} - \bar{g}_j(t_{k+1})) \quad j = 1, \dots, d \quad (3.31) \\ \nabla \cdot (\varphi_\epsilon^{k+1} \mathbf{u}^{k+1}) &= \nabla \varphi_\epsilon^{k+1} \cdot \bar{\mathbf{g}}(t_{k+1}) \quad \text{in } \Omega. \end{aligned}$$

The authors of [JMR06], [JR10] and [LJ08] apply Rosenbrock schemes to the incompressible Navier-Stokes equations and compare it to other time-discretization methods. The system function  $F^{\text{NS}}[\mathbf{x}, t, Y]$  for the Navier-Stokes equations (3.14) in two dimensions and its derivative reads

$$\begin{aligned} F^{\text{NS}}[\mathbf{x}, t, Y] &= \begin{pmatrix} \eta \Delta u_1 - (\mathbf{u} \cdot \nabla) u_1 - \partial_1 p \\ \eta \Delta u_2 - (\mathbf{u} \cdot \nabla) u_2 - \partial_2 p \\ \nabla \cdot \mathbf{u} \end{pmatrix} \quad Y = (\mathbf{u}, p) \\ F_Y^{\text{NS}}[\mathbf{x}, t, Y, X] &= \begin{pmatrix} \eta \Delta v_1 - (\mathbf{v} \cdot \nabla) u_1 - (\mathbf{u} \cdot \nabla) v_1 - \partial_1 q \\ \eta \Delta v_2 - (\mathbf{v} \cdot \nabla) u_2 - (\mathbf{u} \cdot \nabla) v_2 - \partial_2 q \\ \nabla \cdot \mathbf{v} \end{pmatrix} \quad X = (\mathbf{v}, q) \end{aligned} \quad (3.32)$$

using  $H = \text{diag}(1, 1, 0)$ .

Since the Navier-Stokes equations are differential algebraic equations of index 2<sup>1</sup>, special Rosenbrock schemes for such systems must be applied.

## 3.6 Space-discretization

In addition to the time step method, the discretization of the differential operators in space must be performed, to obtain a fully discrete system. Therefore a weak formulation of the differential

<sup>1</sup>See [EG96, JR10] for proof of this statement

equations must be derived. Set  $V := H^1(\Omega)$  the Sobolev space of weakly differential functions that are square integrable in  $\Omega$  and have square integrable derivatives and  $W := L_2(\Omega)$ . We exploit the notation

$$\langle f, v \rangle := \int_{\Omega} f v \, d\mathbf{x}, \quad \|f\| = \sqrt{\langle f, f \rangle} \quad .$$

### 3.6.1 Semi-implicit time-discretization

At first the transport term in the Phase-Field Crystal equation must be modified to obtain the conservative form of the equation. Therefore we use the relation (3.16) and obtain

$$\varphi_{\epsilon} \mathbf{u} \cdot \nabla \varrho = \nabla \cdot (\varphi_{\epsilon} \mathbf{u} \varrho) - \varrho \nabla \varphi_{\epsilon} \cdot \bar{\mathbf{g}} \quad .$$

The last term vanishes due to partial integration of the first one combined with coupling constrained (3.13), that gives conservation of the density. For an arbitrary test function  $\vartheta$  we can write the transport-term in a weak form

$$\begin{aligned} \langle \varphi_{\epsilon} \mathbf{u} \cdot \nabla \varrho, \vartheta \rangle &= \langle \nabla \cdot (\varphi_{\epsilon} \mathbf{u} \varrho), \vartheta \rangle - \langle \varrho \nabla \varphi_{\epsilon} \cdot \bar{\mathbf{g}}, \vartheta \rangle \\ &= -\langle \varphi_{\epsilon} \mathbf{u} \varrho, \nabla \vartheta \rangle + \int_{\partial\Omega} \varphi_{\epsilon} \varrho \mathbf{u} \cdot \mathbf{n} \vartheta \, ds - \langle \varrho \nabla \varphi_{\epsilon} \cdot \bar{\mathbf{g}}, \vartheta \rangle \\ &= -\langle \varphi_{\epsilon} \mathbf{u} \varrho, \nabla \vartheta \rangle + \langle \varrho \nabla \varphi_{\epsilon} \cdot \underbrace{\overline{\mathbf{u}}|_{\Gamma_0}}_{\bar{\mathbf{g}}}, \vartheta \rangle - \langle \varrho \nabla \varphi_{\epsilon} \cdot \bar{\mathbf{g}}, \vartheta \rangle \\ &= -\langle \varphi_{\epsilon} \mathbf{u} \varrho, \nabla \vartheta \rangle \end{aligned} \tag{3.33}$$

Problem (3.27), the semi-implicit Euler discretization of the PFC equations, can be written in variational form:

**Problem 5.** *Let  $\Omega \subset \mathbb{R}^d$ ,  $M > 0$  and  $\varphi_{\epsilon}$  be described by (3.2) for  $\epsilon > 0$  sufficiently small,  $r > -1$ . Find  $\varphi^{k+1} \in V$ ,  $\varrho^{k+1} \in V$ ,  $\mu^{k+1} \in V$  and  $\nu^{k+1} \in V$  for  $k = 0, \dots, N-1$ , such that*

$$\varphi^{k+1} = f(\varphi^k, \varrho^k)$$

where  $f$  describes the evolution of the phase-field, depending on the density  $\varrho$ , and

$$\begin{aligned}
\left\langle \frac{\varphi^{k+1}\varrho^{k+1} - \varphi^k\varrho^k}{\tau^k}, \vartheta \right\rangle &= \langle \varphi^{k+1}\varrho^{k+1}\mathbf{u}(t_{k+1}), \nabla\vartheta \rangle - \langle M\varphi^{k+1}\nabla\mu^{k+1}, \nabla\vartheta \rangle \\
\langle \varphi^{k+1}\mu^{k+1}, \vartheta \rangle &= \langle (1+r)\varphi^{k+1}\varrho^{k+1} + 2\varphi^{k+1}\nu^{k+1}, \vartheta \rangle - \langle \varphi^{k+1}\nabla\nu^{k+1}, \nabla\vartheta \rangle \\
&\quad + \langle 3\varphi^{k+1}\varrho^{k+1}(\varrho^k)^2 - 2\varphi^{k+1}(\varrho^k)^3 + U(t_{k+1}), \vartheta \rangle \\
\langle \varphi^{k+1}\nu^{k+1}, \vartheta \rangle &= \langle \varphi^{k+1}\nabla\varrho^{k+1}, \nabla\vartheta \rangle
\end{aligned} \tag{3.34}$$

for all  $\vartheta \in V$ , subject to initial condition

$$\begin{aligned}
\langle \varphi^0, \vartheta \rangle &= \langle \varphi_\epsilon, \vartheta \rangle \\
\langle \varrho^0, \vartheta \rangle &= \langle \varrho_0, \vartheta \rangle \quad \forall \vartheta \in W \quad .
\end{aligned} \tag{3.35}$$

The variational form of the equations conserves the quantity  $\varrho$  over time as it is constructed, because we obtain the conservation relation

$$\int_{\Omega} \frac{\varphi^{k+1}\varrho^{k+1} - \varphi^k\varrho^k}{\tau^k} \, d\mathbf{x} = 0 \quad \Rightarrow \quad \int_{\Omega_1(t_{k+1})} \varrho^{k+1} \, d\mathbf{x} = \int_{\Omega_1(t_k)} \varrho^k \, d\mathbf{x}$$

by using a test function  $\vartheta \equiv 1$  and testing the first equation in (3.34). Now let  $\Omega$  be a bounded, open and connected domain in  $\mathbb{R}^d$ , with Lipschitz continuous boundary  $\partial\Omega$ , that can be described by a polygonal chain and  $\mathcal{T}_h$  be a conforming triangulation of  $\Omega$  with respect to the grid size  $h$ , equal to the maximal diameter of simplices  $K \in \mathcal{T}_h$ . We use the following Finite Element space to approximate  $V$

$$V \supset V_h := \{v_h \in V : v_h|_K \in \mathbb{P}_m \text{ for all } K \in \mathcal{T}_h, m \geq 1\} \tag{3.36}$$

consisting of all globally continuous piecewise polynomials of degree  $m$  or less. Let  $\Pi_h : V \rightarrow V_h$  be a *projection operator* that satisfies

$$\begin{aligned}
\|\Pi_h v\| &\leq C\|v\| \\
\|v - \Pi_h v\| &\leq C \inf_{v_h \in V_h} \|v - v_h\|
\end{aligned} \tag{3.37}$$

for all  $v \in V$ , with constants  $C$  independent of  $v$  and  $h$ . That means  $\Pi_h v$  is quasi-optimal with respect to the best approximation in  $V_h$ . We can rewrite the problem P5 with discretization in space:

**Problem 6.** Let  $\Omega \subset \mathbb{R}^d$ ,  $M > 0$  and  $\varphi_\epsilon$  be described by (3.2) for  $\epsilon > 0$  sufficiently small,  $r > -1$ .

Find  $\varphi_h^{k+1} \in V_h, \varrho_h^{k+1} \in V_h, \mu_h^{k+1} \in V_h$  and  $\nu_h^{k+1} \in V_h$  for  $k = 0, \dots, N-1$ , such that

$$\varphi_h^{k+1} = f(\varphi_h^k, \varrho_h^k)$$

where  $f$  describes the evolution of the phase-field, depending on the density  $\varrho$ , and

$$\begin{aligned} \left\langle \frac{\varphi_h^{k+1} \varrho_h^{k+1} - \varphi_h^k \varrho_h^k}{\tau^k}, \vartheta_h \right\rangle &= \langle \varphi_h^{k+1} \varrho_h^{k+1} \Pi_h[u_i(t_{k+1})]_i, \nabla \vartheta_h \rangle - \langle M \varphi_h^{k+1} \nabla \mu_h^{k+1}, \nabla \vartheta_h \rangle \\ \langle \varphi_h^{k+1} \mu_h^{k+1}, \vartheta_h \rangle &= \langle (1+r) \varphi_h^{k+1} \varrho_h^{k+1} + 2 \varphi_h^{k+1} \nu_h^{k+1}, \vartheta_h \rangle - \langle \varphi_h^{k+1} \nabla \nu_h^{k+1}, \nabla \vartheta_h \rangle \\ &\quad + \langle 3 \varphi_h^{k+1} \varrho_h^{k+1} (\varrho_h^k)^2 - 2 \varphi_h^{k+1} (\varrho_h^k)^3 + \Pi_h U(t_{k+1}), \vartheta_h \rangle \\ \langle \varphi_h^{k+1} \nu_h^{k+1}, \vartheta_h \rangle &= \langle \varphi_h^{k+1} \nabla \varrho_h^{k+1}, \nabla \vartheta_h \rangle \end{aligned} \quad (3.38)$$

for all  $\vartheta_h \in V_h$ , subject to initial condition

$$\begin{aligned} \langle \varphi_h^0, \vartheta_h \rangle &= \langle \Pi_h \varphi_\epsilon, \vartheta_h \rangle \\ \langle \varrho_h^0, \vartheta_h \rangle &= \langle \Pi_h \varrho_0, \vartheta_h \rangle \quad \forall \vartheta_h \in V_h \end{aligned} \quad (3.39)$$

This leads to a system of linear equations by expressing  $v_h \in V_h$  by a linear combination of basis functions of  $V_h$ :

$$v_h(\mathbf{x}) = \sum_{i=1}^{\dim(V_h)} v_i \phi_i(\mathbf{x})$$

with coefficients  $v_i$ . Choosing  $\{\phi_i\}$  as nodal basis in  $V_h$ , i.e.  $\phi_i(\mathbf{x}_j) = \delta_{ij}$ , with  $\delta_{ij}$  denotes the Kronecker symbol and  $\mathbf{x}_j$  the grid points of the triangulation  $\mathcal{T}_h$ , this leads to  $v_h(\mathbf{x}_j) = v_j$ . Expressing all variables of problem P6 with respect to the basis  $\{\phi_i\}$

$$\begin{aligned} \varphi_h^k(\mathbf{x}) &= \sum_{i=1}^{\dim(V_h)} \varphi_i^k \phi_i(\mathbf{x}), & \boldsymbol{\varphi}^k &:= (\varphi_i^k)_i & \varrho_h^k(\mathbf{x}) &= \sum_{i=1}^{\dim(V_h)} \varrho_i^k \phi_i(\mathbf{x}), & \boldsymbol{\varrho}^k &:= (\varrho_i^k)_i \\ \mu_h^k(\mathbf{x}) &= \sum_{i=1}^{\dim(V_h)} \mu_i^k \phi_i(\mathbf{x}), & \boldsymbol{\mu}^k &:= (\mu_i^k)_i & \nu_h^k(\mathbf{x}) &= \sum_{i=1}^{\dim(V_h)} \nu_i^k \phi_i(\mathbf{x}), & \boldsymbol{\nu}^k &:= (\nu_i^k)_i \end{aligned}$$

and defining  $U_h := \Pi_h U$ ,  $\mathbf{u}_h := \Pi_h \mathbf{u}$ , we arrive at the linear system

$$\begin{aligned} \frac{1}{\tau} \mathbf{M} \boldsymbol{\varrho}^{k+1} + M \mathbf{L} \boldsymbol{\mu}^{k+1} - \mathbf{T}_u \boldsymbol{\varrho}^{k+1} &= \frac{1}{\tau} \mathbf{M}' \boldsymbol{\varrho}^k \\ \mathbf{M} \boldsymbol{\mu}^{k+1} - (1+r) \mathbf{M} \boldsymbol{\varrho}^{k+1} - 2 \mathbf{M} \boldsymbol{\nu}^{k+1} + \mathbf{L} \boldsymbol{\nu}^{k+1} - \mathbf{F}_i \boldsymbol{\varrho}^{k+1} &= \mathbf{F}_e + \mathbf{U} \\ \mathbf{M} \boldsymbol{\nu}^{k+1} + \mathbf{L} \boldsymbol{\varrho}^{k+1} &= 0 \end{aligned} \quad (3.40)$$

with sub-matrices that represent the individual (differential-) operators

$$\begin{aligned} \mathbf{M} &:= \langle \varphi_h^{k+1} \phi_i, \phi_j \rangle_{ij} & \mathbf{M}' &:= \langle \varphi_h^k \phi_i, \phi_j \rangle_{ij} \\ \mathbf{L} &:= \langle \varphi_h^{k+1} \nabla \phi_i, \nabla \phi_j \rangle_{ij} & \mathbf{T}_u &:= \langle \varphi_h^{k+1} \mathbf{u}_h(t_{k+1}) \phi_i, \nabla \phi_j \rangle_{ij} \\ \mathbf{F}_i &:= \langle 3 \varphi_h^{k+1} (\varrho_h^k)^2 \phi_i, \phi_j \rangle_{ij} & \mathbf{F}_e &:= \langle -2 \varphi_h^{k+1} (\varrho_h^k)^3, \phi_j \rangle_j & \mathbf{U} &:= \langle U_h(t_{k+1}), \phi_j \rangle_j \end{aligned} .$$

The resulting system (3.40) can be solved iteratively by using Krylov subspace methods like BiCGStab( $l$ )<sup>2</sup>, or, as it was done for the two-dimensional case, by using a direct solver, e.g. UMFPACK<sup>3</sup>.

### 3.6.2 Rosenbrock method

As well as the semi-implicit time-discretization method, the Rosenbrock version can be discretized in space, using Finite Elements, too. Therefore the system operator  $F$  (3.29) will be written in a weak form. The new operators arise from integration of the vector components of  $F$ , multiplied with a test function  $\vartheta \in V$ , over  $\Omega$  and partial integration, including the boundary conditions. For the PFC equations we get

$$\tilde{F}[\mathbf{x}, t, Y; \vartheta] := \begin{pmatrix} \langle \nu, \vartheta \rangle + \langle \nabla \varrho, \nabla \vartheta \rangle \\ - \langle M \nabla \mu, \nabla \vartheta \rangle + \langle \mathbf{u}(\mathbf{x}, t) \varrho, \nabla \vartheta \rangle \\ \langle \mu - (1+r) \varrho - 2\nu - U(\mathbf{x}, t), \vartheta \rangle + \langle \nabla \nu, \nabla \vartheta \rangle - \langle \varrho^3, \vartheta \rangle \end{pmatrix} .$$

<sup>2</sup>A description can be found in [SF93].

<sup>3</sup>This method is based on [Dav04].

Also the derivatives of  $F$  can be written in such a form:

$$\begin{aligned}\tilde{F}_Y[\mathbf{x}, t, Y, X; \vartheta] &= \begin{pmatrix} \langle \mathbf{n}, \vartheta \rangle + \langle \nabla \mathbf{r}, \nabla \vartheta \rangle \\ \langle -M \nabla \mathbf{m}, \nabla \vartheta \rangle + \langle \mathbf{u}(\mathbf{x}, t) \mathbf{r}, \nabla \vartheta \rangle \\ \langle \mathbf{m} - (1+r) \mathbf{r} - 2\mathbf{n} - 3\varrho^2 \mathbf{r}, \vartheta \rangle + \langle \nabla \mathbf{n}, \nabla \vartheta \rangle \end{pmatrix} \\ \tilde{F}_t[\mathbf{x}, t, Y; \vartheta] &= \begin{pmatrix} 0 \\ \langle \partial_t \mathbf{u}(\mathbf{x}, t) \varrho, \nabla \vartheta \rangle \\ -\langle \partial_t U(\mathbf{x}, t), \vartheta \rangle \end{pmatrix} .\end{aligned}$$

If we take the discrete subspace  $V_h \subset V$  similar to (3.36), the Rosenbrock method can be written in a spatial discrete variational form

$$\begin{aligned}\left\langle \frac{1}{\tau \gamma} H X_i^k, \vartheta_h \right\rangle - \tilde{F}_Y[t_k, Y^k, X_i^k; \vartheta_h] &= \tilde{F}[t_k + \alpha_i \tau, Y^k + \sum_{j=1}^{i-1} a_{ij} X_j^k; \vartheta_h] + \left\langle H \sum_{j=1}^{i-1} \frac{c_{ij}}{\tau} X_j^k, \vartheta_h \right\rangle \\ &\quad + \tau \gamma_i \tilde{F}_t[t_k, Y^k; \vartheta_h] \quad \forall \vartheta_h \in V_h, \quad i = 1, \dots, s \\ Y^{k+1} &= Y^k + \sum_{i=1}^s m_i X_i^k .\end{aligned}\tag{3.41}$$

Again this results in a sequence of linear systems, when using the basis representation of the unknowns  $\varrho, \mu$  and  $\nu$  as linear combinations of elements of a basis of  $V_h$ . The system matrices do not change during the stage iterations, so that a factorization technique for the matrix is appropriate. After the first stage all other stages can be solved with low computational effort.

For the expansion  $\varrho_0(\mathbf{x}) = \sum_{i=1}^{\dim(V_h)} \varrho_{0,i} \phi_i(\mathbf{x})$  with respect to a basis  $\{\phi_i\}$  of  $V_h$  the coefficient vector is called  $\boldsymbol{\varrho}_0 := (\varrho_{0,i})_i$ . The Rosenbrock method to the initial value  $\boldsymbol{\varrho}^0 = \boldsymbol{\varrho}_0$  can be written in a stepwise solution procedure, as can be found in Algorithm 1. We use the notations

$$\begin{aligned}\mathbf{T}'_{\mathbf{u}}(t) &:= \langle \varphi_h^k(\partial_t \mathbf{u})_h(t) \phi_i, \nabla \phi_j \rangle_{ij} & \mathbf{U}'(t) &:= \langle \varphi_h^k(\partial_t U)_h(t), \phi_j \rangle_j \\ \mathbf{F}'_i &:= \langle 3\varphi_h^{k+1}(\varrho_h^k)^2 \phi_i, \phi_j \rangle_{ij} & \mathbf{F}'_e[\boldsymbol{\varrho} = (\varrho_i)_i] &:= \langle \varphi_h^k(\sum_{i=1}^{\dim(V_h)} \varrho_i \phi_i)^3, \phi_j \rangle_j\end{aligned}$$

with

$$(\partial_t \mathbf{u})_h := \Pi_h(\partial_t \mathbf{u}), \quad (\partial_t U)_h := \Pi_h(\partial_t U) .$$

---

**Algorithm 1** Rosenbrock method

---

Set initial value  $\boldsymbol{\varrho}^0 = \boldsymbol{\varrho}_0$ .

Find initial values for  $\boldsymbol{\mu}^0$  and  $\boldsymbol{\nu}^0$ , i.e. solve an initial problem for fixed  $\boldsymbol{\varrho}^0$ .

**for**  $k = 0, \dots, N - 1$  **do**

**for**  $i = 1, \dots, s$  **do**

    Stage iteration: Find  $(\mathbf{n}_i^k, \boldsymbol{\tau}_i^k, \mathbf{m}_i^k)$  subject to

$$\begin{aligned} \begin{pmatrix} -\mathbf{M} & -\mathbf{L} & 0 \\ 0 & \frac{1}{\tau}\mathbf{M} - \mathbf{T}_u & \mathbf{M}\mathbf{L} \\ 2\mathbf{M} - \mathbf{L} & (1+r)\mathbf{M} + \mathbf{F}'_i & -\mathbf{M} \end{pmatrix} \begin{pmatrix} \mathbf{n}_i^k \\ \boldsymbol{\tau}_i^k \\ \mathbf{m}_i^k \end{pmatrix} &= \begin{pmatrix} 0 \\ \sum_{j=1}^{i-1} \frac{c_{ij}}{\tau} \mathbf{M}\boldsymbol{\tau}_j^k \\ -\mathbf{F}'_e[\boldsymbol{\varrho}^k + \sum_{j=1}^{i-1} a_{ij}\boldsymbol{\tau}_j^k] - \mathbf{U}(t_k + \alpha_i\tau) \end{pmatrix} \\ + \begin{pmatrix} \mathbf{M} & \mathbf{L} & 0 \\ 0 & \mathbf{T}_u(t_k + \alpha_i\tau) & -\mathbf{M}\mathbf{L} \\ -2\mathbf{M} + \mathbf{L} & -(1+r)\mathbf{M} & \mathbf{M} \end{pmatrix} \begin{pmatrix} \boldsymbol{\nu}^k + \sum_{j=1}^{i-1} a_{ij}\mathbf{n}_j^k \\ \boldsymbol{\varrho}^k + \sum_{j=1}^{i-1} a_{ij}\boldsymbol{\tau}_j^k \\ \boldsymbol{\mu}^k + \sum_{j=1}^{i-1} a_{ij}\mathbf{m}_j^k \end{pmatrix} &+ \begin{pmatrix} 0 \\ \tau\gamma_i \mathbf{T}'_u(t_k) \\ -\tau\gamma_i \mathbf{U}'(t_k) \end{pmatrix} \end{aligned} \quad (3.42)$$

**end for**

  Calculate new solution  $(\boldsymbol{\nu}^{k+1}, \boldsymbol{\varrho}^{k+1}, \boldsymbol{\mu}^{k+1})$ , by

$$\boldsymbol{\nu}^{k+1} = \boldsymbol{\nu}^k + \sum_{j=1}^s m_j \mathbf{n}_j^k, \quad \boldsymbol{\varrho}^{k+1} = \boldsymbol{\varrho}^k + \sum_{j=1}^s m_j \boldsymbol{\tau}_j^k, \quad \boldsymbol{\mu}^{k+1} = \boldsymbol{\mu}^k + \sum_{j=1}^s m_j \mathbf{m}_j^k \quad (3.43)$$

**end for**

---

### 3.6.3 Space-discretization of Navier-Stokes equations

The Navier-Stokes equations can be solved by discretization in space using Finite Elements like any other second order PDE. As well as in the case of PFC we can write the equations in a weak form by multiplication with test functions and integration over the domain  $\Omega$ . By taking subsets of the space of test functions with discrete base we arrive at a Finite Element formulation of the problem:

For  $k = 0, \dots, N$  find velocity  $\mathbf{u}_h^{k+1} = (u_{h,i}^{k+1})_i \in (V_h)^d \subset H^1(\Omega)^d$  with  $\mathbf{u}_h^{k+1}|_{\Gamma_1} = \mathbf{h}_h(t_{k+1})$  and pressure  $p_h^{k+1} \in P_h \subset \dot{L}_2(\Omega) = \{p \in L_2(\Omega) : \int_{\Omega} p \, dx = 0\}$  such that

$$\begin{aligned} \left\langle \frac{\varphi_h^{k+1} u_{h,j}^{k+1} - \varphi_h^k u_{h,j}^k}{\tau^k}, \vartheta_h \right\rangle &= - \left\langle \varphi_h^{k+1} \mathbf{u}_h^k \cdot \nabla u_{h,j}^{k+1}, \vartheta_h \right\rangle + \left\langle \eta \varphi_h^{k+1} \nabla u_{h,j}^{k+1}, \nabla \vartheta_h \right\rangle \\ &\quad - \left\langle \varphi_h^{k+1} p_h^{k+1}, \partial_j \vartheta_h \right\rangle - \left\langle \partial_j (\varphi_h^{k+1}) p_h^{k+1}, \vartheta_h \right\rangle \\ &\quad - \left\langle \frac{\beta}{\varepsilon^3} (1 - \varphi_h^{k+1}) (u_{h,j}^{k+1} - g_{h,j}(t_{k+1})), \vartheta_h \right\rangle \quad j = 1, \dots, d \\ \left\langle \varphi_h^{k+1} \nabla \cdot \mathbf{u}_h^{k+1}, \theta_h \right\rangle &= \left\langle \nabla \varphi_h^{k+1} \cdot (\mathbf{g}_h(t_{k+1}) - \mathbf{u}_h^{k+1}), \theta_h \right\rangle \end{aligned} \quad (3.44)$$

for every  $\vartheta \in V_h$  with  $\vartheta_h|_{\Gamma_1} = 0$  and  $\theta_h \in P_h$ , subject to initial conditions  $\mathbf{u}_h^0 = \Pi_h \mathbf{u}_0$ . The discrete boundary functions are defined by  $g_{h,j} = \Pi_h \bar{g}_j$ , with  $\mathbf{g}_h = (g_{h,j})_j$ .

For reasons of stability the selection of an appropriate Finite Element subspace is not arbitrary. It has to fulfill the Ladyschenskaja-Babuska-Brezzi condition (LBB-condition)

$$\inf_{0 \neq p_h \in P_h} \left\{ \sup_{0 \neq \vartheta_h \in V_h} \left\{ \frac{\langle p_h, \nabla \cdot \vartheta_h \rangle}{\|p_h\| \|\nabla \vartheta_h\|} \right\} \right\} \geq \beta > 0$$

a sufficient condition for stability of mixed Finite Element problems with saddle-point structure. One special choice is a triangular element, introduced by Hood and Taylor, with quadratic polynomials for velocity and linear pressure ( $P_2/P_1$ -element).

### Projection method

A projection method based on the ideas of Chorin (SIMPLE or SIMPLE-R, to be more precise) is now introduced since the direct solution of the problem (3.44) still seems very difficult. The idea is to make a prediction step without any pressure term and without conservation of mass at first, then a pressure calculation is done and at the end a projection into the space of divergence-free velocities is performed. The pressure variable loses its meaning during these steps. In Algorithm 2 these steps are performed and in the Appendix C this algorithm is derived in more detail.

---

#### Algorithm 2 SIMPLE-R

---

**for**  $\mathfrak{b} = 0, 1$  **do**

1.) prediction step ("Burgers equation"): Find  $\bar{\mathbf{u}} \in (V_h)^d$ , with  $\bar{\mathbf{u}}|_{\Gamma_1} = \mathbf{h}$  s.t. for  $j = 1, \dots, d$

$$\begin{aligned} \left\langle \frac{\varphi_h^{k+1} \bar{u}_j - \varphi_h^k u_{h,j}^k}{\tau^k}, \vartheta_h \right\rangle &= - \langle \varphi_h^{k+1} \mathbf{u}_h^k \cdot \nabla \bar{u}_j, \vartheta_h \rangle + \langle \eta \varphi_h^{k+1} \nabla \bar{u}_j, \nabla \vartheta_h \rangle \\ &\quad - \mathfrak{b} \left( \langle \varphi_h^{k+1} p_h^{k+1}, \partial_j \vartheta_h \rangle + \langle \partial_j (\varphi_h^{k+1}) p_h^{k+1}, \vartheta_h \rangle \right) \\ &\quad - \left\langle \frac{\beta}{\varepsilon^3} (1 - \varphi_h^{k+1}) (\bar{u}_j - \bar{g}_{h,j}(t_{k+1})), \vartheta_h \right\rangle \end{aligned} \quad (3.45)$$

for all  $\vartheta_h \in V_h$ , subject to  $\vartheta_h|_{\Gamma_1} = 0$ .

2.) pressure Poisson problem: Find  $p_b \in W_h \subset \dot{H}^1(\Omega) = \{p \in H^1(\Omega) : \int_{\Omega} p \, d\mathbf{x} = 0\}$ , s.t.

$$-\tau^k \langle \varphi_h^{k+1} \nabla p_b, \nabla \theta \rangle = \langle \nabla \varphi_h^{k+1} \cdot (\bar{\mathbf{u}} - \mathbf{g}_h(t_{k+1})), \theta \rangle + \langle \varphi_h^{k+1} \nabla \cdot \bar{\mathbf{u}}, \theta \rangle \quad (3.46)$$

for all  $\theta_h \in W_h$

**end for**

3.) projection step  $\bar{\mathbf{u}} \mapsto \mathbf{u}^{k+1} : \nabla \cdot \mathbf{u}^{k+1} = 0$  in  $\Omega_1$ :

$$\mathbf{u}_h^{k+1} = \bar{\mathbf{u}} - \tau \nabla p_1 \quad (3.47)$$


---



# Chapter 4

## Simulations

In order to solve the problem P6 for semi-implicit time discretization, or to process the Algorithm 1 we use the Finite Element toolbox AMDiS<sup>1</sup>. This toolbox provides functions for mesh refinement and coarsening, depending on local error estimates or predefined requirements on the mesh structure near obstacles, boundaries or regions of interest. The assemblage of the linear systems, using Lagrangian Finite Elements of polynomial degree  $\leq 4$ , can be performed and the linear systems can be solved with various internal or external solvers. Iterative methods like BiCGStab( $l$ )<sup>2</sup> are found to produce good results in admissible time for non-symmetric systems. The external tool UMFPACK [Dav04], a method for sparse LU factorization using pre-ordering and pivoting strategies to preserve fill-in upper bounds, can be used as direct solver. In two-dimensional simulations this solver is preferred compared to iterative methods. It needs less time to solve the linear systems, but matrices from the three-dimensional case produce a much higher fill-in that slows down the factorization process of the direct solvers rapidly.

Simulations were performed on Quad-Core computer with 1.8 Ghz per core and 4 Gb memory (called *Q18*), on a Quad-core with 4 times 3.2 Ghz CPU clock rate and 8 Gb memory (called *Q32*) and on the PC-farm Deimos<sup>3</sup> at TU-Dresden with 2.6 Ghz per core and maximum 2 Gb RAM each process (called *Deimos*). Most of the simulations were done sequentially but tests with distributed domains and parallel assembling were performed, as well.

---

<sup>1</sup>Adaptive Multi-Dimensional Simulation Toolbox [VV07]

<sup>2</sup>An improvement of stabilized bi-conjugate gradient method, [SF93]

<sup>3</sup>2576 cores AMD Opteron 2.6 Ghz, 5.4 TB memory, 724 nodes with 1,2, or 4 Opteron dual-core CPUs each up to 32 Gb main memory, 68 TB SAN disk storage, 13.9 TFlops/s peak performance: [Dei]

## 4.1 Validation

In the literature the problem of non-equilibrium Soft Matter systems - polymer solutions - and that of driven steady states is not analyzed much and, if at all, then often using molecular or Brownian dynamic simulations, see e.g. [GKK<sup>+</sup>08, HZWH08]. Recently some simulations were published [PDT03, PRDK07, DLL03], that make use of diffusion equations for non-interacting particles and dynamic density functional theory for interacting particles. Spherical obstacles are included in the polymeric solution.

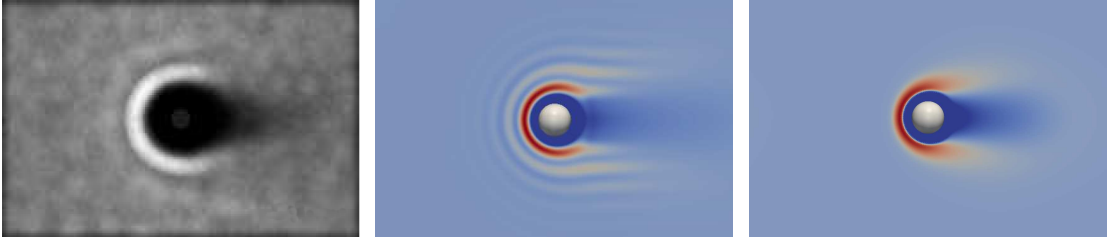


**Figure 4.1:** polymer density around a colloidal particle. Left: Brownian dynamics simulation from [HZWH08], average over 2000 snapshots, lighter colors indicate higher densities. Center: phase-field crystal simulation with  $R^* = 0.6, c^* = 0.8$  for the parameters  $r = -0.1, \bar{\varrho} = -0.3$ , right: advection-diffusion simulation with  $R^* = 0.6, c^* = 1.0$  for parameter  $\bar{\varrho} = -0.3$ . Red indicates high density whereas blue indicates low density.

In figure 4.1 a result from Brownian dynamics simulation is compared to a solution of the PFC problem P2 and to diffusion problem P1. The characteristic first density wave can be seen in each one of the pictures above. Brownian dynamics indicate more than one such wave, but the second one is less intensive, than the first one. Simple advection-diffusion does not produce further waves, though the Phase-Field Crystal simulation does. This implies that a simulation of interacting particles using the Phase-Field Crystal model reproduces more effects (properties) in the quality of the polymer solution than a diffusion model does. Figure 4.2 shows a comparison of the plot over the  $x$ -axis. There one can see the decay of density waves in the BD simulation as well as in the PFC simulation.

The authors of [PRDK07] analyze the dependency of density to radius of the colloid ( $R^* := R_p/R_c$ ), as well as density to Peclet number of the fluid (in my simulations defined as  $c^* := cR_p r/\bar{\varrho}$ , where  $c$  is the velocity of the fluid and  $r$  the temperature parameter of the PFC model). However, this is only done for ideal polymers, i.e. the non-interacting situation. We have studied the same relations for non- and interacting polymer particles. Peclet number dependency for ideal solutions can be found in figure 4.3 and the same dependency for interacting particles - Phase-Field Crystal simulations - is visualized in figure 4.4. We have plotted the density profile over the  $x$ -axis, since

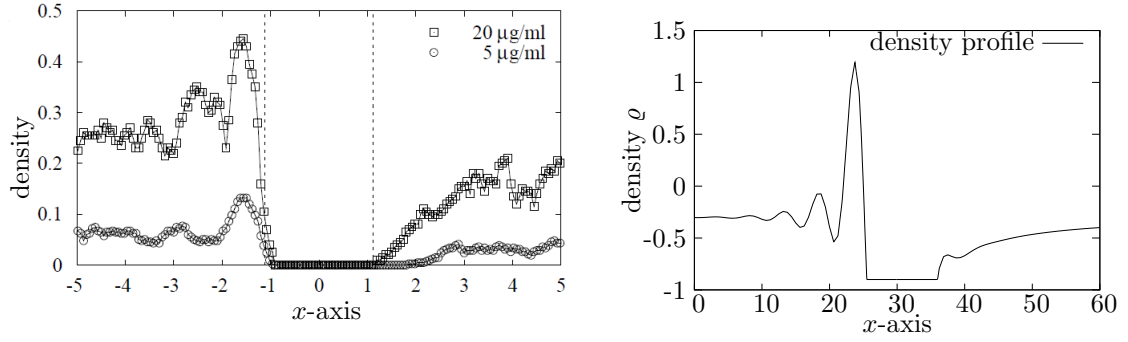


**Figure 4.2:** Plot over the  $x$ -axis. Left: Brownian dynamics simulation [GKK<sup>+</sup>08], right: Phase-Field Crystal simulation. Parameter as above. Scaling of domain and density are different in both simulations.

the fluid flows through a channel in  $x$  direction. At the inflow boundary a parabolic velocity profile is set with maximal velocity at the  $x$ -axis with norm depending of the Peclet number. The radius of the obstacle is fixed at  $R^* = 0.6$ , thus the colloid is bigger than the polymer coils.

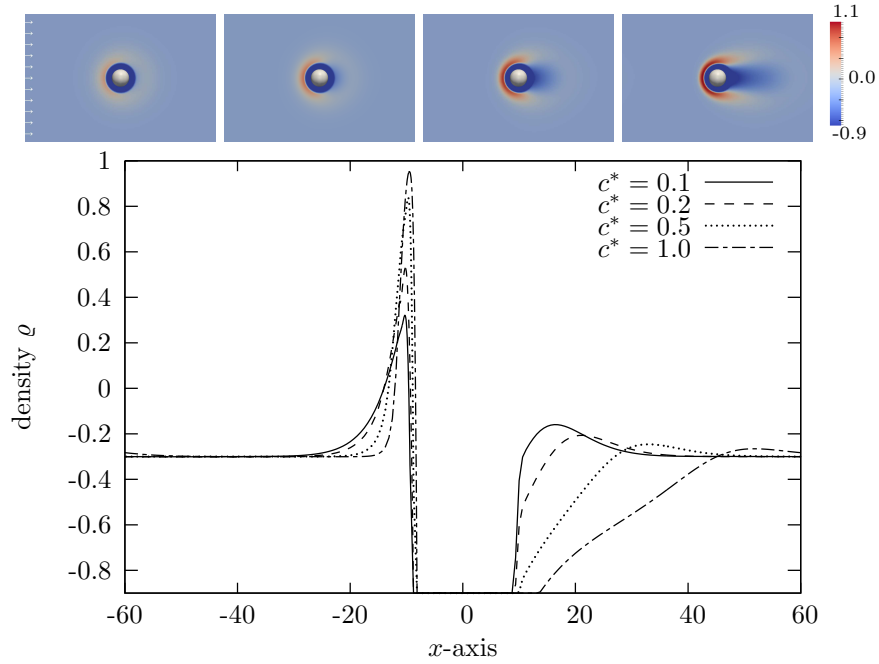


**Figure 4.3:** Density-profile of solution with non-interacting particles for different Peclet numbers of the fluid, at fixed radius  $R^* = 0.6$  of the obstacle.

The other relation of density to radius is plotted in figure 4.5, where we fixed the Peclet number at  $c^* = 0.6$ . For radii bigger than the polymer coil radius, i.e.  $R^* > 0.5$ , the density shows an additional wave behind the obstacle, whereas for smaller radii one can not see such an effect. The above simulations were performed on the Q32 computer. Since the lattice constant is fixed in the PFC model, we scaled the domain. For simulations with one spherical obstacle, like above, a domain

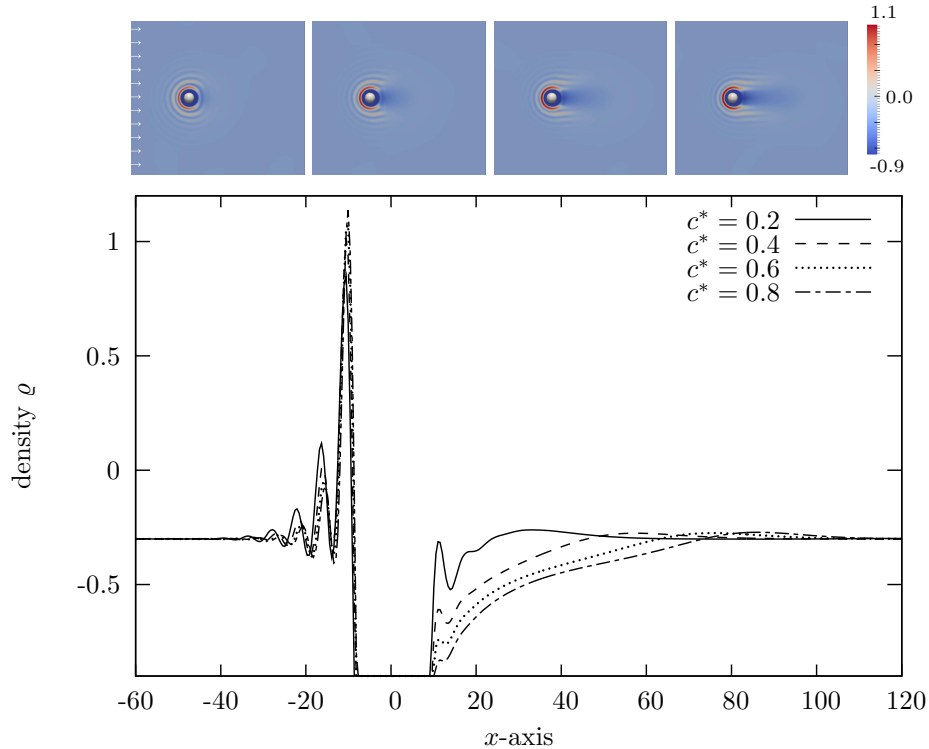


**Figure 4.4:** Density-profile of solution with interacting particles for different Peclet number of the fluid, at fixed radius  $R^* = 0.6$  of the obstacle.

of size  $120 \times 80$  was set up. Far away from the colloid - the inner boundary  $\Gamma_1$  - a grid size of  $a/5$  was used. For  $a = 2\pi/\sqrt{3}$  this gives approximately  $h = 0.72$ . Near the interface the grid size must solve the phase-transition area, that means  $h < \epsilon/5 \approx 0.06$ , for  $\epsilon := 0.3$ . In an area between the interface and a region "far" away from it, we linearly interpolate between both grid size. Thus a number of discretization points of about 80565 and a number of triangular elements of 160488 is obtained. It turns out, that a discretization of polymeric particles with 10 grid points in each dimension, that is used in [BRV07] upon others, is not sufficient to solve the first maxima near the obstacle. This first peak is much steeper than the density waves in colloidal crystals, that are analyzed in their paper.

For more obstacles the domain size must be increased so that density waves around colloids near the boundary of the domain can decay down to nearly constant density. In figure 4.6 the domain is scaled up to include 5 obstacles. The number of degrees of freedom is now on the limit that can be solved with a simple personal computer on one core. For bigger systems parallelization strategies, like domain decomposition or matrix distribution are necessary.

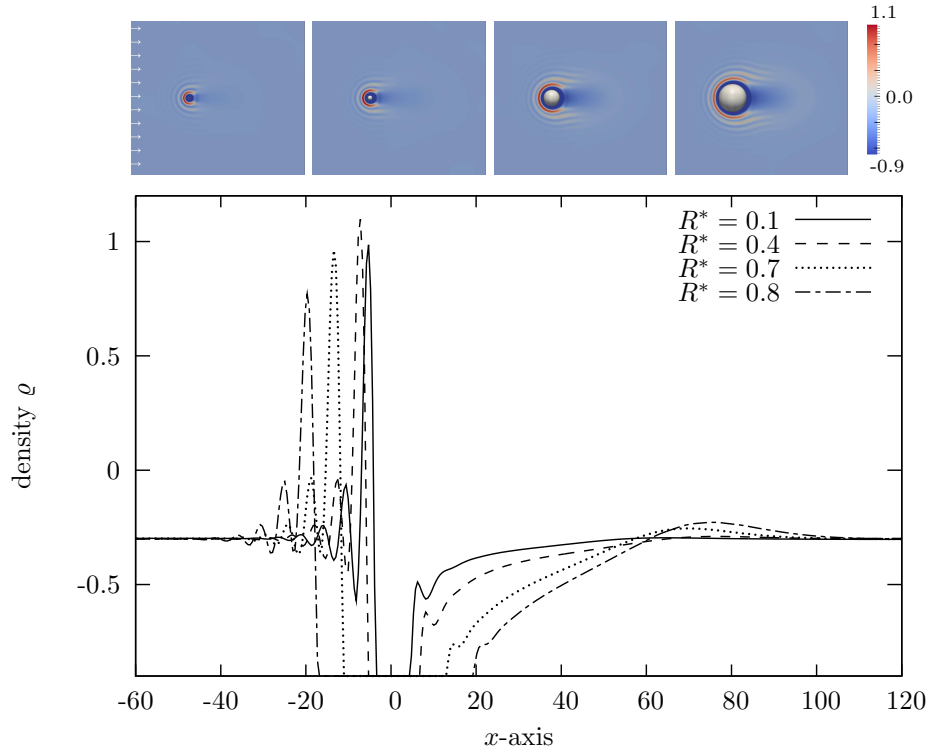


**Figure 4.5:** Density-profile of solution with interacting particles for different radii of the obstacle at constant Peclet number  $c^* = 0.6$  of the fluid.

#### 4.1.1 Validation of mathematical properties

The Phase-Field Crystal equations are an evolutionary system that minimizes the appropriate energy functional. Minimization is done via a gradient descent method. So a crucial property of the simulations is that the energy decreases over time. In figure 4.7 the energy-curve of a stationary system is plotted, i.e. the transport velocity is zero. One can see that at the end decreasing slows down very much and one has to take larger time steps to decrease the energy slightly in reasonable time.

The second mathematical property that can be analyzed easily is the conservation of density (see section 2.1.4). Due to numerical errors and the phase-field approximation we expect the density not conserve absolutely, but with small deviation. In figure 4.8 the density deviation from initial density is plotted for a system of particles in a flow field. The global deviation is of order  $10^{-4}$  and linear increasing is due to constant local deviations. For a system without flow field the deviation from initial density is very small, of order  $10^{-7}$ .

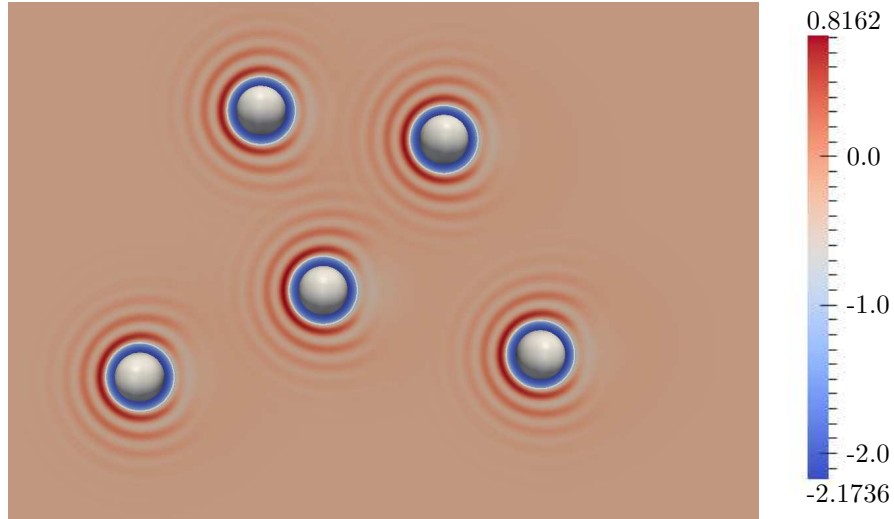


**Figure 4.6:** Five obstacles in flow field - Peclet number  $c^* = 0.2$ , density profile of polymer solution plotted. Around the spherical obstacles circles with radius  $R_p$  are plotted that indicate the area of repulsion. The simulation are performed with a grid of 374069 points and 746901 elements.

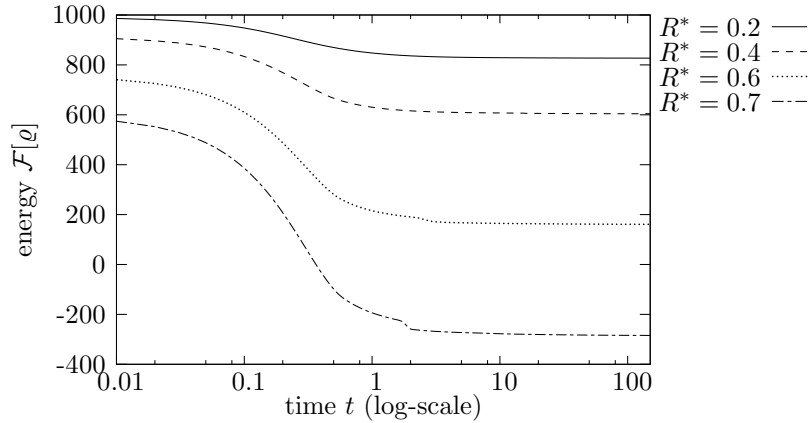


**Figure 4.7:** Energy evolution of system for  $c^* = 0$  and different radii  $R^*$ .

## 4.2 Modification of the model

As can be seen in figure 4.9 the density near the obstacle decrease deeply down to values less than  $-0.9$ . This value, that is the minimum in all plots above, is a physical boundary on the density. Since in the modeling of the PFC equations, the density is shifted and scaled, this value is negative. Physical densities are greater than zeros. By performing the shifting and scaling on the boundary of the original variable  $\rho$  one obtains the formula  $\varrho_{\min} = 3\bar{\varrho} = -0.9$  for  $\bar{\varrho} = -0.3$ . In the modeling we approximate the original evolution equation for the one-particle density (2.5) by an evolution with constant mobility, that was one assumption to obtain the standard-form of the PFC equations. With a mobility depending on the density, i.e. low mobility when density is low, the effect of unnatural

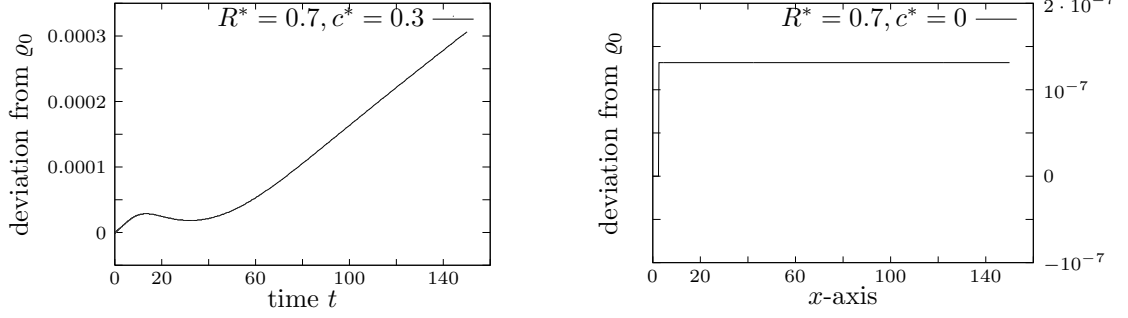


**Figure 4.8:** Deviation of the density from the initial value:  $1 - (\int_{\Omega_1} \varrho \, d\mathbf{x}) / (\int_{\Omega_1} \varrho_0 \, d\mathbf{x})$ , left:  $R^* = 0.7$ ,  $c^* = 0.3$ , right:  $R^* = 0.7$ ,  $c^* = 0$

negative densities is avoided.

To modify the standard PFC model to guarantee physical densities (scaled and shifted), different ideas can be implemented: non-constant mobility in the standard PFC model or a penalty term in the energy minimization.

#### 4.2.1 Non-constant mobility

The assumption of constant mobility enforces an approximation of the ideal solution part in the energy by a Taylor expansion around a reference density. Since this approximation also leads to comparable solutions of the diffusion part, one can perform the approximation if the mobility is not constant, as well. All other approximations and transformations are similar to the modeling of the standard equations. We obtain the PFC1-model introduced in [vTBVL09] but approximate the ideal solution term:

$$\begin{aligned}
 \partial_t \varrho + \nabla \cdot (\varrho \mathbf{u}) &= \nabla \cdot (M(\varrho) \nabla \mu) \\
 \mu &= (1+r)\varrho + \varrho^3 + 2\nu + \Delta\nu + U \\
 \nu &= \Delta\varrho
 \end{aligned} \tag{4.1}$$

where  $M(\varrho) = \frac{1}{2}(1 - \varrho/\bar{\varrho})\bar{\rho} + \bar{\rho}$ . This non-constant mobility function leads to a different Jacobian that must be used in the Rosenbrock method. For a system function  $F$  similar to (3.29), but including the mobility depending on the density, the Jacobian matrix can be written as:

$$F_Y[\mathbf{x}, t, Y, X] = \begin{pmatrix} \mathbf{n} - \Delta\mathbf{r} \\ \nabla \cdot (\mathbf{r} M'(\varrho) \nabla \mu) + \nabla \cdot (M(\varrho) \nabla \mathbf{m}) + \nabla \cdot (\mathbf{u}(\mathbf{x}, t)\mathbf{r}) \\ \mathbf{m} - (1+r)\mathbf{r} - 2\mathbf{n} - \Delta\mathbf{n} - 3\varrho^2\mathbf{r} \end{pmatrix}$$

with  $X = (\mathbf{n}, \mathbf{r}, \mathbf{m})$ ,  $Y = (\nu, \varrho, \mu)$  and  $M'(\varrho) = -\bar{\rho}/(2\bar{\varrho})$ . In the semi-implicit time-discretization one can take the mobility function explicit and the other terms like in (3.27). Ignoring the phase-field approximation, one can write the time-discrete system as

$$\begin{aligned} \frac{\varrho^{k+1} - \varrho^k}{\tau^k} &= \nabla \cdot \{M(\varrho^k) \nabla \mu^{k+1}\} + \nabla \cdot (\mathbf{u}(t_{k+1}) \varrho^{k+1}) \\ \mu^{k+1} &= (1+r)\varrho^{k+1} + 2\nu^{k+1} + \Delta \nu^{k+1} + 3\varrho^{k+1}(\varrho^k)^2 - 2(\varrho^k)^3 + U(t_{k+1}) \\ \nu^{k+1} &= \Delta \varrho^{k+1} \quad . \end{aligned} \tag{4.2}$$

Phase-Field Crystal equations with non-constant mobility can be seen as a gradient flow subject to a scalar-product with mobility, like (1.3). For the PFC energy  $\mathcal{F}$  in (2.19) this gradient flow reads

$$\partial_t \varrho = -C \operatorname{grad}_{H^{-1}, M(\varrho)} \mathcal{F}[\varrho]$$

where  $C$  is a constant depending on the scaling of the energy. For  $M(\varrho^0) > 0$  this gradient flow is a descent method. The densities  $\varrho$  which approach the lower boundary are slowed down to almost no movement and stay there. Numerically this is more tricky since the evolution of one time step can violate the property  $M(\varrho) > 0$ . This has to be taken into account, e.g. by  $M(\varrho) := \max\{10^{-8}, \frac{1}{2}(1 - \varrho/\bar{\varrho})\bar{\rho} + \bar{\rho}\}$ , and we expect the density to be bounded by the analytic lower bound only approximately.

#### 4.2.2 Penalization of low densities

The PFC equations can be seen as a minimization evolution for the functional  $\mathcal{F}$  in (2.19), using a gradient flow approach (and additional transportation by a flow field). The idea of penalization is to include an additional constrained to the problem of energy minimization, namely

$$\varrho \geq \varrho_{\min} \quad \text{in } \Omega_1 \quad .$$

Different methods to penalize the violation of such a constrained are known. We use a barrier function, that forces the density to be strictly greater than the lower bound. A logarithmic barrier function subject to the constrained above reads

$$b_\eta(\varrho) := \begin{cases} -\eta \log(\varrho - \varrho_{\min}) & \text{for } \varrho > \varrho_{\min} \\ \infty & \text{otherwise} \end{cases}$$



with  $\eta$  a small parameter that can be decreased asymptotically to zero. The modified energy functional, including the barrier function, is given by

$$\mathcal{F}[\varrho] = \int_{\Omega_1} \frac{1}{2} \varrho (r + (1 + \Delta)^2) \varrho + \frac{1}{4} \varrho^4 + \varrho U + b_\eta(\varrho) \, dx$$

with the variational derivative

$$\delta_\varrho \mathcal{F}[\varrho] = (r + (1 + \Delta)^2) \varrho + \varrho^3 + U + b'_\eta(\varrho)$$

where the derivative of the barrier function reads

$$b'_\eta(\varrho) = \begin{cases} \frac{-\eta}{\varrho - \varrho_{\min}} & \text{for } \varrho > \varrho_{\min} \\ \infty & \text{otherwise} \end{cases} .$$

In the Jacobian matrix of the Rosenbrock method the second derivative of  $b$  must be included in the component of the chemical potential  $\mu$ :

$$b''_\eta(\varrho) = \begin{cases} \frac{\eta}{(\varrho - \varrho_{\min})^2} & \text{for } \varrho > \varrho_{\min} \\ \infty & \text{otherwise} \end{cases} .$$

Semi-implicit time-discretization takes this penalization explicitly or uses a linearization around the old time step:

$$\frac{-\eta}{\varrho^{k+1} - \varrho_{\min}} \approx \eta \frac{\varrho^{k+1}}{(\varrho^k - \varrho_{\min})^2} - \eta \frac{2\varrho^k - \varrho_{\min}}{(\varrho^k - \varrho_{\min})^2}$$

The case of  $\infty$  is handled numerically by high penalization around  $10^6 - 10^{10}$ . We arrive at a semi-implicit scheme

$$\begin{aligned} \frac{\varrho^{k+1} - \varrho^k}{\tau^k} &= \Delta \mu^{k+1} + \nabla \cdot (\mathbf{u}(t_{k+1}) \varrho^{k+1}) \\ \mu^{k+1} &= (1 + r) \varrho^{k+1} + 2\nu^{k+1} + \Delta \nu^{k+1} + 3\varrho^{k+1} (\varrho^k)^2 - 2(\varrho^k)^3 + U(t_{k+1}) \\ &\quad + \eta \frac{\varrho^{k+1}}{\max\{(\varrho^k - \varrho_{\min})^2, 10^{-8}\}} - \eta \frac{2\varrho^k - \varrho_{\min}}{\max\{(\varrho^k - \varrho_{\min})^2, 10^{-8}\}} \\ \nu^{k+1} &= \Delta \varrho^{k+1} \quad . \end{aligned} \tag{4.3}$$

Penalty-methods are known to produce bad conditioned linear systems. The iterative solvers need more iterations to solve the linear system than without the penalty term.

In figure 4.9 a comparison of both modifications to the original model is visualized. The modified models produce different density profiles and maxima. Since the non-constant mobility method relies on the more physical PFC1-model and uses fewer approximations than the standard model (with(out) constraints), we would prefer this modification upon the other.

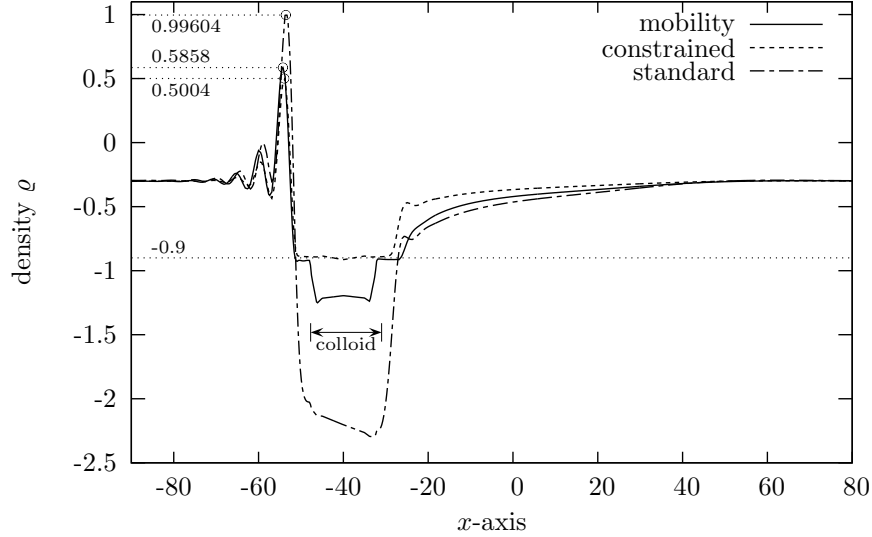


**Figure 4.9:** Simulation with three different models for  $R^* = 0.7, c^* = 0.5$ : non-constant mobility,  $\rho$ -constrained and without both modifications. As can be seen, some modification is necessary to enforce density  $\rho \gtrsim -0.9$ . In the standard-model the density falls far below the lower bound, mobility depending on the density overcome this problem, but is slightly below  $-0.9$  due to numerical reasons. The  $\rho$ -constrained approaches the lower bound but never crosses it (in the domain outside the colloid). The maxima and density profiles look quite different and it is not clear which modification is the best.

### 4.3 Depletion forces

Properties of colloid dispersion can be tuned and modified by adding polymer particles to the solvent. One way of changing the interaction between colloidal particles is by adsorption. Coating the surface of the particles with a polymer layer leads to steric repulsion. Another way of tuning the interaction is by depletion interaction.

Non-adsorbing polymer particles, or other non-adsorbing Brownian particles, are depleted in a zone

around the colloidal surface, due to a repulsive colloid-polymer interaction  $U_i$ . If the two depletion zones overlap, i.e. two colloidal particles are positioned close to each other, a free energy gain

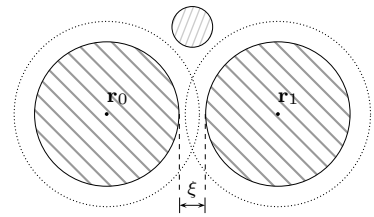


**Figure 4.11:** System of two colloidal particles with gap of width  $\xi$ . The third smaller particle indicates the size of a polymer coil.

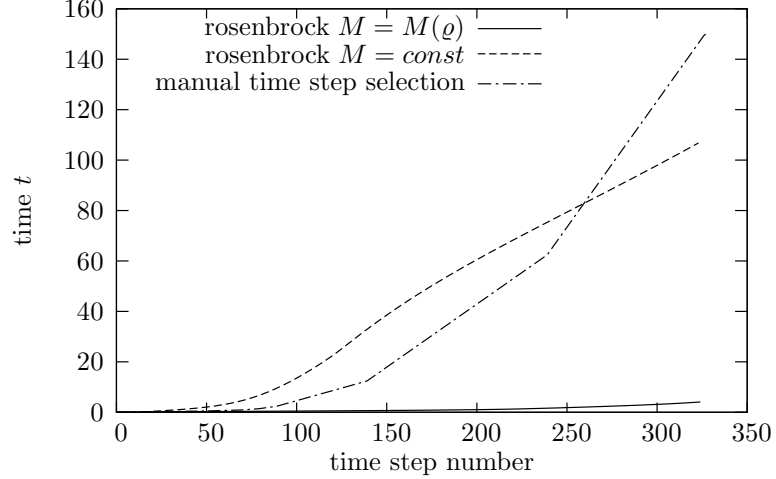


**Figure 4.10:** Comparison of time step widths obtained by Rosenbrock time step control for the PFC model with constant mobility, non-constant mobility modification and time step pre-selection used for semi-implicit time-discretization, where the increase of time step is set by numerical experiment. All Rosenbrock simulations were performed with the same time tolerance  $10^{-4}$ , for  $R^* = 0.7, c^* = 0.5$ . The scaling of time step width in the non-constant mobility case is much worth than with constant mobility. Additional techniques, e.g. combination of fixed time steps and automatic scaling, are necessary for an efficient method.

of the polymers relative to the situation with separated colloids results in an effective attraction between the particles. The region of depletion is of order  $a$ , the width of the colloid-polymer interaction region. A system of two colloidal particles is visualized schematically in figure 4.11.

For positions  $\mathbf{r}_i, i = 0, 1$  of the colloids, the width of the gap  $\xi$  between the particles is defined by

$$\xi = \|\mathbf{r}_1 - \mathbf{r}_0\| - 2R_h \quad .$$

The *effective force* between (soft interacting) colloids can be found as the integral expression for each colloid  $i$ , as

$$\mathbf{F}_{\text{eff},i} := - \int_{\Omega_1} \rho \nabla V_{1,i} \, d\mathbf{x} = - \frac{k_B T \bar{\rho}}{144 \bar{\varrho}^3} \int_{\Omega_1} \left( 3 - \frac{\varrho}{\bar{\varrho}} \right) \nabla U_i \, d\mathbf{x} = \frac{k_B T \bar{\rho}}{144 \bar{\varrho}^4} \int_{\Omega_1} \varrho \nabla U_i \, d\mathbf{x}$$

since  $U_i|_{\Gamma_1} \approx 0$ . The derivation can be found in [GED97] (equations 2.4 and A4). For the special case of hard spherical particles, the gradient of the external potential is not defined in the classical sense any more. In the limit one gets the formula

$$\mathbf{F}_{\text{eff},i}^{\text{HS}} := k_B T \int_{S_i} \rho \hat{\mathbf{n}}_i \, ds = \frac{k_B T \bar{\rho}}{2} \int_{S_i} \left( 3 - \frac{\varrho}{\bar{\varrho}} \right) \hat{\mathbf{n}}_i \, ds$$

where  $S_i$  describes the surface of a sphere with radius  $R_p$  and center  $\mathbf{r}_i$  and  $\hat{\mathbf{n}}_i$  the unit normal vector pointing outwards from this sphere. In a model where we assume hard core interactions between the colloids and between colloids and polymers and non-interacting spherical polymers, the effective interaction can be described by the Asakura-Oosawa model and is proportional to the overlapping volume of the depletion zones. The resulting force is attractive for  $\xi < 2a$  and repulsive otherwise.

The effective forces correspond to the so-called *depletion forces* in the equilibrium case, in absence of a flow field. The authors of [DLL03] study the non-equilibrium case by subtracting the drift forces induced by a flow field on a single colloid from the effective forces. The *drift force* can be calculated by the same formula as above, but with only one colloid present in the system (see figure 4.14 for a relation of Peclet number to drift force). As a result the depletion forces simplify to

$$\mathbf{F}_{\text{depl},i} := \mathbf{F}_{\text{eff},i}(\varrho) - \mathbf{F}_{\text{eff},i}(\varrho^{[1]}) = \frac{k_B T \bar{\rho}}{144 \bar{\varrho}^4} \int_{\Omega_1} (\varrho - \varrho^{[1]}) \nabla U_i \, d\mathbf{x}$$

where  $\varrho^{[1]}$  is the density field, obtained by considering only one colloid. In a similar way the formula for the hard sphere depletion force can be calculated.

In the article above an idealized case of non-interacting polymers was studied and density for a system with two colloidal particles is calculated by a dynamical superposition approximation:

$$\rho(\mathbf{x}) \approx \rho^{[1]}(\mathbf{x} - \mathbf{r}_0) \rho^{[1]}(\mathbf{x} - \mathbf{r}_1) / \bar{\rho}$$

This principle of superposition is applicable for the equilibrium case in absence of a flow field and used as an approximation for the dynamical case, as well. It is not clear whether this superposition works for interacting bath particles also, obtained by our PFC simulation, so we simulate a system with two obstacles directly and use fewer approximations. In the figures 4.13, 4.15 and 4.16 the superposition method is compared to the case of direct simulations. As can be seen in the plots of the depletion

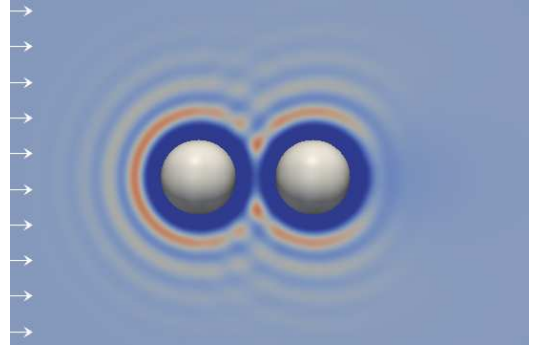


**Figure 4.12:** System of two colloidal particles in a flow field with direction from left to right.

forces, superposition and simulation results in similar curves but with different scalings. This leads to qualitative different forces. Additional pass through the zero line, i.e. change in the direction of the force, is not present in the simulation of depletion forces in equilibrium situation (figure 4.15). The sum of the forces acting on both colloids separately shows a qualitative difference, too. But, since

the simulation results do not produce a smooth curve, the values and the second conflict has to be taken with a pinch of salt. The key conclusion of simulations of depletion forces in non-equilibrium is the long-ranged structure of the attractive force.

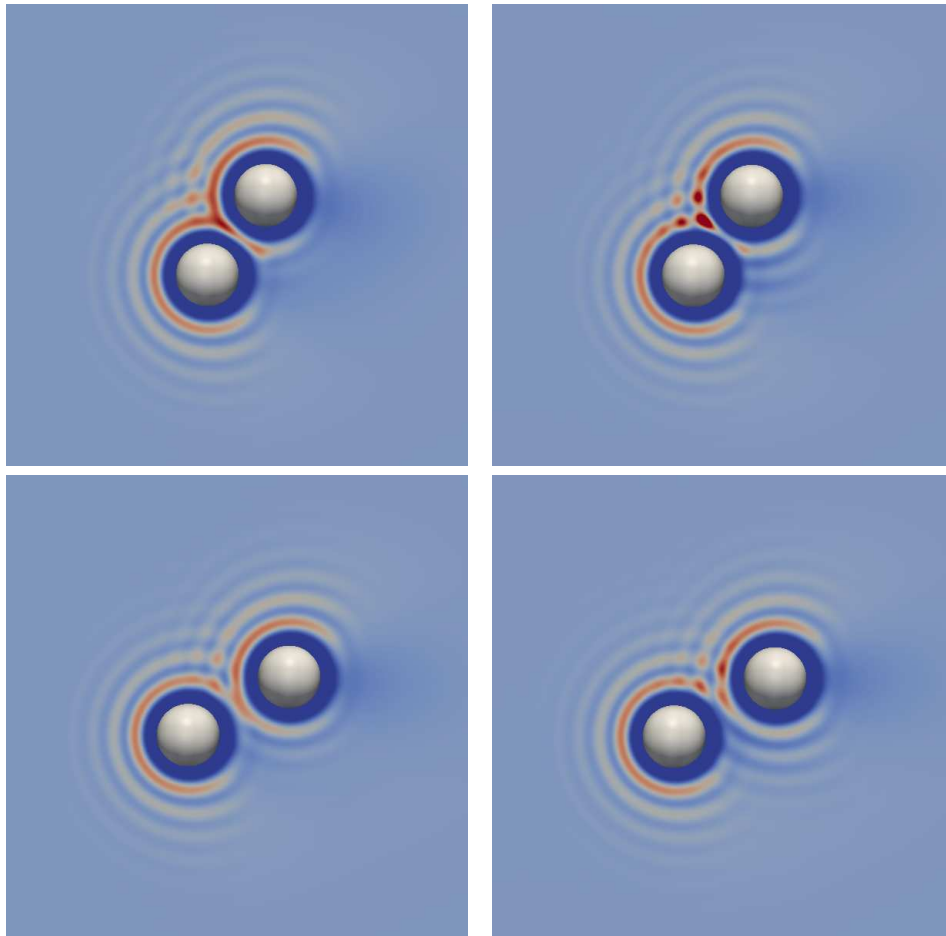


**Figure 4.13:** Comparison of direct simulation and superposition of simulation with one colloid only, for parameters  $R^* = 0.7$ ,  $c^* = 0.3$ . Left: direct simulation, right: superposition, top and bottom: different positions of colloidal particles.

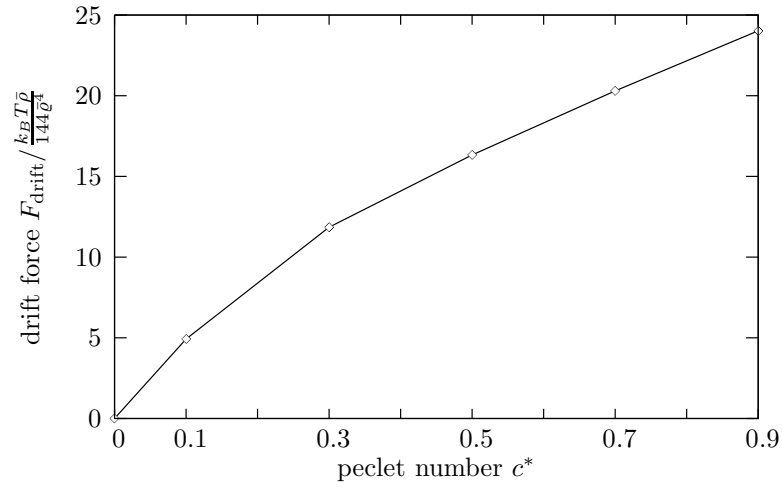


**Figure 4.14:** Drift force acting on a single colloid with radius  $R^* = 0.7$ , depending on the Peclet number of the fluid. For non-flowing solutions, i.e.  $c^* = 0$ , this force is zero because of the rotational symmetry of the density field.

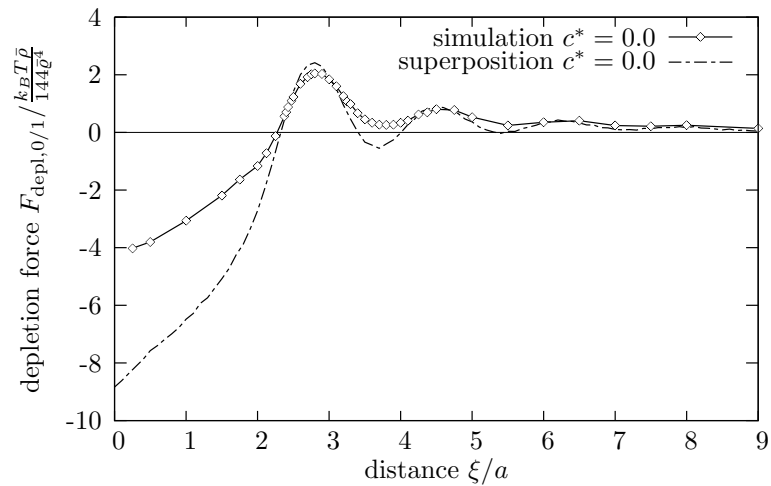


**Figure 4.15:** Depletion forces acting on one colloidal particle in the presence of a second one at a distance  $\xi$ . The  $x$ -component is plotted only and the distance is scaled by the radius of the polymer coils  $a$ . Negative forces indicate an attractive force between the particles. Dots mark performed simulations. The depletion force is symmetric with respect to the colloids.

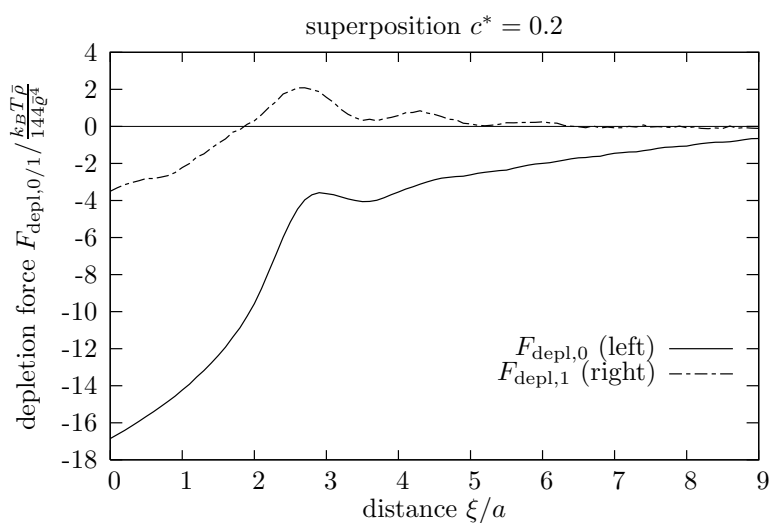


**Figure 4.16:** Depletion forces acting on one colloidal particle in the presents of a second one in a distance  $\xi$ . Both particles are positioned on the  $x$ -axis, i.e. behind each other. The  $x$ -component is plotted only and the distance is scaled by the radius of the polymer coils  $a$ . The simulations in the flow field are obtained by a superposition method.

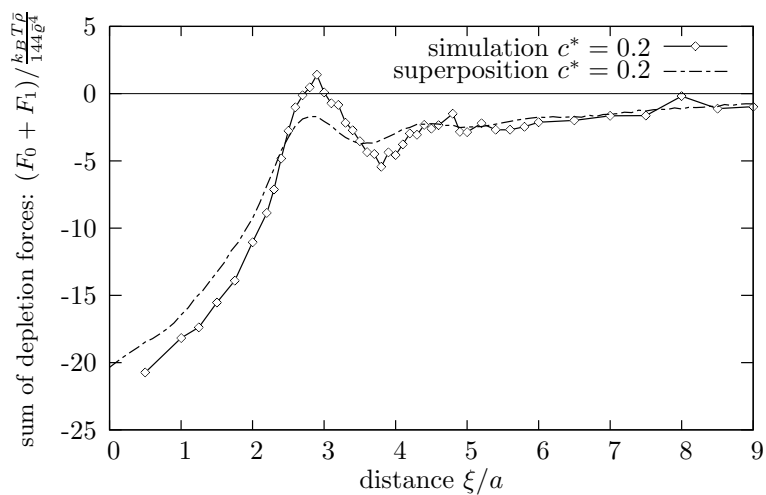


**Figure 4.17:** Depletion forces acting on one colloidal particle in the presents of a second one in a distance  $\xi$ . Both particles are positioned on the  $x$ -axis, i.e. behind each other. The  $x$ -component is plotted only and the distance is scaled by the radius of the polymer coils  $a$ . The sum over the forces on both colloids is visualized. A simulation obtained by a superposition method is compared to the direct simulation of two colloids.

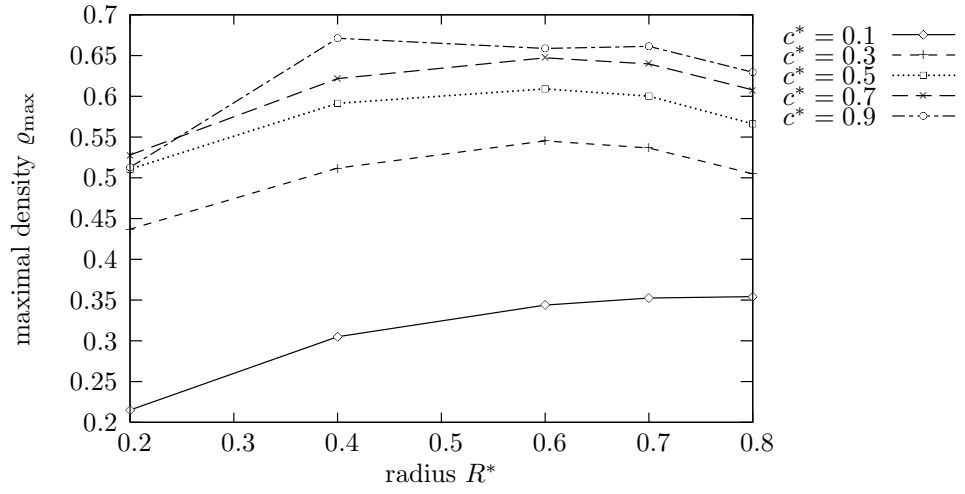


**Figure 4.18:** Maximal values of the density-field  $\rho$  depending on the Peclet number of the fluid  $c^*$  for different radii  $R^*$ .

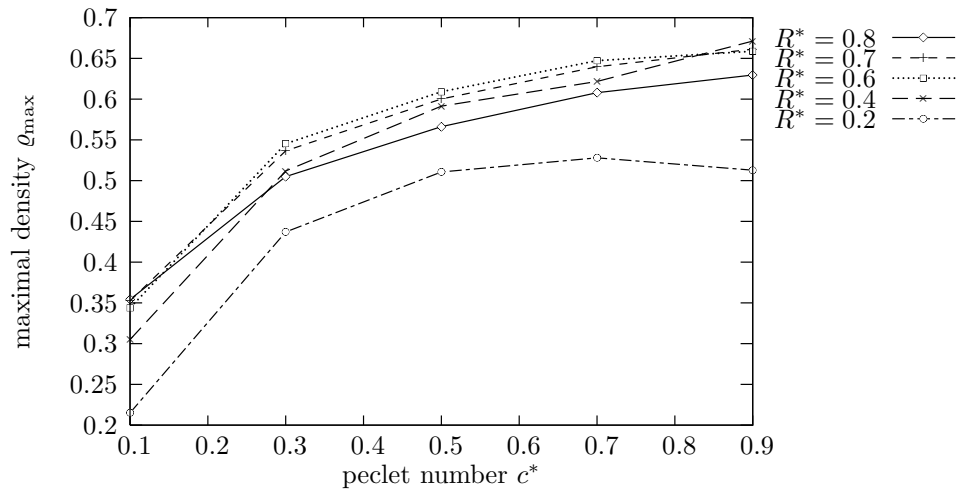


**Figure 4.19:** Maximal values of the density-field  $\rho$  depending on the radius  $R^*$  for different Peclet numbers of the fluid  $c^*$ .



# Chapter 5

## Conclusion and Outlook

### 5.1 Conclusion

We have presented, derived and analyzed the Phase-Field Crystal model to describe interacting particles in a flowing solvent. The interesting situation of additional obstacles in the domain was treated by a diffuse domain ansatz and repulsive potentials in the equations. A weak coupling to Navier-Stokes simulations for the flowing bath where the particles are immersed in and the coupling to a motion of the obstacles was explained. Numerical solutions of the resulting equations were obtained by different discretization schemes in time - semi-implicit Euler method and Rosenbrock-method - and Finite Element discretization in space. Finally simulations were performed to validate the model and compare results to a few calculations found in the literature.

In conclusion we can say that the Phase-Field Crystal model can describe some phenomena of particles in flowing solvents in the presence of obstacles. However, the standard form of the PFC equation can not be used to obtain quantitative results. Because of the external potential, the density gets unphysical values near the obstacles that influence the complete density profile. The further the lower the minima at the colloids fall, the higher is the next maxima. So no relations between maxima, depending on different radii for the obstacles, make sense with the standard model. The minima can not be controlled without further modifications. These changes in the model were explained and added to the equations and simulations with more physical minima were performed. Nevertheless, it remains unclear which model is the best since different modifications produce different results. Further comparisons with own dynamic density functional simulations must be done, to get more rigorous clarification. The mobility modifications lead to bad behavior of the time control

of the Rosenbrock method. The mobility fluctuates at the beginning of the simulations throughout the domain. This produces high time step errors or bad error estimates. Further studies and modifications are necessary to obtain more efficient time stepping control mechanisms.

Diffuse domain approach was applied to both, Phase-Field Crystal equations and Navier-Stokes equations, to describe the obstacles not part of the domain. This leads to fine meshes around the colloids and coarse meshes inside the obstacles. The motion of the fluid can be described with this phase-field approach and boundary conditions for moving obstacles can be included easily. In the PFC model the colloids are described by a repulsive potential in addition to the cut out of the domain via phase-field multiplication. So perhaps the diffuse domain extension is not necessary to describe obstacles in the density field. An alternative to diffuse domain for the Navier-Stokes equation is an immersed boundary method that seems to be an efficient method for complex (moving) domains. So an extension of the proposed model could be the coupling of different meshes for Navier-Stokes and Phase-Field Crystal and different techniques to describe the obstacles. This could possibly lead to a more efficient solver. Recently an extension to the Finite-Element toolbox AMDiS was published ([VW10]), that implements a multi-mesh method to handle different meshes for different quantities effectively. Further modifications could be to take different Finite Elements for Navier-Stokes and Phase-Field Crystal equations, as it has been shown that for the PFC system higher order elements lead to faster convergence.

Depletion forces were calculated using direct simulation of a flow field around two spherical obstacles, i.e. colloidal particles, and simulation of interacting Brownian bath particles, i.e. soft particles as an approximation to polymer coils, by Phase-Field Crystal equations. The results were compared to a superposition approach, that uses calculation of flow field and density profile around one obstacle and superposing this result at different distances of the obstacles. We found qualitative differences to direct simulations in the equilibrium case, i.e. zero solvent velocity, and assume qualitative differences in the non-equilibrium situation, as well. The last one needs additional consideration, since the simulation results show errors in the calculation of the forces.

At the moment the simulation of a high number ( $N \gg 100$ ) of Brownian particles using the Phase-Field Crystal method is quite expensive. Using domain-decomposition techniques (for AMDiS see [VW10]) parallelization in space can lead to higher particle numbers. Parallelization of matrix assemblage improves the performance not very much. The simulation of colloidal particles in the polymer solution using diffuse domain methods is also not very efficient and restricted to a very small number of colloids. So only considerations of specific behavior, e.g. calculation of forces induced by polymer particles on the colloids, make sense. The simulation of a system of many colloids mediated

by Brownian particles need other methods, than the proposed ones.

## 5.2 Outlook

As it was stated in the physical modeling, different assumptions were necessary to obtain these simple Phase-Field Crystal equations. Hydrodynamic interactions were neglected completely, for example. Recently the dynamic density functional theory was extended to include approximations to the hydrodynamic interactions ([RL08]), that could lead more realistic behavior than no such influence. To include this derivations in the Phase-Field Crystal approximations, some work has to be done. Their main idea is to extend the evolution equation (2.8) of density functional theory by two terms including two hydrodynamic interaction tensors  $\boldsymbol{\omega}_{11}, \boldsymbol{\omega}_{12}$ , that approximate the diffusion tensor

$$\mathbf{D}_{ij}(\vec{\mathbf{r}}) \approx D_0 \left( \mathbb{I} \delta_{ij} + (1 - \delta_{ij}) \boldsymbol{\omega}_{12}(\mathbf{r}_i - \mathbf{r}_j) + \delta_{ij} \sum_{k \neq i} \boldsymbol{\omega}_{11}(\mathbf{r}_i - \mathbf{r}_k) \right)$$

where  $D_0$  denotes the diffusion constant of a single particle. For the Rothne-Prager approximation we could write

$$\boldsymbol{\omega}_{11}(\mathbf{r}) = 0, \quad \boldsymbol{\omega}_{12}(\mathbf{r}) = \frac{3}{8} \frac{\sigma}{\|\mathbf{r}\|} (\mathbb{I} + \mathbf{r} \otimes \mathbf{r}) + \frac{1}{16} \left( \frac{\sigma}{\|\mathbf{r}\|} \right)^3 (\mathbb{I} - 3\mathbf{r} \otimes \mathbf{r})$$

with  $\sigma$  the hydrodynamic diameter and  $\otimes$  the dyadic product. The evolution equation for the one-particle density can then be written as

$$\frac{k_B T}{D_0} \partial_t \rho(\mathbf{r}, t) = \nabla \cdot \left( \rho(\mathbf{r}, t) \nabla \frac{\delta \mathcal{F}[\rho(\mathbf{r}, t)]}{\delta \rho(\mathbf{r}, t)} + \mathbf{j}_2 + \mathbf{j}_3 \right) \quad (5.1)$$

where we have neglected the advection term, with additional fluxes

$$\begin{aligned} \mathbf{j}_2 &= \int \rho^{(2)}(\mathbf{r}, \mathbf{r}', t) \boldsymbol{\omega}_{11}(\mathbf{r} - \mathbf{r}') \cdot \nabla \frac{\delta \mathcal{F}[\rho(\mathbf{r}, t)]}{\delta \rho(\mathbf{r}, t)} d\mathbf{r}' \\ &\approx \int \rho(\mathbf{r}, t) \rho(\mathbf{r}', t) g(\|\mathbf{r} - \mathbf{r}'\|, \bar{\rho}) \boldsymbol{\omega}_{11}(\mathbf{r} - \mathbf{r}') \cdot \nabla \frac{\delta \mathcal{F}[\rho(\mathbf{r}, t)]}{\delta \rho(\mathbf{r}, t)} d\mathbf{r}' \\ \mathbf{j}_3 &= \int \rho^{(2)}(\mathbf{r}, \mathbf{r}', t) \boldsymbol{\omega}_{12}(\mathbf{r} - \mathbf{r}') \cdot \nabla \frac{\delta \mathcal{F}[\rho(\mathbf{r}', t)]}{\delta \rho(\mathbf{r}', t)} d\mathbf{r}' \\ &\approx \int \rho(\mathbf{r}, t) \rho(\mathbf{r}', t) g(\|\mathbf{r} - \mathbf{r}'\|, \bar{\rho}) \boldsymbol{\omega}_{12}(\mathbf{r} - \mathbf{r}') \cdot \nabla \frac{\delta \mathcal{F}[\rho(\mathbf{r}', t)]}{\delta \rho(\mathbf{r}', t)} d\mathbf{r}' \quad . \end{aligned}$$

Here  $g(\|\mathbf{r}-\mathbf{r}'\|, \bar{\rho})$  denotes the pair correlation function for a system with average density  $\bar{\rho}$ . Analytic expressions for  $g$  are available in the literature (see the references in [RL08]).

For the extension of Phase-Field Crystal equations to hydrodynamic interactions, we have to find good approximations to the integral expressions in  $\mathbf{j}_2, \mathbf{j}_3$ , maybe similar to the approximation of the direct correlation function  $c^{(2)}$  in the original model.

## 5.3 Anisotropic PFC

Recently extensions to the classical PFC model were proposed in the direction of oriented, ellipsoidal particles. Phenomenological description, by coordinate-transformation of the derivatives, was done by Backofen and Voigt et.al., whereas Löwen et.al. [Löw10, WLB10] derived a Phase-Field Crystal model for liquid crystals from density functional theory for liquid crystals that has been known for a while. Both ideas are based on the relaxation of an orientation field and couple this with the PFC energy minimization. For the dynamics of rod-like particles see [Dho98], for example. Liquid crystals were studied in [PJ95] among many others and a summary can be found in [And06].

### 5.3.1 Transformed PFC-energy

First results were obtained with the method of Backofen, that is described here. The basic idea is a coordinate-transform of the Laplacian in direction  $d$  with  $\|d\| = 1$ . A general Laplace-Beltrami operator can be written in the form  $\frac{1}{\sqrt{g}}\nabla\cdot(\sqrt{g}G^{-1}\nabla\cdot)$ . Consider stretching and rotation as coordinate transform  $T := R(d) \circ S(k)$ , with scaling-matrix  $S$  and rotation-matrix  $R$ : i.e.

$$S(k) := \begin{pmatrix} 1 & 0 \\ 0 & k \end{pmatrix}, \quad R(d) := \|d\|^{-1} \begin{pmatrix} d_1 & d_0 \\ -d_0 & d_1 \end{pmatrix}$$

the inverse transformation  $T^{-1}$  defines a mapping  $\mathbf{x} \mapsto T^{-1}\mathbf{x}$  with image  $t(\mathbf{x})$ . A metric tensor defined by this transformation can be obtained

$$\begin{aligned} G &:= (\partial_i t_k \partial_j t_k)_{ij} \\ G^{-1} &= \frac{1}{\|d\|^2} \begin{pmatrix} k^2 d_0^2 + d_1^2 & d_0 d_1 (k^2 - 1) \\ d_0 d_1 (k^2 - 1) & d_0^2 + k^2 d_1^2 \end{pmatrix} \\ g &:= |\det(G)| = \frac{1}{k^2} \quad . \end{aligned} \tag{5.2}$$

The anisotropic PFC-energy is made up of the PFC-energy by transformation of  $\Delta$  to  $\nabla \cdot (G^{-1}\nabla\circ)$ :

$$\mathcal{F}^{\text{apfc}}[\varrho, d] := \int_{\Omega} \frac{1}{4}\varrho^4 + \frac{1}{2}\varrho[r + (1 + \nabla \cdot (G(d)^{-1}\nabla\circ))^2]\varrho + \varrho U \, \mathbf{d}\mathbf{x} \quad .$$

It follows for the variational derivative of  $\mathcal{F}^{\text{apfc}}$  with respect to  $\varrho$ :

$$\begin{aligned} \delta_{\varrho}\mathcal{F}^{\text{apfc}}[\varrho, d] &= \varrho^3 + (r+1)\varrho + 2\nabla \cdot (G(d)^{-1}\nabla\varrho) + \nabla \cdot (G(d)^{-1}\nabla(\nabla \cdot (G(d)^{-1}\nabla\varrho))) + U \\ &= \varrho^3 + (r+1)\varrho + 2\Delta_G\varrho + \Delta_G^2\varrho + U \quad \text{with} \quad \Delta_G := \nabla \cdot (G(d)^{-1}\nabla\circ) \quad . \end{aligned} \quad (5.3)$$

### 5.3.2 Modeling of nematic liquid crystals

Oseen and Frank introduced the following energy-density to describe the orientation of liquid crystals (e.g. [AG97],[And06],[MZ10]):

$$f_{OF}(d) := \frac{1}{2}\kappa_1(\nabla \cdot d)^2 + \frac{1}{2}\kappa_2(d \times (\nabla \times d))^2 + \frac{1}{2}\kappa_3(d \cdot (\nabla \times d))^2 \quad \text{with} \quad \|d\| = 1 \quad (5.4)$$

where  $\kappa_1, \kappa_2$  and  $\kappa_3$  are (positive) material constants for influence of different types of deformations, that can occur: splay, bend and twist.

For the special case  $\kappa_1 = \kappa_2 = \kappa_3 =: \kappa$  the energy-density  $f_{OF}$  reduces to the *one constant approximation*, the so-called Harmonic mapping case, that has been studied in great depth in [Alo97, Shk02, Ura93, AG97].

$$f_{OF}^{(1)}(d) := \frac{\kappa}{2}\|\nabla d\|_F^2 = \frac{\kappa}{2}\text{tr}(\nabla d \cdot \nabla d^T) \quad . \quad (5.5)$$

This is also known as Dirichlet energy density for the director  $d$ . If we want to handle the constraints of the Oseen-Frank-functional  $\|d\| = 1$ , we could do this with a penalty-approach. We get an energy similar to Ginzburg-Landau-functional:

$$\mathcal{F}_{OF,\epsilon} = \int_{\Omega} \frac{\kappa}{2}\|\nabla d\|^2 + \frac{1}{4\epsilon^2}(\|d\|^2 - 1)^2 \, \mathbf{d}\mathbf{x}, \quad \epsilon \in \mathbb{R}^+ \quad .$$

The  $L^2$ -gradient flow of this energy is a system of equations with parameter  $\epsilon > 0$

$$\partial_t d = -\delta_d \mathcal{F}_{OF,\epsilon}[d] = \kappa \Delta d - \frac{1}{\epsilon^2}(\|d\|^2 - 1) d \quad . \quad (5.6)$$

The existence of critical points of  $\mathcal{F}_{OF,\epsilon}$  on more general Riemannian manifolds with  $\epsilon$  sufficiently

small and the convergence  $\mathcal{F}_{OF,\epsilon} \xrightarrow{\epsilon \rightarrow 0} \mathcal{F}_{OF} = \int_{\Omega} \frac{\kappa}{2} \|\nabla d\|^2 dx$  is shown in [Mes09]. The last equation (5.6) contains a nonlinear term that will be linearized in order to solve this evolution equation numerically

$$\frac{1}{\epsilon^2} (\|d\|^2 - 1) d \approx \frac{3}{\epsilon^2} \|d^{\text{old}}\|^2 d - \frac{2}{\epsilon^2} \|d^{\text{old}}\|^2 d^{\text{old}} - \frac{1}{\epsilon^2} d \quad . \quad (5.7)$$

Combination of  $\mathcal{F}^{\text{apfc}}$  and Ginzburg-Landau energy  $\mathcal{F}_{OF,\epsilon}$  gives new "weak" energy of anisotropic Phase-Field Crystals

$$\mathcal{F}_{\epsilon}^{\text{apfc}}[\varrho, d] = \int_{\Omega} \frac{\kappa}{2} \|\nabla d\|^2 + \frac{1}{4\epsilon^2} (\|d\|^2 - 1)^2 + \frac{1}{4} \varrho^4 + \frac{1}{2} \varrho [r + (1 + \Delta_G)^2] \varrho + \varrho U dx \quad .$$

Variational derivatives of this energy with respect to  $\varrho$  are similar to (5.3), for derivative with respect to  $d$  one gets

$$\delta_d \mathcal{F}_{\epsilon}^{\text{apfc}}[\varrho, d] = -\kappa \Delta d + \frac{1}{\epsilon^2} (\|d\|^2 - 1) d - [\nabla \varrho \cdot ([G_{d_i}] (\nabla \varrho + \nabla \nu))]_i \quad . \quad (5.8)$$

The derivative of  $G^{-1}$  in direction  $d$  is a tensor of grade 3:

$$\begin{aligned} \partial_d (G^{-1}) &= [\partial_{d_i} (G^{-1})]_i =: [G_{d_i}]_i \\ G_{d_0} &= \frac{k^2 - 1}{\|d\|^4} \begin{pmatrix} 2d_0 d_1^2 & -d_1 (d_0^2 - d_1^2) \\ -d_1 (d_0^2 - d_1^2) & 2d_0 d_1^2 \end{pmatrix}, \\ G_{d_1} &= \frac{k^2 - 1}{\|d\|^4} \begin{pmatrix} -2d_0^2 d_1 & d_0 (d_0^2 - d_1^2) \\ d_0 (d_0^2 - d_1^2) & 2d_0^2 d_1 \end{pmatrix} \end{aligned}$$

and multiplied by the vector  $\nabla \varrho$  gives a matrix.

The evolution equation that follows from this variational derivative, using an  $L^2$ -gradient flow approach gives the system

$$\partial_t d = \kappa \Delta d - \frac{1}{\epsilon^2} (\|d\|^2 - 1) d + [\nabla \varrho \cdot ([G_{d_i}(d)] (\nabla \varrho + \nabla \nu))]_i \quad . \quad (5.9)$$

A first discretization approach uses semi-implicit Euler method for time-discretization, where the nonlinear term is treated by the (5.7) and the matrices  $G_{d_i}$  are taken explicitly. We arrive at

$$\frac{d^{k+1} - d^k}{\tau^k} = \kappa \Delta d^{k+1} - \frac{3}{\epsilon^2} \|d^k\|^2 d^{k+1} + \frac{2}{\epsilon^2} \|d^k\|^2 d^k + \frac{1}{\epsilon^2} d^{k+1} + [\nabla \varrho^k \cdot ([G_{d_i}(d^k)] (\nabla \varrho^k + \nabla \nu^k))]_i \quad . \quad (5.10)$$

Depending on the coupling to the evolution of  $\varrho$  in the last term  $\varrho^k$  or  $\nu^k$  can be replaced by  $\varrho^{k+1}$  or  $\nu^{k+1}$  accordingly.

### 5.3.3 Simulation of stretched particles

Some simulations were done using the anisotropic PFC model but the results need further consideration. The first example in figure 5.1 shows a Phase-Field Crystal simulation in a circle  $\Omega_1$  described as diffuse domain using boundary conditions to force normal orientation on the boundary  $\partial\Omega_1$ .

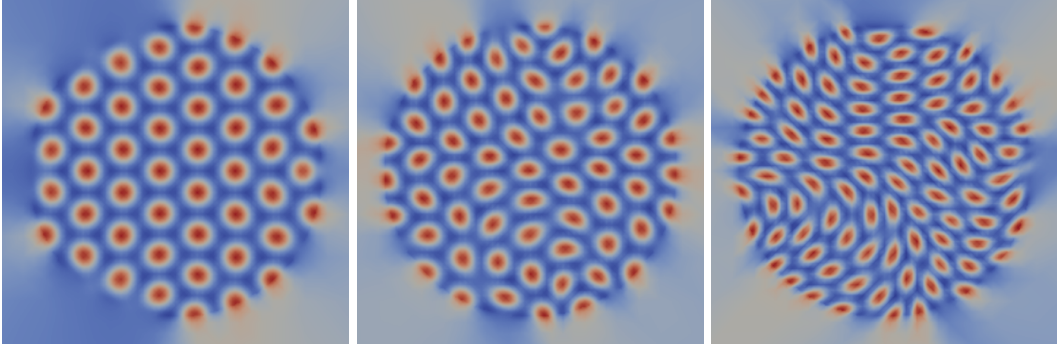


**Figure 5.1:** Snapshots of anisotropic Phase-Field Crystal simulation in solid parameter regime for different scaling factors  $k$ . Left:  $k = 1$ , center:  $k = 1.5$ , right:  $k = 2$ .

Performing similar simulations in a liquid parameter regime, this time the domain  $\Omega_1$  is similar to the one in figure 3.1, gives different behavior for normal and tangential oriented particles at the boundary. Snapshots of the density profile can be seen in figure 5.2 and a comparison using different scaling factors  $k$  of plots of the  $x$ -axis is shown in figure 5.3.

Flowing liquid crystal particles can be modeled by liquid crystal flows (e.g. [LSY07]) by including a transport term in the evolution equation (5.9):

$$\partial_t d + \mathbf{u} \cdot \nabla d = \kappa \Delta d - \frac{1}{\epsilon^2} (\|d\|^2 - 1) d + [\nabla \varrho \cdot ([G_{d_i}] (\nabla \varrho + \nabla \nu))]_i \quad . \quad (5.11)$$

First results for a flow around a spherical obstacle can be seen in figure 5.4.

The extension of the Phase-Field Crystal model to stretched particles is very new. Various interesting questions arise, for example dependency of orientation, stretching factor to depletion forces between obstacles, defect dynamic in the liquid crystal field depending on Phase-Field Crystal particle interactions and obstacles. A more rigorous modeling of rigid particles was done by [Löw10] recently and includes an additional order parameter. Since modeling of liquid crystals without coupling to Phase-Field Crystal equations is yet a difficult and complex problem, this coupling

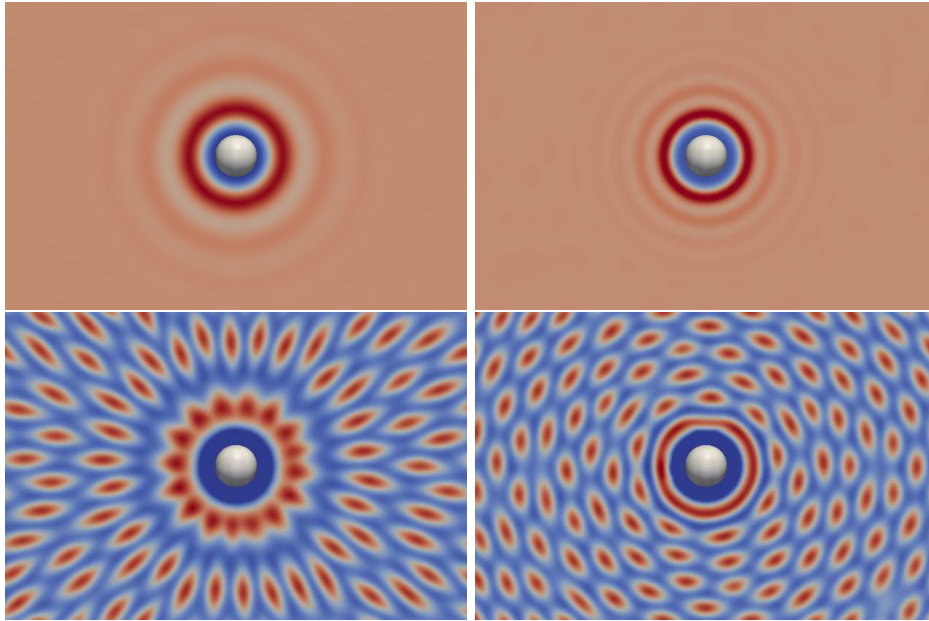


**Figure 5.2:** Simulation of liquid crystal particles with normal (left) or tangential (right) orientation on the boundary of the colloid. Top: liquid parameter regime, bottom: solid parameter regime.

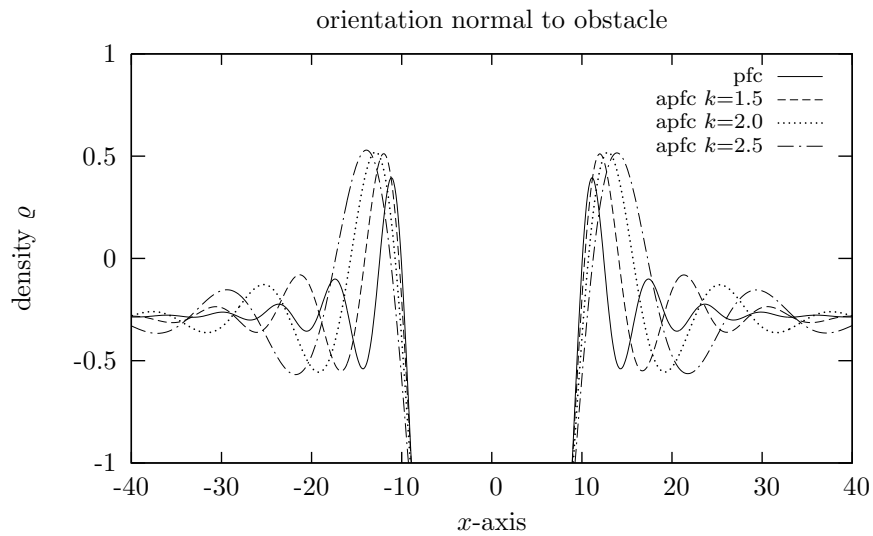


**Figure 5.3:** Comparison between isotropic and anisotropic PFC solution for different stretching parameters  $k$ , with normal director-field.

needs to be done very carefully and many questions concerning boundary conditions near obstacles, influence of attractive or repulsive potentials for the obstacles to the orientation of the liquid crystals, has to be answered. So it remains open for further research.



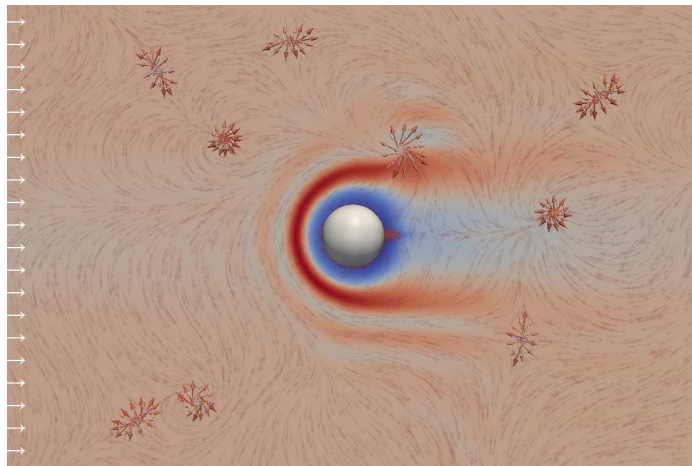


**Figure 5.4:** Simulation of liquid crystal particles flowing around spherical obstacle. Defects in the director field are highlighted.

# Appendix A

## Solution Theory

For existence and uniqueness of solutions of evolutionary equations a wide range of theories is available in literature. One class of equations, called *linear material laws*, is analyzed by Rainer Picard in [Pic10, Pic09] recently and his solution theory is quoted here for the analysis of a diffusion advection equation.

**Definition A.0.1.** A Hilbert space, called *weighted  $L_2$ -space* and denoted by  $H_{\nu,0}$ , is defined as the completion of  $C_0^\infty(\mathbb{R})$  with respect to the inner product

$$(f, g)_{\nu,0} := \int_{\mathbb{R}} f(t)^* g(t) e^{-2\nu t} dt$$

where  $t \mapsto e^{-2\nu t}$  is called *exponential weight function* of the space, and  $*$  denoted the conjugated complex. The associated norm will be denoted by  $\|\cdot\|_{\nu,0}$ .

**Theorem A.0.1.** (*Solution theory*)

Let  $H$  be a complex Hilbert space,  $(M(z))_{z \in B_{\mathbb{C}}(r,r)}$  be a holomorphic family of uniformly bounded linear operators on  $H$ ,  $\nu \geq \frac{1}{2r}$ , satisfying the condition

$$\exists c \in \mathbb{R} : \forall z \in B_{\mathbb{C}}(r,r) : \frac{1}{2} (z^{-1}M(z) + (z^*)^{-1}M(z)^*) \geq c > 0 \quad (\text{A.1})$$

and  $A$  be skew-self-adjoint in  $H$ , then we have for every  $f \in H_{\nu,0} \otimes H$  a unique solution  $(U, V) \in (H_{\nu,0} \otimes H)^2$  of the problem

$$(\partial_t M(\partial_t^{-1}) + A)U = f, \quad V = M(\partial_t^{-1})U \quad (\text{A.2})$$

Moreover, the solution depends continuously on the data in  $H_{\nu,0} \otimes H$ .

*Proof.* see [Pic10] □

Now consider the evolutionary problem P1 of the advection diffusion system. We can show existence and uniqueness properties and the relation to initial and boundary data. Similar results can be obtained using other theorems and techniques, too.

**Example A.0.1.** Let  $(0, \nabla U_0)$  be in the tensor-product space  $H_{\nu,0} \otimes H$ , then Problem P1 has a unique solution  $\rho \in H_{\nu,0} \otimes H$  and the solution depends continuously on the data in  $H_{\nu,0} \otimes H$  where  $\nu > 0$  depends on  $\mathbf{u}$  and  $D$ .

*Proof.* The proof based on Theorem A.0.1. Therefore we rewrite the equation into the standard form of the material laws and see that the requirements of the theorem are fulfilled. The equation now reads

$$(\partial_t M(\partial_t^{-1}) + A) X = f, \quad \text{with } X = (\rho, \mathbf{j})^\top$$

where  $M(z) = M_0 + zM_1$  with

$$M_0 = \begin{pmatrix} 1 & 0 \\ 0 & 0 \end{pmatrix}, \quad M_1 = D^{-1} \begin{pmatrix} 0 & 0 \\ -\mathbf{u} & 1 \end{pmatrix}, \quad A = \begin{pmatrix} 0 & \nabla \cdot \\ \overset{\circ}{\nabla} & 0 \end{pmatrix}, \quad f = \begin{pmatrix} 0 \\ -\nabla U_0 \end{pmatrix}.$$

We are in the (P)-Degenerate case as  $M_0$  is self-adjoint and  $M_0 \geq 0$ . On the range  $M_0[H]$  it holds  $M_0 \geq 1 > 0$  and we see that  $M_1$  is positive definite on the null space  $N[M_0]$  since  $D^{-1} > 0$ . So  $M(z)$  is (holomorphic), uniformly bounded and  $\exists c, r > 0$  s.t.  $\Re(z^{-1}M(z)) \geq c > 0$  for all  $z \in B_{\mathbb{C}}(r, r)$  (see [Pic09] for derivation of the last implication and explanation of the (P)-Degenerate case).

The operator-matrix  $A$  is skew-self-adjoint, because the operator  $\overset{\circ}{\nabla}$  is the gradient including homogeneous Dirichlet boundary conditions.

All requirements are fulfilled and for  $\nu \geq \frac{1}{2r}$  the theorem A.0.1 of Picard states the existence and continuous dependence on the data in  $H_{\nu,0} \otimes H$  what completes the proof. □

# Appendix B

## Stability analysis

### B.1 Energy-stability

In [WWL09] an energy-stable time-discretization scheme for the standard PFC-model in  $\Omega \subset \mathbb{R}^2$  has been derived. The basic ideas from this paper are extended to the case of PFC with external potentials here.

The following Energy-splitting is proposed by different authors (e.g. [WWL09]). They split the energy (2.19) in a purely convex ("contractive") and concave ("expansive") part:  $\mathcal{F} = \mathcal{F}_c - \mathcal{F}_e$ , with  $\mathcal{F}_c = \int f_c \, d\mathbf{x}$ ,  $\mathcal{F}_e = \int f_e \, d\mathbf{x}$  defined by the free energies

$$f_c := \frac{1}{4}\varrho^4 + \frac{1}{2}(1+r)\varrho^2 + \frac{1}{2}(\Delta\varrho)^2 + \varrho U', \quad f_e := \|\nabla\varrho\|^2 \quad .$$

*Remark.* For  $r < -1$  one can find an other splitting of the energy in a convex and concave part so that the following calculations can be done in similar way.

In the following we rewrite the Theorem 1.1 from [WWL09] for the slightly altered PFC-equation including an external potential  $U' = U + \Psi$  that contains a contribution to a transport by potential-flow  $\mathbf{u} \sim -\nabla\Psi$ . We follow the argumentation used in the paper.

**Theorem B.1.1.** *Let  $\Omega \subseteq \mathbb{R}^d$  be a simply connected domain and  $\phi, \psi : \Omega \rightarrow \mathbb{R}$  sufficiently smooth, and let  $r > -1$ . Consider the canonical splitting of the PFC-energy  $\mathcal{F}$  into  $\mathcal{F} = \mathcal{F}_c - \mathcal{F}_e$ . Then*

$$\mathcal{F}(\phi) - \mathcal{F}(\psi) \leq (\delta_\varrho \mathcal{F}_c(\phi) - \delta_\varrho \mathcal{F}_e(\psi), \phi - \psi)_{L_2(\Omega)}$$

where  $\delta_\varrho$  denotes the variational derivative and  $(\cdot, \cdot)_{L_2(\Omega)}$  the  $L^2$ -scalar product in  $\Omega$ .

*Proof.* Consider the (abstract) free energy-functions  $\tilde{f}_{c/e}(\boldsymbol{\phi})$  with  $\boldsymbol{\phi} = (\phi_1, \phi_2, \phi_3)$  and

$$\tilde{f}_c(\boldsymbol{\phi}) = \frac{1}{4}\phi_1^4 + \frac{1}{2}(1+r)\phi_1^2 + \frac{1}{2}\phi_2^2 + \phi_1 U', \quad \tilde{f}_e(\boldsymbol{\phi}) := \boldsymbol{\phi}_3 \cdot \boldsymbol{\phi}_3 \quad .$$

Since  $\tilde{f}_{c/e}$  are both convex in all of its arguments the following statements hold:

$$\tilde{f}_c(\boldsymbol{\psi}) - \tilde{f}_c(\boldsymbol{\phi}) \geq \nabla \tilde{f}_c(\boldsymbol{\phi})^\top (\boldsymbol{\psi} - \boldsymbol{\phi})$$

$$\tilde{f}_e(\boldsymbol{\phi}) - \tilde{f}_e(\boldsymbol{\psi}) \geq \nabla \tilde{f}_e(\boldsymbol{\psi})^\top (\boldsymbol{\phi} - \boldsymbol{\psi})$$

for any  $\boldsymbol{\phi}, \boldsymbol{\psi} \in \mathbb{R} \times \mathbb{R} \times \mathbb{R}^n$ . Following the argumentation in [WWL09], by setting  $\boldsymbol{\phi} := (\phi, \Delta\phi, \nabla\phi)$  and  $\boldsymbol{\psi} := (\psi, \Delta\psi, \nabla\psi)$  and integrating over  $\Omega$ , one gets

$$\begin{aligned} \mathcal{F}_c(\boldsymbol{\psi}) - \mathcal{F}_c(\boldsymbol{\phi}) &\geq \int_{\Omega} \partial_1 \tilde{f}_c(\boldsymbol{\phi}, \Delta\phi, \nabla\phi)(\boldsymbol{\psi} - \boldsymbol{\phi}) + \partial_2 \tilde{f}_c(\boldsymbol{\phi}, \Delta\phi, \nabla\phi)(\Delta\psi - \Delta\phi) \, \mathrm{d}\mathbf{x} \\ &= \int_{\Omega} (\phi^3 + (1+r)\phi + U')(\boldsymbol{\psi} - \boldsymbol{\phi}) + \Delta\phi(\Delta\psi - \Delta\phi) \, \mathrm{d}\mathbf{x} \\ &= \int_{\Omega} (\phi^3 + (1+r)\phi + U' + \Delta^2\phi)(\boldsymbol{\psi} - \boldsymbol{\phi}) \, \mathrm{d}\mathbf{x} \\ \mathcal{F}_e(\boldsymbol{\phi}) - \mathcal{F}_e(\boldsymbol{\psi}) &\geq \int_{\Omega} \partial_3 \tilde{f}_e(\boldsymbol{\psi}, \Delta\psi, \nabla\psi) \cdot (\nabla\phi - \nabla\psi) \, \mathrm{d}\mathbf{x} \\ &= \int_{\Omega} \nabla\psi \cdot \nabla\phi - \nabla\psi \cdot \nabla\psi \, \mathrm{d}\mathbf{x} \\ &= \int_{\Omega} (-2\Delta\psi)(\phi - \psi) \, \mathrm{d}\mathbf{x} \end{aligned}$$

for appropriate boundary conditions. With the variational derivatives of the energies  $\delta_{\varrho}\mathcal{F}_c(\varrho) = \varrho^3 + (1+r)\varrho + U' + \Delta^2\varrho$  and  $\delta_{\varrho}\mathcal{F}_e(\varrho) = -2\Delta\varrho$  one obtains

$$\begin{aligned} \mathcal{F}(\boldsymbol{\psi}) - \mathcal{F}(\boldsymbol{\phi}) &= \mathcal{F}_c(\boldsymbol{\psi}) - \mathcal{F}_e(\boldsymbol{\psi}) - \mathcal{F}_c(\boldsymbol{\phi}) + \mathcal{F}_e(\boldsymbol{\phi}) \\ &\geq (\delta_{\varrho}\mathcal{F}_c(\boldsymbol{\phi}), \boldsymbol{\psi} - \boldsymbol{\phi})_{L^2(\Omega)} + (\delta_{\varrho}\mathcal{F}_e(\boldsymbol{\psi}), \boldsymbol{\phi} - \boldsymbol{\psi})_{L^2(\Omega)} \\ &= (\delta_{\varrho}\mathcal{F}_c(\boldsymbol{\phi}) - \delta_{\varrho}\mathcal{F}_e(\boldsymbol{\psi}), \boldsymbol{\psi} - \boldsymbol{\phi})_{L^2(\Omega)} \quad . \end{aligned}$$

□

## Energy-stable time discretization

We consider the gradient flow of  $\mathcal{F}$  for conserved dynamics, i.e. the  $H^{-1}$ -gradient flow with mobility-term  $M$ :

$$\partial_t \varrho = \nabla \cdot \{M \nabla \mu\} = \nabla \cdot \{M \nabla \delta_{\varrho} \mathcal{F}\} \quad .$$

An energy-stable time-discretization uses a semi-implicit discretization of the convex-splitting scheme by taking the contractive-part implicitly and the expanding-part explicitly. The discretization of time  $t_0 < t_1 < \dots < t_k < \dots$  gives a time step size  $\tau^k := t_{k+1} - t_k$  for  $k = 0, 1, \dots$  and function-values at specific time:  $\varrho^k := \varrho(t_k)$ . So we get the discretization-scheme:

$$\varrho^{k+1} - \varrho^k = \tau^k \nabla \cdot \{M \nabla [\delta_{\varrho} \mathcal{F}_c(\varrho^{k+1}) - \delta_{\varrho} \mathcal{F}_e(\varrho^k)]\} \quad . \quad (\text{B.1})$$

**Theorem B.1.2.** *Let  $M > 0$ . Then the proposed discretization-scheme in (B.1) is unconditionally energy-stable, i.e. non-increasing in time, regardless of time step size:*

$$\mathcal{F}(\varrho^{k+1}) \leq \mathcal{F}(\varrho^k), \quad \forall k \quad .$$

*Proof.* We use theorem B.1.1 by setting  $\phi := \varrho^{k+1}$ ,  $\psi := \varrho^k$ . Additionally we define the discrete potential  $\tilde{\mu}(\varrho^{k+1}, \varrho^k) := \delta_{\varrho} \mathcal{F}_c(\varrho^{k+1}) - \delta_{\varrho} \mathcal{F}_e(\varrho^k)$  and find:

$$\begin{aligned} \mathcal{F}(\varrho^{k+1}) - \mathcal{F}(\varrho^k) &\leq (\delta_{\varrho} \mathcal{F}_c(\varrho^{k+1}) - \delta_{\varrho} \mathcal{F}_e(\varrho^k), \varrho^{k+1} - \varrho^k)_{L_2(\Omega)} \\ &= \tau^k (\tilde{\mu}, \nabla \cdot \{M \nabla \tilde{\mu}\})_{L_2(\Omega)} \\ &= -\tau^k \int_{\Omega} M \nabla \tilde{\mu} \cdot \nabla \tilde{\mu} \, d\mathbf{x} \leq 0 \quad . \end{aligned}$$

□

## B.2 Linear stability analysis

The choice of parameters for the PFC model, to obtain an evolution that ends in a liquid or solid/crystalline structure, depends on the stability of a constant phase. A constant density profile is characteristic for the liquid phase. If we start our evolution in this phase and add some perturbations, we expect that on the one hand this perturbations decrease and we end up with the original constant phase (then we are in a liquid parameter regime). On the other hand the perturbation grows and build a crystalline structure, we speak of solidification.

The discrete evolution equation should be consistent with these phenomena and should adopt the stability properties. One way to get a basic idea of the parameters is a linear stability analysis that is done for the PFC equation by [CW08]. We adopt their derivation and apply it to the PFC model, but without including external potentials. This potential-terms changes the constant (meta-)stable liquid phase to a solution that oscillates near high potential values. Transport terms are neglected

in this first analysis, as well since they lead to complicated terms that can not be handled directly by the proposed analysis.

**Theorem B.2.1.** *The Phase-Field Crystal equations are unstable with respect to small perturbations of a constant phase  $\bar{\varrho}$ , if the following inequality holds for the parameters  $r$  and  $\bar{\varrho}$*

$$3\bar{\varrho}^2 + r < 0 \quad .$$

*Necessary for stability is  $3\bar{\varrho}^2 + r > 0$ .*

*Proof.* To derive the stability statements, we write the density-field as  $\varrho = \bar{\varrho} + \eta$ . By linearization of the PFC equation in  $\eta = \eta(x, t)$  we get the evolution equation for the perturbation

$$\partial_t \eta = \nabla \cdot M \nabla \left( \{3\bar{\varrho}^2 + r + (1 + \Delta)^2\} \eta \right) \quad . \quad (\text{B.2})$$

This can be Fourier transformed using  $\hat{\eta} := \hat{\eta}(\mathbf{k}, t) = \mathfrak{F}(\eta)(\mathbf{k}, t)$  to the evolution equation in Fourier space

$$\partial_t \hat{\eta} = - \underbrace{M \mathbf{k}^2 \{3\bar{\varrho}^2 + r + (1 - \mathbf{k}^2)^2\}}_A \hat{\eta} =: -A \hat{\eta} \quad . \quad (\text{B.3})$$

The stability condition, to ensure that the perturbation tends to zero, is known to be  $\sigma(A) \in \mathbb{R}_{>0} + i\mathbb{R}$ . This is equivalent to  $3\bar{\varrho}^2 + r + (1 - \mathbf{k}^2)^2 > 0$  for  $\mathbf{k} \neq 0$  since  $M > 0$  and in the limit  $\mathbf{k} \rightarrow 0$  we obtain the relation  $3\bar{\varrho}^2 + r > 0$ . For  $3\bar{\varrho}^2 + r < 0$  there exists a  $\mathbf{k}$  such that the stability condition does not hold anymore. Thus the equation is unstable due to small perturbations.  $\square$

Similar analysis can be done for the discrete version of the evolution equation (B.2) for a general splitting scheme (with  $a_1, a_2, a_3 \in \mathbb{R}$ )

$$\begin{aligned} \varrho^{k+1} - \tau^k \Delta \left[ \{(1 - a_1)(1 + r) + 2(1 - a_2)\Delta + (1 - a_3)\Delta^2\} \varrho^{k+1} + (\varrho^{k+1})^3 \right] \\ = \varrho^k + \tau^k \Delta \left[ \{a_1(1 + r) + 2a_2\Delta + a_3\Delta^2\} \varrho^k \right] \quad . \end{aligned} \quad (\text{B.4})$$

This leads to a discretization scheme for the perturbation  $\eta^k = \eta(t_k)$  after construction of  $\varrho^k = \bar{\varrho} + \eta^k$  and linearization around  $\bar{\varrho}$

$$\begin{aligned} \eta^{k+1} - \tau^k \Delta \left[ \{(1 - a_1)(1 + r) + 2(1 - a_2)\Delta + (1 - a_3)\Delta^2 + 3\bar{\varrho}^2\} \eta^{k+1} \right] \\ = \eta^k + \tau^k \Delta \left[ \{a_1(1 + r) + 2a_2\Delta + a_3\Delta^2\} \eta^k \right] \quad . \end{aligned} \quad (\text{B.5})$$

The aim is to obtain the same stability properties like in the continuous version for the same model parameters  $\bar{\varrho}$  and  $r$ .

**Theorem B.2.2.** *Let  $r > -1$  and let the discrete scheme adopt the stability of the continuous system, i.e. (B.4) is stable as to small perturbations of a constant phase if and only if  $3\bar{\varrho}^2 + r > 0$  and unstable otherwise, then it holds for the parameters of the time-discretization scheme (B.4)*

$$a_1 < \frac{1}{2} + \frac{3\bar{\varrho}^2}{2(1+r)}, \quad a_2 \geq \frac{1}{2}, \quad a_3 \leq \frac{1}{2} \quad .$$

*Proof.* The spitting scheme for the perturbation (B.5) can also be Fourier transformed to

$$\begin{aligned} \hat{\eta}^{k+1} \left[ 1 + \tau^k \underbrace{M\mathbf{k}^2 \{ (1-a_1)(1+r) - 2(1-a_2)\mathbf{k}^2 + (1-a_3)\mathbf{k}^4 + 3\bar{\varrho}^2 \}}_{\mathcal{L}_{\mathbf{k}}} \right] \\ = \hat{\eta}^k \left[ 1 + \tau^k \underbrace{(-M\mathbf{k}^2) \{ a_1(1+r) - 2a_2\mathbf{k}^2 + a_3\mathbf{k}^4 \}}_{\mathcal{R}_{\mathbf{k}}} \right] \end{aligned}$$

with  $\hat{\eta}^k = \hat{\eta}^k(\mathbf{k}) = \mathfrak{F}(\eta^k)(\mathbf{k})$ . One can write this equation more short:

$$\hat{\eta}^{k+1} [1 + \tau^k \mathcal{L}_{\mathbf{k}}] = \hat{\eta}^k [1 + \tau^k \mathcal{R}_{\mathbf{k}}] \quad .$$

Note that  $A = \mathcal{L}_{\mathbf{k}} - \mathcal{R}_{\mathbf{k}}$  of proof to Theorem B.2.1. Recognize that the scheme should be stable iff  $A > 0$  and unstable iff  $A < 0$ . The discrete system is stable if  $|\hat{\eta}^{k+1}| < |\hat{\eta}^k|$  and unstable for  $|\hat{\eta}^{k+1}| > |\hat{\eta}^k|$ . We get conditions for stable and unstable systems

$$\begin{aligned} [1 + \tau^k \mathcal{L}_{\mathbf{k}}]^2 &> [1 + \tau^k \mathcal{R}_{\mathbf{k}}]^2 \quad \text{for } A > 0 \\ [1 + \tau^k \mathcal{L}_{\mathbf{k}}]^2 &< [1 + \tau^k \mathcal{R}_{\mathbf{k}}]^2 \quad \text{for } A < 0 \end{aligned}$$

We get restrictions independent of time step  $\tau^k$  by dividing both by  $A$ :  $\mathcal{L}_{\mathbf{k}} + \mathcal{R}_{\mathbf{k}} > 0$ . Using  $r > -1$  and mode independent considerations this results in conditions for  $a_1, a_2$  and  $a_3$ :

$$a_1 < \frac{1}{2} + \frac{3\bar{\varrho}^2}{2(1+r)}, \quad a_2 \geq \frac{1}{2}, \quad a_3 \leq \frac{1}{2} \quad .$$

□

*Remark.* In contrast to the work of [CW08], we take the nonlinear term implicitly in the stability



analysis. For an explicit treatment the inequality for  $a_1$  changes to

$$a_1 < \frac{1}{2} - \frac{3\bar{\varrho}^2}{2(1+r)}$$

that is more restrictive. Linearization of the nonlinear term  $\varrho^3$  by Taylor expansion around  $\bar{\varrho}$  for a better approximation of  $\varrho$  is justified in our analysis since this leads to the same linearized perturbation equation (B.5).

*Remark.* The splitting scheme obtained by convex splitting of the energy in (B.1) is conform to this parameter restrictions by taking  $a_1 = 0$ ,  $a_2 = 1$  and  $a_3 = 0$ .

## Appendix C

# Derivation of SIMPLE-R algorithm

Pressure-projection methods to solve the Navier-Stokes equations are introduced by Chorin and are developed further by Prohl, Liu and others. A collection of some ideas is given by [Ran99]. The following derivation is based on [Im05, Bar98, Iss84] upon others.

We start from the velocity  $\mathbf{u}^k$  at time  $t = t_k$  and want to calculate values  $\mathbf{u}^{k+1}$  after on time step at time  $t = t_{k+1}$ . The velocity and pressure can be split into a predicted value and the remaining difference

$$\mathbf{u}^{k+1} = \mathbf{u}_1 + \delta\mathbf{u}_1, \quad \mathbf{u}_1 = \mathbf{u}_0 + \delta\mathbf{u}_0, \quad p = p_0 + \delta p \quad .$$

The SIMPLE-R algorithm starts with a prediction equation for the velocity where we neglect the pressure and the incompressibility condition:

$$\frac{\varphi^{k+1} \mathbf{u}_0 - \varphi^k \mathbf{u}^k}{\tau} + \varphi^{k+1} (\mathbf{u}^k \cdot \nabla) \mathbf{u}_0 = \eta \nabla \cdot (\varphi^{k+1} \nabla \mathbf{u}_0) - \frac{\beta}{\varepsilon^3} (1 - \varphi^{k+1}) (\mathbf{u}_0 - \bar{\mathbf{g}}) \quad . \quad (\text{C.1})$$

Take the same equation, but with a predicted pressure term, for the wanted  $\mathbf{u}_1$ , that is the first approximation to  $\mathbf{u}^{k+1}$ :

$$\frac{\varphi^{k+1} \mathbf{u}_1 - \varphi^k \mathbf{u}^k}{\tau} + \varphi^{k+1} (\mathbf{u}^k \cdot \nabla) \mathbf{u}_1 + \varphi^{k+1} \nabla p_0 = \eta \nabla \cdot (\varphi^{k+1} \nabla \mathbf{u}_1) - \frac{\beta}{\varepsilon^3} (1 - \varphi^{k+1}) (\mathbf{u}_1 - \bar{\mathbf{g}}) \quad . \quad (\text{C.2})$$

Subtract (C.2) from (C.1) where we assume that the following identities hold:

$$\begin{aligned}
\nabla \cdot (\varphi^{k+1} \nabla \mathbf{u}_0) &= \nabla \cdot (\varphi^{k+1} \nabla \mathbf{u}_1) = \nabla \cdot (\varphi^{k+1} \nabla \mathbf{u}^{k+1}) \\
\varphi^{k+1} (\mathbf{u}^k \cdot \nabla) \mathbf{u}_0 &= \varphi^{k+1} (\mathbf{u}^k \cdot \nabla) \mathbf{u}_1 = \varphi^{k+1} (\mathbf{u}^k \cdot \nabla) \mathbf{u}^{k+1} \\
(1 - \varphi^{k+1}) \mathbf{u}_0 &= (1 - \varphi^{k+1}) \mathbf{u}_1 = (1 - \varphi^{k+1}) \mathbf{u}^{k+1} \quad .
\end{aligned} \tag{C.3}$$

These are the main assumptions/approximations in the projection method of SIMPLE-R. Other methods like SIMPLE-C try to improve these approximations. The last assumption comes from the boundary conditions where we assume that this must be fulfilled in both, the predicted and final velocity field. We get an equation for  $\delta \mathbf{u}_0$ :

$$(\text{C.1}) - (\text{C.2}) \Rightarrow \frac{1}{\tau} \varphi^{k+1} \underbrace{(\mathbf{u}_0 - \mathbf{u}_1)}_{-\delta \mathbf{u}_0} = \varphi^{k+1} \nabla p_0 \quad . \tag{C.4}$$

Additionally we want to get divergence-free velocity  $\nabla \cdot \mathbf{u}_1 = 0$  in  $\Omega_1$ :

$$\nabla \cdot (\varphi^{k+1} \mathbf{u}_1) = \underbrace{\nabla \varphi^{k+1} \cdot \mathbf{u}_1}_{\nabla \varphi^{k+1} \cdot \mathbf{g}, \text{ since } \nabla \varphi \neq 0 \text{ in } \partial \Omega_1} \quad .$$

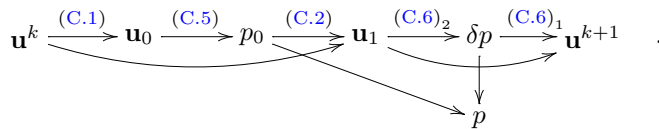
So we take the divergence on both sides of (C.4)

$$\nabla \cdot (\varphi^{k+1} \mathbf{u}_0) - \nabla \varphi^{k+1} \cdot \mathbf{g} = \tau \nabla \cdot (\varphi^{k+1} \nabla p_0) \quad . \tag{C.5}$$

This is an equation for the predicted pressure  $p_0$ . Now repeat the calculation of (C.1), including this predicted pressure (solution will be called  $\mathbf{u}_1$ ) and do the same procedure with the difference to final pressure  $p$  in (C.2) to get the pressure difference  $\delta p$  in (C.5) and the velocity difference  $\mathbf{u}^{k+1} = \mathbf{u}_1 + \delta \mathbf{u}_1$  in (C.4). We get the following equations by requiring  $\nabla \cdot \mathbf{u}^{k+1} = 0$  in  $\Omega_1$

$$\frac{1}{\tau} \varphi^{k+1} \underbrace{(\mathbf{u}_1 - \mathbf{u}^{k+1})}_{-\delta \mathbf{u}_1} = \varphi^{k+1} \nabla \underbrace{(p - p_0)}_{\delta p}, \quad \frac{1}{\tau} \nabla \cdot (\varphi^{k+1} \mathbf{u}_1) - \nabla \varphi^{k+1} \cdot \mathbf{g} = \nabla \cdot (\varphi^{k+1} \nabla \delta p) \quad . \tag{C.6}$$

The solution-procedure can be described schematically by



# Bibliography

- [AG97] Francois Alouges and J.M. Ghidaglia. Minimizing oseen-frank energy for nematic liquid crystals: Algorithms and numerical results. *Annales De L'I.H.P., Section A*, 66(4):411–447, 1997.
- [Alo97] Francois Alouges. A new algorithm for computing liquid crystal stable configurations: The harmonic mapping case. *SIAM Journal on Numerical Analysis*, 34(5):1708–1726, 1997.
- [And06] Denis Andrienko. Introduction to liquid crystals. *Modelling of Soft Matter*, 09 2006. Max Planck Research School.
- [Arc09] A.J. Archer. Dynamical density functional theory for molecular and colloidal fluids: A microscopic approach to fluid mechanics. *Journal of Chemical Physics*, 130(1), 2009.
- [Bar98] I.E. Barton. Comparison of Simple- and Piso-Type Algorithms for transient flows. *Int.J.Numer.Meth.Fluids*, 26:459–483, 1998.
- [BRV07] Rainer Backofen, Andreas Rätz, and Axel Voigt. Nucleation and growth by a phase field crystal (pfc) model. *Philosophical Magazine*, 87, 2007.
- [Cow04] Craig Cowan. The Cahn-Hilliard Equation as Gradient Flow. Master’s thesis, Simon Fraser University, 2004.
- [CW08] Mowei Cheng and James A. Warren. An efficient algorithm for solving the phase field crystal model. *Journal of Computational Physics*, 227(12):6241–6248, 2008.
- [Dav04] Timothy A. Davis. A Column Pre-Ordering Strategy for the Unsymmetric-Pattern Multifrontal Method. *ACM Transactions on Mathematical Software*, 30(2):165–195, 2004.
- [Dei] [http://tu-dresden.de/die\\_tu\\_dresden/zentrale\\_einrichtungen/zih/hpc/hochleistungsrechner/deimos](http://tu-dresden.de/die_tu_dresden/zentrale_einrichtungen/zih/hpc/hochleistungsrechner/deimos).
- [dG92] P.-G de Gennes. Soft Matter (Nobel Lecture). *Angewandte Chemie International Edition in English*, 31(7):842–845, 1992.
- [Dho98] Jan K.G. Dhont. *An Introduction to Dynamics of Colloids*. Elsevier, 1998.
- [DLL03] J. Dziubella, H. Löwen, and C.N. Likos. Depletion Forces in Nonequilibrium. *Physical Review Letter*, 91(24), 2003.
- [Dro05] Marc Droske. *On Variational Problems and Gradient Flows in Image Processing*. PhD thesis, university Duisburg-Essen, 2005.
- [EG96] E.Hairer and G.Wanner. *Solving ordinary differential equations II: Stiff and differential-algebraic problems*, volume 14 of *Springer Series in Computational Mathematics*, second ed. Springer, 1996.
- [EG05] K.R. Elder and Martin Grant. Modeling elastic and plastic deformations in non-equilibrium processing using phase field crystals. *Physical Review E*, 70, 2005.

- [Emm03] Heike Emmerich. *The Diffuse Interface Approach in Material Science*. Springer, 2003.
- [EPB<sup>+</sup>07] K.R. Elder, Nikolas Provatas, Joel Berry, Peter Stefanovic, and Martin Grant. Density functional theory of freezing and phase field crystal modeling. *Physical Review B*, 75, 2007.
- [Eva05] R.M.L. Evans. Detailed balance has a counterpart in non-equilibrium steady states. *Journal of Physics A: Mathematical and General*, 38(2), 2005.
- [Eva09] Robert Evans. Density functional theory for inhomogeneous fluids: Statics, dynamics and applications i. Technical Report 3, Heinrich-Heine University Düsseldorf, Germany, Kazimierz Dolny, Poland, 2009.
- [Gar96] C.W. Gardiner. *Handbook of Stochastic Methods: for Physics, Chemistry and the Natural Science*, volume 13 of *Springer Series in synergetics*. Springer, 1996.
- [GED97] B. Götzdelmann, R. Evans, and S. Dietrich. Depletion forces in fluids. *Physical Review E*, 57(6):6785–6800, 1997.
- [GKK<sup>+</sup>08] Christof Gutsche, Friedrich Kremer, Matthias Krüger, Markus Rauscher, Rudolf Weeber, and Jens Harting. Colloids dragged through a polymer solution: experiment, theory and simulation. *Journal of Chemical Physics*, 129(8), 2008. 084902.
- [GL99] Hartmut Graf and Hartmut Löwen. Density functional theory for hard sphericylinders: phase transitions in the bulk and in the presence of external fields. *Journal of Physics: Condensed Matter*, 11:1435–1452, 1999.
- [GR05] Christian Großmann and Hans-Görg Roos. *Numerische Behandlung partieller Differentialgleichungen*, volume 3. Teubner, 2005.
- [HZWH08] Jens Harting, Thomas Zauner, Rudolf Weeber, and Rudolf Hilfer. Numerical modeling of fluid flow in porous media and in driven colloidal suspensions. Technical report, computational physics, university Stuttgart, Pfaffenwaldring 27, 70569 Stuttgart, Germany, 2008.
- [IJ08] Ioan Teleaga and Jens Lang. Higher-Order Linearly Implicit One-Step Methods for Three-Dimensional Incompressible Navier-Stokes Equations. *Studia.Univ. "Babeş-Bolyai", Mathematica*, 53(1):109–121, 2008.
- [Im05] Hong G. Im. Numerical Methods for the Navier-Stokes Equations. presentation, 2005. University of Michigan.
- [Iss84] R.I. Issa. Solution of the Implicitly Discretised Fluid Flow Equations by Operator-Splitting. *Journal of Chemical Physics*, 62:40–65, 1984.
- [Jaa06] Akusti Jaatinen. Applicability of the phase field crystal model in predicting phase diagrams. Master’s thesis, Helsinki University of Technology, Department of Materials Science and Engineering, 2006.
- [JMR06] Volker John, Gunar Matthies, and Joachim Rang. A comparison of time-discretization/linearization approaches for the incompressible navier-stokes equations. *Computer Methods in Applied Mechanics and Engineering*, 165:5995–6010, 2006.
- [JR10] Volker John and Joachim Rang. Adaptive time step control for the incompressible navier-stokes equations. *Computer Methods in Applied Mechanics and Engineering*, 199:514–524, 2010.
- [Kab99] Winfried Kaballo. *Einführung in die Analysis III*, volume 3. Spektrum, Akademischer Verlag, 1999.

- [KGG<sup>+</sup>04] Evelina B. Kim, Orlando Guzman, Sylvain Grollau, Nicholas L. Abbott, and Juan J. de Pablo. Interactions between spherical colloids mediated by a liquid crystal: A molecular simulation and mesoscale study. *Journal of Chemical Physics*, 121(4):1949–1961, 2004.
- [KR07] Matthias Krüger and Markus Rauscher. Colloid-colloid and colloid-wall interactions in driven suspensions. *Journal of Chemical Physics*, 127(034905), 2007.
- [LÖ9] Hartmut Löwen. 3rd Warsaw School of Statistical Physics. presentation, Kazimierz Dolny, Poland, 2009.
- [Lan01] J. Lang. *Adaptive Multilevel Solutions of Nonlinear Parabolic PDE Systems. Theory, Algorithm, and Applications*, volume 16 of *Lecture notes in Computational Science and Engineering*. Springer, 2001.
- [LBF<sup>+</sup>02] A.A. Louis, P.G. Bolhuis, R. Finken, V. Krakoviack, E.J. Meijer, and J.P. Hansen. Coarse-graining polymers as soft colloids. *Physica A*, 306:251–261, 2002.
- [LBHM00] A.A. Louis, P.G. Bolhuis, J.P. Hansen, and E.J. Meijer. Can Polymer Coils Be Modeled as "Soft Colloids"? *Physical Review Letters*, 85(12):2522–2525, 2000.
- [LLVAR09] X. Li, John Lowengrub, Axel Voigt, and Andreas Rätz. Solving pde's in complex geometries: A diffuse domain approach. *Communication in Mathematical Sciences*, 7(1):81–107, 2009.
- [Löw09] Hartmut Löwen. Density functional theory for inhomogeneous fluids ii (freezing, dynamics, liquid crystals). Technical Report 3, Heinrich-Heine University Düsseldorf, Germany, Kazimierz Dolny, Poland, 2009.
- [Löw10] Hartmut Löwen. Phase-field-crystal model for liquid crystals. preprint, 2010.
- [LSY07] Chun Liu, Jie Shen, and Xiaofeng Yang. Dynamics of Defect Motion in Nematic Liquid Crystal Flow: Modeling and Numerical Simulation. *preprint submitted to Elsevier*, 2007.
- [Mes09] Jeff Meszaric. *Existence of Critical Points for the Ginzburg-Landau Functional on Riemannian Manifolds*. PhD thesis, Department of Mathematics University of Toronto, 2009.
- [MT99] Umberto Marini Bettolo Marconi and Petro Tarazona. Dynamic density functional theory of fluids. *Journal of Chemical Physics*, 110(16), 1999. 8032.
- [MZ10] Apala Majumdar and Arghir Zarnescu. Landau-de gennes theory of nematic liquid crystals: The oseen-frank limit and beyond. *Archive for Rational Mechanics and Analysis*, 196(1):227–280, 2010.
- [OS88] Stanley Osher and James A. Sethian. Fronts propagating with curvature dependent speed: algorithms based on hamilton-jacobi formulations. *Journal of Computational Physics*, 79:12–49, 1988.
- [PDT03] Florencia Penna, Joachim Dzubiella, and Pedro Tarazona. Dynamic density functional study of a driven colloidal particle in polymer solutions. *Physical Review E*, 68, 2003.
- [Pic09] Rainer Picard. A structural observation for linear material laws on classical mathematical physics. *Math.Meth.Appl.Sci.*, 32:1768–1803, 2009.
- [Pic10] Rainer Picard. On a comprehensive class of linear material laws in classical mathematical physics. *Discrete and Continuous Dynamical Systems Series S*, 3(2):339–349, 2010.
- [PJ95] P.G. de Gennes and J. Prost. *The Physics of Liquid Crystals*, volume 2. Clarendon Press, Oxford, paperback edition edition, 1995.

- [PRDK07] Florencia Penna, Markus Rauscher, Alvaro Domínguez, and Matthias Krüger. A dynamic density functional theory for particles in a flowing solvent. *Journal of Chemical Physics*, 24, 2007.
- [PS04] Per-Olof Persson and Gilbert Strang. A simple mesh generator in matlab. *SIAM Review*, 46(2), 2004.
- [Ran99] Rolf Rannacher. Finite Element Methods for the Incompressible Navier-Stokes Equations. Technical report, Institute of Applied Mathematics University of Heidelberg, 1999.
- [Ris89] Hannes Risken. *Focke-Planck Equation Methods of Solutions Applications*, volume 18 of *Springer Series in synergetics*. Springer, 1989.
- [RL08] M. Rex and Hartmut Löwen. Dynamic density functional theory with hydrodynamic interactions and colloids in unstable traps. *Physical Review Letters*, 101, 2008.
- [RL09] M. Rex and Hartmut Löwen. Dynamic density functional theory for colloidal dispersions including hydrodynamic interactions. *European Physical Journal*, E 28:139–146, 2009.
- [Ros63] H.H. Rosenbrock. Some general implicit processes for the numerical solution of differential equations. *The Computer Journal*, 5(4):329–330, 1963.
- [RY79] T.V. Ramakrishnan and M. Yussouff. First -principles order-parameter theory of freezing. *Physical Review B*, 15(5), 1979.
- [SF93] Gerard L.G. Sleijpen and Diederik R. Fokkema. BiCGStab( $l$ ) for Linear Equations Involving Unsymmetric Matrices with Complex Spectrum. *Elec.Trans.Numer.Anal*, 1:11–32, 1993.
- [SH77] J. Swift and P.C. Hohenberg. Hydrodynamic fluctuations at the convective instability. *Physical Review A*, 15(1), 1977.
- [Shk02] Steve Shkoller. Well-posedness and global attractors for liquid crystal on riemannian manifolds. *Communications in Partial Differential Equations*, 27(5-6):1103–1137, 2002.
- [SS03] James A. Sethian and Peter Smereka. Level set methods for fluid interfaces. *Annual Reviews in Fluid Mechanics*, 35:341–372, 2003.
- [Ura93] Hajim Urakawa. *Calculus of Variations and Harmonic Maps*, volume 132 of *Translations of mathematical monographs*. American Mathematical Society, 1993.
- [VR07] M.H. Veinstein and J.M. Rubi. Gaussian noise and time-reversal symmetry in nonequilibrium langevin models. *Physical Review E*, 75, 2007. 031106.
- [vTBVL09] Sven van Teeffelen, Rainer Backofen, Axel Voigt, and Hartmut Löwen. Derivation of the phase field crystal model for colloidal solidification. *Physical Review E*, 79, 2009.
- [VV07] Simon Vey and Axel Voigt. Amdis: Adaptive multidimensional simulations. *Computing and Visualization in Science*, 10:57–67, 2007.
- [VW10] Axel Voigt and Thomas Witkowski. A multi-mesh finite element method for lagrange elements of arbitrary degree. submitted, 2010.
- [Wer06] Dirk Werner. *Funktionalanalysis*, volume 5. Springer, extended edition, 2006.
- [WLB10] Raphael Wittkowski, Hartmut Löwen, and Helmut R. Brand. Derivation of a three-dimensional phase-field-crystal model for liquid crystals from density functional theory. preprint, 2010.
- [WWL09] S.M. Wise, C. Wang, and J.S. Lowengrub. An energy-stable and convergent finite-difference scheme for the phase field crystal equation. *SIAM Journal on Numerical Analysis*, 47(3):2269–2288, 2009.

# ERKLÄRUNG

Hiermit erkläre ich, dass ich die am heutigen Tag eingereichte Diplomarbeit zum Thema "Interacting Particles in Flowing Solvents – Modeling, Numerics and High-Performance Computing" unter Betreuung von Prof. Dr.rer.nat.habil. Axel Voigt selbstständig erarbeitet, verfasst und Zitate kenntlich gemacht habe. Andere als die angegebenen Hilfsmittel wurden von mir nicht benutzt.

Datum

Unterschrift